Juan Palacios Ortega

Molecular Basis of the Sticholysin-Membrane Interaction

On the Structure of the Pore and the Effect of Lipids

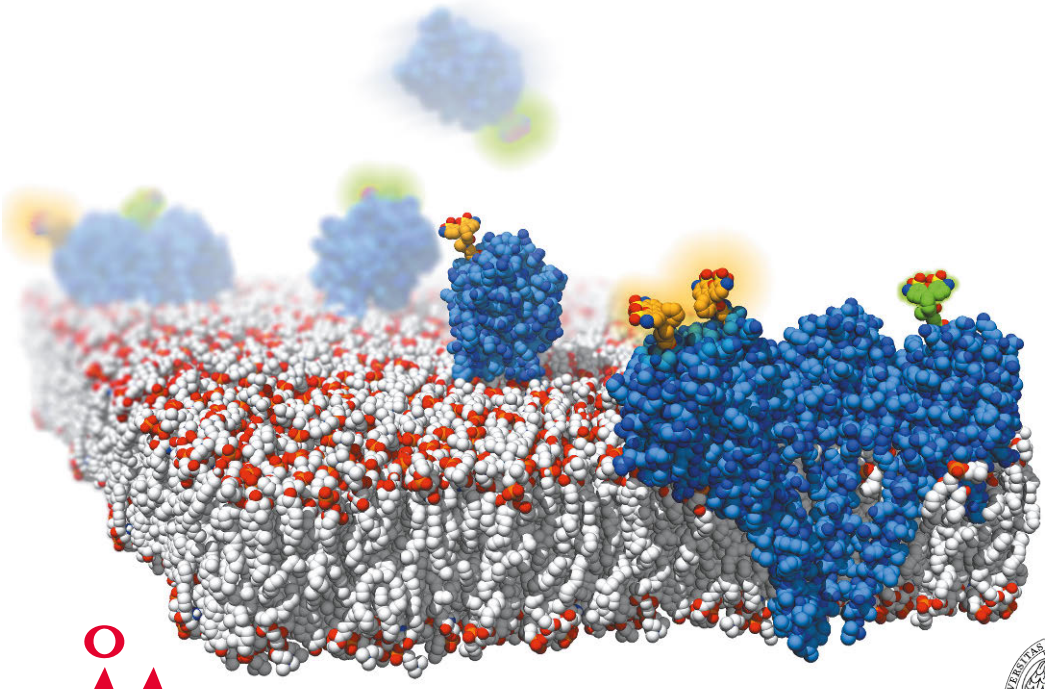

Åbo Akademi University

UNIVERSIDAD COMPLUTENSE MADRID

Juan Palacios Ortega

Born March 12th, 1994 in Madrid, Spain

Juan received his BSc in Biochemistry form Complutense University of Madrid in 2016, which included an Erasmus stay at the laboratory of Professor J. Peter Slotte in Åbo Akademi in 2015-2016. He completed his MSc in Biochemistry, Molecular Biology and Biomedicine in 2017, from Complutense University of Madrid, while working at the laboratory of Professor Álvaro Martínez del Pozo. This PhD thesis project took place from September 2017 to June 2021 under the joint co-supervision of Professor Slotte from Åbo Akademi and Professor Martínez del Pozo from Complutense University of Madrid. During this time, Juan worked at both institutions alternately.

MOLECULAR BASIS OF THE STICHOLYSIN-MEMBRANE INTERACTION

On the Structure of the Pore and the Effects of Lipids

Juan Palacios Ortega

Biochemistry, Faculty of Science and Engineering
Åbo Akademi University
Turku, Finland

Bioquímica y Biología Molecular, Facultad de Ciencias Químicas
Universidad Complutense de Madrid
Madrid, España

2021

Supervised by:

Professor J. Peter Slotte
Biochemistry, Faculty of Science and Engineering
Åbo Akademi University
Turku, Finland

Professor Álvaro Martínez-del-Pozo
Department of Biochemistry and Molecular Biology, Faculty of Chemistry
Complutense University of Madrid
Madrid, Spain

Reviewed by:

Docent Katariina Öörni
Biochemistry
Wihuri Research Institute and University of Helsinki
Helsinki, Finland

Professor Alicia Alonso Izquierdo
Dept. of Biochemistry and Molecular Biology, Faculty of Science and Technology
University of the Basque Country
Leioa, Spain

Opponent:

Professor Ilpo Tapio Vattulainen
Department of Physics
University of Helsinki
Helsinki, Finland

Cover: Artistic all-atom representation of the process of pore formation of fluorescently labeled sticholysins. Table of contents from paper IV. Copyright (2021) American Chemical Society.

ISBN 978-952-12-4073-7 (print)
ISBN 978-952-12-4074-4 (pdf)
Painosalama Oy – Turku, Finland 2021

To everyone that
got me here

Table of Contents

LIST OF ORIGINAL PUBLICATIONS

The thesis is based on the original publications listed below. These are referred to by the indicated Roman numerals throughout the thesis.

I. Palacios-Ortega, J., García-Linares, S., Rivera-de-Torre, E., Gavilanes, J. G., Martínez-del-Pozo, Á., & Slotte, J. P. (2017). **Differential Effect of Bilayer Thickness on Sticholysin Activity**. *Langmuir*, 33(41), 11018-11027.

II. Palacios-Ortega, J., García-Linares, S., Rivera-de-Torre, E., Gavilanes, J. G., Martínez-del-Pozo, Á., & Slotte, J. P. (2019). **Sticholysin, Sphingomyelin, and Cholesterol: A Closer Look at a Tripartite Interaction**. *Biophysical Journal*, 116(12), 2253-2265.

III. Palacios-Ortega, J., Rivera-de-Torre, E., Gavilanes, J. G., Martínez-del-Pozo, Á., & Slotte, J. P. (2020). **Evaluation of Different Approaches Used to Study Membrane Permeabilization by Actinoporins on Model Lipid vesicles**. *Biochimica et Biophysica Acta (BBA)-Biomembranes*, 1862(9), 183311.

IV. Palacios-Ortega, J., García-Linares, S., Rivera-de-Torre, E., Gavilanes, J. G., Martínez-del-Pozo, Á., & Slotte, J. P. (2021**). Oligomerization of Sticholysins from Förster Resonance Energy Transfer**. *Biochemistry*, 60(4), 314-323. (The author is the corresponding author of this publication.)

Publications II and III were selected by the Spanish Society of Biochemistry and Molecular Biology (SEBBM) to feature in the section *Article of the Month* of the Society's webpage in August 2019 and August 2020, respectively.

CONTRIBUTIONS OF THE AUTHOR

I. The author designed the experiments together with supervisors. The author performed the anisotropy, SPR, ITC and calcein release experiments. The author analyzed the results and conceived the model presented in the paper. Professor Slotte synthesized 14:0-SM. The author contributed to the manuscript writing together with Professor Slotte and Professor Martínez-del-Pozo, with help from the other authors.

II. The author designed the calcein release experiments together with supervisors and Sara García-Linares. Professor Slotte devised the pyrene excimer-monomer experiments. The author came up with the SLPC-CTL experiment and optimized it with help from Professor Slotte. The author developed the FRET experiments together with both supervisors. Sara García-Linares performed and analyzed the calcein release experiments. The author performed all remaining experiments, calculations, and analyses. The author contributed to the manuscript writing together with Professor Slotte and Professor Martínez-del-Pozo, with aid from the other authors.

III. The author designed the experiments together with supervisors. The author suggested the use of R6G and Tb^{3+}. The author and Esperanza Rivera-de-Torre suggested and designed the H^{+}-fluorescein experiment. Professor Martínez-del-Pozo proposed the test of the dithionite-induced quenching of NBD-PE assay. The author and Esperanza Rivera-de-Torre performed the probe release experiments. The author performed the dithionite experiments. The author contributed to the manuscript writing together with Professor Slotte and Professor Martínez-del-Pozo, with help from the other authors.

IV. The author designed the experiments. The author designed, produced, purified, and labeled the sticholysin mutants. The author preformed the experiments and analyzed the results. The author developed the model used to evaluate stoichiometry from FRET. The author wrote the manuscript with contributions from Professor Slotte and Professor Martínez-del-Pozo, with help from the other authors.

ADDITIONAL PUBLICATIONS NOT INCLUDED IN THE THESIS MANUSCRIPT

García-Linares, S., Palacios-Ortega, J., Yasuda, T., Åstrand, M., Gavilanes, J. G., Martínez-del-Pozo, Á., & Slotte, J. P. (2016). **Toxin-induced Pore Formation Is Hindered by Intermolecular Hydrogen Bonding in Sphingomyelin Bilayers.** *Biochimica et Biophysica Acta (BBA)-Biomembranes,* 1858(6), 1189-1195.

Palacios-Ortega, J., García-Linares, S., Åstrand, M., Al Sazzad, M. A., Gavilanes, J. G., Martínez-del-Pozo, Á., & Slotte, J. P. (2016). **Regulation of Sticholysin II-induced Pore Formation by Lipid Bilayer Composition, Phase State, and Interfacial Properties**. *Langmuir*, 32(14), 3476-3484.

Rivera-de-Torre, E., Palacios-Ortega, J., García-Linares, S., Gavilanes, J. G., & Martínez-del-Pozo, Á. (2017). **One Single Salt Bridge Explains the Different Cytolytic Activities Shown by Actinoporins Sticholysin I and II from the Venom of *Stichodactyla helianthus***. *Archives of Biochemistry and Biophysics*, 636, 79-89.

García-Linares, S., Rivera-de-Torre, E., Palacios-Ortega, J., Gavilanes, J. G., & Martínez-del-Pozo, Á. (2017). **The Metamorphic Transformation of a Water-soluble Monomeric Protein into an Oligomeric Transmembrane Pore**. *Advances in Biomembranes and Lipid Self-Assembly* (Vol. 26, pp. 51-97). Academic Press.

García-Ortega, L. Palacios-Ortega, J., & Martínez-del-Pozo, Á. (2017). **Fungal Ribotoxins**. *eLS*, 1 9.

Al Sazzad, M. A., Möuts, A., Palacios-Ortega, J., Lin, K-. L., Nyholm, T. K. M., & Slotte, J. P. (2019). **Natural Ceramides and Lysophospholipids Cosegregate in Fluid Phosphatidylcholine Bilayers**. *Biophysical Journal*, 116(6), 1105-1114.

Rivera-de-Torre, E., Palacios-Ortega, J., Gavilanes, J. G., Martínez-del-Pozo, Á., & García-Linares, S. (2019). **Pore-Forming Proteins from Cnidarians and Arachnids as Potential Biotechnological Tools**. *Toxins*, 11(6), 370.

Rivera-de-Torre, E., Palacios-Ortega, J., Garb, J. E., Slotte, J. P., Gavilanes, J. G., & Martínez-del-Pozo, Á. (2020). **Structural and Functional Characterization of Sticholysin III: A Newly Discovered Actinoporin within the Venom of the Sea Anemone *Stichodactyla helianthus***. *Archives of Biochemistry and Biophysics*, 108435.

Rivera-de-Torre, E., Palacios-Ortega, J., Slotte, J. P. Gavilanes, J. G., Martínez-del-Pozo, Á., & García-Linares, S. (2020). **Functional and Structural Variations among Sticholysins, Pore-forming Proteins from the Sea Anemone *Stichodactyla helianthus*.** *International Journal of Molecular Sciences*, 21(23), 8915.

Palacios-Ortega, J., Rivera-de-Torre, E., Gavilanes, J. G., Slotte, J. P., Martínez-del-Pozo, Á., & García-Linares, S. (2021) **Biophysical Approaches to Study Actinoporin-lipid Interactions.** *Methods in Enzymology*, *649*, 307-339.

ACKNOWLEDGEMENTS

This work was performed at the Laboratory of Lipid and Membrane Biochemistry at the Faculty of Science and Engineering of Åbo Akademi University, Turku, and at the Laboratory of Protein Structure and Function, at the Faculty of Chemistry of Complutense University of Madrid, from 2017 to 2020.

I would like to thank my supervisors, Professor *J. Peter Slotte* and Professor *Álvaro Martínez del Pozo*, for giving me the chance to work in their respective research groups, first as an undergrad, then as a master's, and, finally, as a PhD student, and for their guidance and help while I worked on the research presented here. I would also like to thank them for their help when travelling back and forth between Finland and Spain.

I would also like to thank Professor *Mark S. Johnson* for agreeing to be my official supervisor once Professor *Slotte* retired from office. I also wish to thank Professor *José G. Gavilanes*, who has always been a source of wisdom and counsel.

Next, I would like to thank *Esperanza Rivera de Torre* and *Sara García Linares* for initially taking me on as their apprentice and instructing me on how to work in a laboratory. I would also like to thank them for their collaboration in all the projects we have shared over the years, and for helping me whenever I needed them.

I would also like to thank all present and past members of both research groups—especially *Thomas Nyholm, Oskar Engberg, Kai-Lan Lin, Anna Möuts, Henrik Nurmi, Victor Hautala,* and *Max Lönnfors* from the Finnish laboratory. From the Spanish side, *Moisés Maestro López*, *Rodrigo Lázaro Gorines, Javier Narbona Corral*, *Diego Heras Márquez*, and everyone from the L1, our neighbor laboratory.

My most especial thanks to *Sara Hernández Pérez*, for sharing this adventure in the cold lands of Finland, and always being there for me.

Finally, I would like to express my deepest gratitude to my family, specially to my parents *Francisco Javier Palacios Muñoz* and *Concepción Ortega Pérez*, my sister *María Palacios Ortega*, my grandparents, and the rest of my family. With their care, their wisdom, and the value they have always place on knowledge, culture, and hard work, they made me the person I am today.

I am grateful for the financial support provided by Åbo Akademi University and the National Doctoral Program of Informational and Structural Biology (ISB). This work was supported by grants from the Sigrid Juselius Foundation, the Magnus Ehrnrooth foundation, and the Jane and Aatos Erkko foundation.

Juan Palacios Ortega
May 2021

ABBREVIATIONS

14:0-SM	*N*-myristoyl-D-*erythro*-sphingosylphosphorylcholine
7-SLPC	1-palmitoyl-2-(7-doxyl)-stearoyl-*sn*-glycero-3-phosphocholine
BLAST	Basic local alignment search tool
$C_{12}E_8$	Octaethylene glycol monododecyl ether
Cer	Ceramide
CHAPS	3-[(3-cholamidopropyl)-dimethylammonio]-1-propanesulfonate
Chol	Cholesterol
CTL	Cholestatrienol
di-14:1-PC	1,2-dimirystoleoyl-*sn*-glycero-3-phosphocholine
di-16:1-PC	1,2-dipalmitoleoyl-*sn*-glycero-3-phosphocholine
di-18:1-PC	1,2-dioleoyl-*sn*-glycero-3-phosphocholine, also DOPC
di-20:1-PC	1,2-dieicosenoyl-*sn*-glycero-3-phosphocholine
di-22:1-PC	1,2-dierucoyl-*sn*-glycero-3-phosphocholine
DOPC	1,2-dioleoyl-*sn*-glycero-3-phosphocholine, also di-18:1-PC
DPH	1,6-diphenyl-1,3.5-hexatriene
E/M	Excimer/monomer
eSM	Egg sphingomyelin
FraC	Fragaceatoxin C
FRET	Förster resonance energy transfer
ITC	Isothermal titration calorimetry
L/P	Lipid / protein
L_d	Liquid-disordered phase
L_o	Liquid-ordered phase
LUV	Large unilamellar vesicle
M_w	Molecular weight
NBD	*N*-(7-Nitrobenz-2-Oxa-1,3-Diazol-4-yl)
OCer	*N*-oleoyl-D-*erythro*-sphingosine
PC	Phosphatidylcholine
PFTs	Pore-forming toxins
p*I*	Isoelectric point
PL	Phospholipid
PnSL	Phosphonosphingolipids
POC	Phosphocholine
POPC	1-palmitoyl-2-oleoyl-*sn*-glycero-3-phosphocholine
PSM	*N*-palmitoyl-D-*erythro*-sphingosylphosphorylcholine
Pyr-SM	*N*-C10-pyrene-D-*erythro*-sphingosylphosphorylcholine

R_0	Förster distance
SEM	Standard error of the mean
SM	Sphingomyelin
S_o	Solid-ordered or gel phase
StnI	Sticholysin I
StnII	Sticholysin II
TCDB	Transporter classification database
tPa	*trans*-Parinaric acid
tPa-SM	*trans*-Parinaroyl- D-*erythro*-sphingosylphosphorylcholine
WT	Wild type

ABSTRACT

The usefulness of toxicity across the tree of life is far beyond doubt. Most, if not all, organisms produce compounds that can be used for attack and/or defense against external entities. Some of the most specialized of these compounds are toxic proteins, among which pore-forming toxins (PFTs) particularly excel. PFTs are present in all kingdoms of life. Given the wide variety of PFTs, one can expect a multitude of different specificities and mechanisms of action, of which we will certainly take advantage at some point. For that, a thorough characterization of PFTs and their functionality is necessary. In this thesis, we have taken further the characterization of sticholysins, small PFTs produced by the sea anemone *Stichodactyla helianthus*.

In paper I, the influence of bilayer thickness on the pore forming activity of sticholysins has been studied. Model lipid bilayers made mainly of a phosphatidylcholine (PC), with two monounsaturated acyl chains that determined membrane thickness, were used. Myristoyl-sphingomyelin (14:0-SM) was included to ensure membrane recognition by sticholysins. The effect of cholesterol (Chol) was also evaluated. The preferred thickness for sticholysins was that of di-18:1-PC membranes. This seems to be a result of evolutionary pressure since it agrees with the most common acyl chains found in analyzed fish.

In paper II, different fluorescent derivatized lipids, Sticholysin II (StnII) tryptophan mutants, and oleoyl-ceramide (OCer) were used to delve into the relationship between StnII and Chol and sphingomyelin (SM). We found that Chol favored SM recognition by StnII while, concomitantly, StnII rearranged the membrane, extracting Chol from the SM-rich domains. In fact, Chol was preferentially distributed near StnII.

In paper III, we evaluated the mechanism of the release of aqueous contents from vesicles. Several different probes were employed. We found that the StnII pore is too small for calcein to leak through. We propose that molecules of comparable size to calcein are released through the membrane perturbations produced by StnII during pore formation. The final pore would only let through very small molecules, such as dithionite.

In paper IV, a single-cysteine mutant of StnI was used to study oligomerization directly in unrestrained environments, such as that of model membranes. The results are consistent with previous structures obtained for other actinoporins. Furthermore, we have observed that the stoichiometry of the complex was maintained when StnII was included in the complex. The results in solution also support the previously observed ability of StnII to promote StnI binding to membranes.

SAMMANDRAG

Nyttan av toxicitet hos olika organismer är långt bortom tvivel. De flesta, om inte alla, organismer producerar föreningar som kan användas för attack och/eller försvar mot externa hot. Några av de mest specialiserade av dessa föreningar är toxiska proteiner, bland vilka por-bildande toxiner (eng., *pore-forming toxins*, PFT) är särskilt utmärkande. PFT finns i alla livets riken. Med tanke på det stora utbudet av PFT kan man förvänta sig en mängd olika specificiteter och verkningsmekanismer, som vi kan komma att dra nytta i olika tillämpningar. Därför är en grundlig karakterisering av PFT-peptider och deras funktionalitet nödvändig. I denna avhandling har vi undersökt och karakteriser olika stickolysiner, vilka är små PFT-peptider producerade av havsanemonen *Stichodactyla helianthus*.

I arbete I har påverkan av membraners dubbelskiktstjocklek på den porbildande aktiviteten hos stikolysiner studerats. Modellmembraner tillverkade huvudsakligen av en fosfatidylkolin (PC), med två enkelomättade acylkedjor. Genom att variera acylkedjans längd kunde de bildade bilagrens tjocklek påverkas. Myristoyl-sfingomyelin (14:0-SM) inkluderades för att säkerställa membranigenkänning hos stickolysinerna. Effekten av kolesterol (eng., cholesterol, Chol) utvärderades också eftersom det också påverkar bilagertjockleken. Den mest optimala membrantjockleken för stickolysiner var den tillverkad av di-18: 1-PC. Detta verkar vara ett resultat av evolutionärt tryck eftersom det överensstämmer med de vanligaste acylkedjorna som finns i membraner hos tex fisk.

I arbete II användes olika fluorescerande lipider, tryptofanmutanter av sticholysin II (StnII) och oleoyl-ceramid (OCer) för att studera samverkan mellan StnII och membrane innehållande Chol och sfingomyelin (SM). Vi fann att Chol gynnade SM-igenkänning av StnII medan StnII samtidigt ordnade upp membranet och drog ut Chol från de SM-rika domänerna. I själva verket distribuerades Chol företrädesvis nära StnII.

I arbete III utvärderade vi mekanismen för frisättning av vattenlösliga småmolekylära föreningar från membranvesikler. Flera olika sonder användes vid studierna. Vi fann att StnII-poren är för liten för att kalcein skall läcka igenom. Eftersom kalcein ändå frigörs från vesikler när de exponeras för stickolysiner, antar vi att andra orsaker än porer förorsakar ökad membranpermeabilitet i närvaro av stickolysiner. Den slutliga poren kan bara släppa igenom mycket små molekyler, såsom ditionit.

I arbete IV användes en cysteinmutant av StnI för att studera oligomerisering direkt i lösning eller i bilagermembraner. Resultaten som erhölls överensstämmer med tidigare visade strukturer för andra aktinoporiner. Vidare har vi observerat att

porkomplexets stökiometri bibehölls när StnII inkluderades med StnI i komplexet. Resultaten med Stn i lösning stöder den tidigare observerade förmågan hos StnII att främja Stnl-bindning till membran.

ABSTRACT

La toxicidad es indudablemente útil para los seres vivos. La mayoría, si no todos los organismos, producen compuestos para usarlos contra otros seres vivos, ya sea con fines de defensa o de ataque. Algunos de los más especializados de estos compuestos son las proteínas tóxicas, entre las que destacan las toxinas formadoras de poros (ing., *pore-forming toxins*, PFT). Estas proteínas pueden encontrarse en todos los reinos de la vida. Dada su amplia diversidad, puede esperarse que tengan una gran variedad de especificidades y mecanismos de acción. Una caracterización detallada de las PFT y su funcionalidad es un requisito fundamental para, en un futuro, poder beneficiarse de la acción de estas toxinas. Por ello, en esta tesis se ha profundizado en el comportamiento de las esticolisinas, pequeñas PFT producidas por la anémona del mar Caribe *Stichodactyla helianthus*.

En el artículo I, se estudió la influencia del grosor de membrana en la actividad de formación de poros de las esticolisinas. Para ello, se utilizaron bicapas lipídicas hechas principalmente de fosfatidilcolina (PC) con cadenas de acilo monoinsaturadas, cuya longitud determinaba el grosor de la membrana. La miristoil-esfingomielina (14:0-SM) fue incluida para asegurar la unión a la membrana de las esticolisinas. Se evaluó también el efecto del colesterol (ing., *cholesterol*, Chol). El grosor preferido resultó ser el de las membranas que incluían di-18:1-PC. Esta preferencia parece ser resultado de la presión evolutiva, ya que coincide con la longitud de las cadenas de acilo más comunes en los peces analizados.

En el artículo II, se profundizó en la relación entre la esticolisina II (StnII), el Chol y la esfingomielina (SM). Para ello, se utilizaron diferentes lípidos fluorescentes, mutantes de triptófano de la esticolisina II (StnII) y oleoil-ceramida (OCer). Los resultados obtenidos sugieren que el Chol favorece el reconocimiento de la SM por parte de StnII mientras que, simultáneamente, StnII remodela la membrana, extrayendo el Chol de los dominios ricos en SM. De hecho, una vez alcanzado el equilibrio, el Chol resulta estar distribuido preferentemente cerca de StnII.

En el artículo III, se evaluó el mecanismo de liberación de contenidos acuosos de vesículas modelo, empleando diferentes sondas fluorescentes. De acuerdo con las observaciones, el poro de StnII es demasiado pequeño para que la calceína pueda pasar a través de él. Se propone, por tanto, que la liberación de moléculas de tamaño comparable al de la calceína se produce a través de perturbaciones en la membrana inducidas por StnII durante la formación del poro. El poro final sólo dejaría pasar moléculas de menor tamaño, como puede ser la molécula de ditionito.

En el artículo IV, se utilizó un mutante puntual de cisteína de StnI para estudiar la oligomerización de las esticolisinas directamente en un ambiente sin restricciones, como es el de la superficie de las membranas modelo. Los resultados obtenidos son coherentes con las estructuras anteriores obtenidas para otras actinoporinas. Además, hemos observado que la estequiometria del complejo se mantiene cuando al mezclar ambas esticolisinas. Los resultados obtenidos en ausencia de membranas refuerzan las observaciones previas que sugerían que StnII es capaz de facilitar la actividad de StnI, presumiblemente porque estaría favoreciendo su unión a la membrana.

1. INTRODUCTION

Toxicity, though not always obvious, is widespread in life. All kind of organisms, from bacteria to mammals, produce toxic compounds. The nature and targets of these compounds, however, can be extremely varied. Toxins can be as simple as small molecules or as intricate as a large protein complex. Their targets can be structures inside of cells, such as ribosomes, or on their outside, such as membrane receptors. There is, however, one structure that particularly stands out as a target for toxins, which is the cellular membrane, and particularly the lipid bilayer. The structure of the bilayer is very similar in all living beings. The plasma membrane is of capital importance to all cells, providing the barrier between the self and the non-self, while fulfilling many other functions. In eukaryotes, membranes additionally provide compartmentalization, helping optimize cellular processes [1]. Most cells have lipid membranes that are completely exposed to the outside world.

For these reasons, membranes can be considered as excellent toxin targets due to their availability and vital importance. They are targeted various toxins, many of which are pore-forming toxins (PFTs) [2-5]. PFTs are usually produced by bacteria, but many other organisms produce them as well. In many animals, PFTs are a constituent of the immune system [6-9]. In many other organisms, they are a fundamental component of their venoms. Such is the case with many sea anemones, in whose venom actinoporins play a major role [10].

Actinoporins are small, basic proteins [11-13]. They specifically bind to their target membranes by recognition of sphingomyelin (SM), often considered to be the actinoporin receptor [14-16]. However, other physicochemical features of the membrane can greatly influence actinoporin functionality [16-25]. The presence and effect of cholesterol (Chol) in the membrane is possibly the most remarkable of these [15, 19, 22, 23, 25-28]. The pores made by these toxins, which are cation-selective, are formed once the oligomers are bound to the membrane [17]. The oligomerization steps, however, as well as the stoichiometry of the pore complex, remain to be solved in full detail.

Various actinoporins, from many different sea anemones, have been found and described so far. Nevertheless, the soluble structure of only four of them, sticholysin I (StnI) and II (StnII), equinatoxin II (EqtII), and fragaceatoxin C (FraC), has been resolved in atomic detail [29-35]. StnI and StnII are both produced by the same sea anemone, *Stichodactyla helianthus*, and despite years of research, many details regarding their behavior and mechanism of action still remain unknown. Some of those questions, such as the effect of membrane thickness and the details of Chol's

effect on actinoporin activity, the probe selectivity of the pores, and the stoichiometry adopted by these proteins in unrestrained environments, have been tackled here. Using a variety of biophysical techniques, new information is brought to light regarding these issues. The results obtained have contribute to a better understanding of the behavior of these metamorphic proteins.

2. REVIEW OF THE LITERATURE

2.1. Early reports on *Stichodactyla helianthus'* toxins and other actinoporins

Sea anemones have been known to be toxic since ancient times. One only needs to touch these animals to feel the effect of their venom. However, it was not until after the coming of the molecular sciences that the attention of a part of the scientific community was drawn to venomous animals in order to systematically find within them compounds and substances that might have potential therapeutic uses. This attention first focused on coelenterates in the 1960s and early 1970s [36-38]. The purification of toxins from the sea anemone, then known as *Stoichactis helianthus*, was first reported in Canada in 1974 by J. P. Devlin who had obtained the anemones from Barbados [39]. The toxin was not shown to be purified to homogeneity. However, the obtained cocktail displayed strong hemolytic activity.

As early the following year, in 1975, Bernheimer and co-workers at New York University (New York, NY) reported the specific binding of that toxin to SM [40]. In their paper, the researchers also presented the first estimates of the molecular weight (M_w), amino acid composition, and p*I* of the toxin. Not only that but they also pointed out the resemblance of the purified toxin with "*the nematocysts toxin of the sea anemone* Actinia equina" [40], which would be referred to as equinatoxin. Follow-up studies were published by the same group, focusing mainly on the SM-specificity displayed by the toxin, and its potential interaction with the choline moiety of SM [41, 42]. One paper presented the earliest report of toxin-induced release of aqueous contents by a *S. helianthus* toxin, performed using ^{14}C-labeled glucose [41]. In another paper, a toxin-ferritin conjugate was used to highlight the toxin specificity for sphingomyelin by taking electron micrographs of liposomes with and without SM. The researchers observed that liposomes were only labeled if SM was present. However, the authors apparently missed what was their most remarkable result: the first micrographs of the pore structures. These can be clearly appreciated in Figure 8A of the paper, shown here in Figure 1 [42].

Figure 1. *Electron micrograph of* S. helianthus *toxin's membrane-bound structures, now known to be pores, as shown by Linder* et al.*, 1977 [42]. Reproduced under Elsevier's license number 4961291129782.*

After that, in 1979, a double paper was published by D. W. Michaels and colleagues from the Johns Hopkins University in Baltimore, MD, still using Devlin's extract and/or the New York purified version [43, 44]. These papers were the first to report that the formation of transmembrane channels was responsible for increased membrane permeability. Furthermore, the cation-selectivity of these pores was then first demonstrated. Channel conductance was further explored by Varanda and Finkelstein at the Albert Einstein College of Medicine in New York [17]. They showed that the channels were selective to univalent cations in a pH-dependent manner, which was indicative of negatively charged residues at the pore lumen. Poor selectivity to Ca^{2+} was observed, being accounted for by Ca^{2+} binding to negatively charged sidechains and blocking the pore lumen.

In 1982, Blumenthal and Kem, at the University of Florida, were the first to sequence the toxin, termed by them "Cytolysin III," with no mention of the previous I and II [45, 46]. They also made the first prediction of its secondary structure elements. From their analysis, now we can see that, even with some flaws (essentially, residues 30 to 52 are missing), they sequenced StnII. It was not until 1988 that Kem and Dunn reported the discovery of four "sequence variants" of the *S. helianthus* toxin, still referring to them as Cytolysins [47]. Cytolysin III, being hemolytically strongest, was chosen to be further characterized in subsequent studies [48, 49]. At the same time, other smaller peptide components, which turned out to be neurotoxins, were being found in the venom of *S. helianthus* [50]. After this, however, no more studies would be published on this subject by groups based in the United States. Nevertheless, in the late 1980s, the first immunotoxins based on these proteins would be reported from a group in Cuba [51, 52]. This country would be the origin of the second wave of studies of *S. helianthus* toxins.

Meanwhile, equinatoxin, from *A. equina*, was being characterized in Europe. It had been first purified and characterized, as the *Stoichactis* toxin, in 1974, by the group of Ferlan and Lebez in Ljubljana, Slovenia [53-55]. The first partial sequence of equinatoxin was reported nine years later, in 1983 [56]. By that time, equinatoxin had been described as hemolytic and assayed *in vivo* [54, 57-59], and three different equinatoxin isoforms would be identified shortly after [60]. In fact, equinatoxins would be subject to much more scrutiny over the following 10 years [61-67], when it was reported that EqtII also formed cation-selective channels, modifying the Ca^{2+} fluxes in the affected cells and, most importantly, that its N-terminal sequence would fold as an amphipathic α-helix, which was in turn responsible for membrane penetration. EqtII would then be the first actinoporin to be cloned, sequenced at the DNA level, and produced in a heterologous system in 1996 [68].

It was in 1994 when the term *sticholysin* first appeared in the literature in a report from the group of Lanio and Pazos at the University of Havana, in La Habana, Cuba [69]. In that report, the full amino acid sequence of a sticholysin (in fact, StnII) was first reported complete and compared to those of the former Cytolysin III and EqtII. Shortly after, StnI and StnII were given the names they still have today [70, 71]. The group from La Habana would then continue characterizing these proteins, both on their own and in collaboration with Spanish and Italian groups [18, 72], forming the seed from which this thesis, many years later, would come to be.

The major findings of the subsequent studies in the field, by the aforementioned groups and some other researchers, shall be the focus of the subsequent sections. Before moving on, it should be mentioned that the first reports on FraC, now one of the four best characterized actinoporins, did not appear until 2009 [33, 73]. Finally, we should also acknowledge the great number of studies regarding toxins (both actinoporins and other) from many other sea anemones, such as *Anemonia sulcata*, *Heteractis magnifica*, *Heteractis crispa*, and *Actinia tenebrosa*, to name a few, that were published during the years reviewed in this section [74-84].

2.2. Classification and general characteristics of sticholysins

Sticholysins belong to the actinoporin family. They are small, cysteinless proteins with basic p*I* [11-13, 85]. They form cation-selective pores of 1–2 nm in diameter on their targeted cells, provoking cell death by means of osmotic shock [17, 18, 66, 72, 86]. These proteins are said to be hemolytic since they have the ability to disrupt erythrocytes, which is the basis of a widely used activity assay [60, 65, 84]. The classification, origin, and structural and functional features of these proteins are detailed in the following sections.

2.2.1. Channels, pore-forming toxins, and the actinoporin family

The Transporter Classification Database (TCDB) has organized all membrane transport proteins according to their class, subclass (which usually refers to the energy source of the transporter), family, and subfamily. PFTs are classified as channels, under the code 1.C and, in this classification, comprise 128 different families. Actinoporins, which in the TCDB are referred to as "the Pore-forming Equinatoxin Family," are classified in a single subfamily under the code 1.C.38.1 [87].

The classic way of classifying PFTs, however, ranks actinoporins as one of the three major families of α-PFTs [3]. The basis of this classification, unlike that of the TCDB, lies on the secondary structure lining the walls of the pores of the corresponding PFT

[4, 5, 88-93]. Actinoporins, as colicins and cytolysin A-related toxins, form a pore whose walls are lined with α-helices. The remaining PFTs, which comprise the families of bacterial haemolysins, cholesterol-dependent cytolysins, and aerolysins, are β-PFTs, based on their pore walls being lined by β-strands [3]. In spite of sharing a category, each of the families displays its own fold and pore formation mechanism. Membrane specificities can differ within the families, with the receptors being as varied as specific sugar moieties, lipids, such as Chol or SM, and specific proteins of the target organism, which can be the case of some pathogen-produced toxins.

2.2.2. Actinoporins in sea anemones and other organisms

Actinoporins, among which sticholysins are found, are cytolysins produced by sea anemones. These proteins are the main component of their venom, used for hunting purposes. Yet since they can be found not only in the venom but also in the coelomic fluid and the surroundings of these animals as well, they are also considered to play a role in the defense of these organisms [11, 94]. The reason for the existence of several actinoporin isoforms within a single species of sea anemones is not known, although it has been proposed that it could, among other things, broaden the range of targets [95, 96].

At least 20 different species of sea anemones have been observed to produce actinoporins though not all actinoporins have been sequenced [11, 13, 73, 97]. In spite of having multiple actinoporin sequences encoded in their genome, most sea anemones generally produce only a small number of these toxins in detectable quantities [10, 11, 13, 96, 98, 99]. If a basic local alignment (with the basic local alignment search tool, BLAST) is performed on UniProtKB [100] using the sequence of StnII as the query, 31 of the obtained results (as of November 2020) are proteins produced by species in the Cnidaria phylum, of which 24 come from the Actinaria order (sea anemones), and 8 from the Scleractinia order (stony corals). All sequenced and characterized actinoporins display high sequence identity (57–90%, Figure 2). If a sequence alignment is performed with the 20 sequences that have been reviewed in UniProtKB, the analysis shows that 55 residues are conserved in all of them, 36 have "strongly similar properties," and 19 show weakly similar properties, according to the scoring they obtain in the Gonnet PAM 250 matrix. There are still five positions more that are conserved in at least 18 of the sequences, adding up to 115 out of the 175 residues that make StnII (~66%).

It is interesting to note that, among all the reviewed sequences that showed up on the BLAST, there was a protein, bryoporin, from *Physcomitrella patens* (a moss), which shows some of the conserved motifs that are considered to be landmarks in the

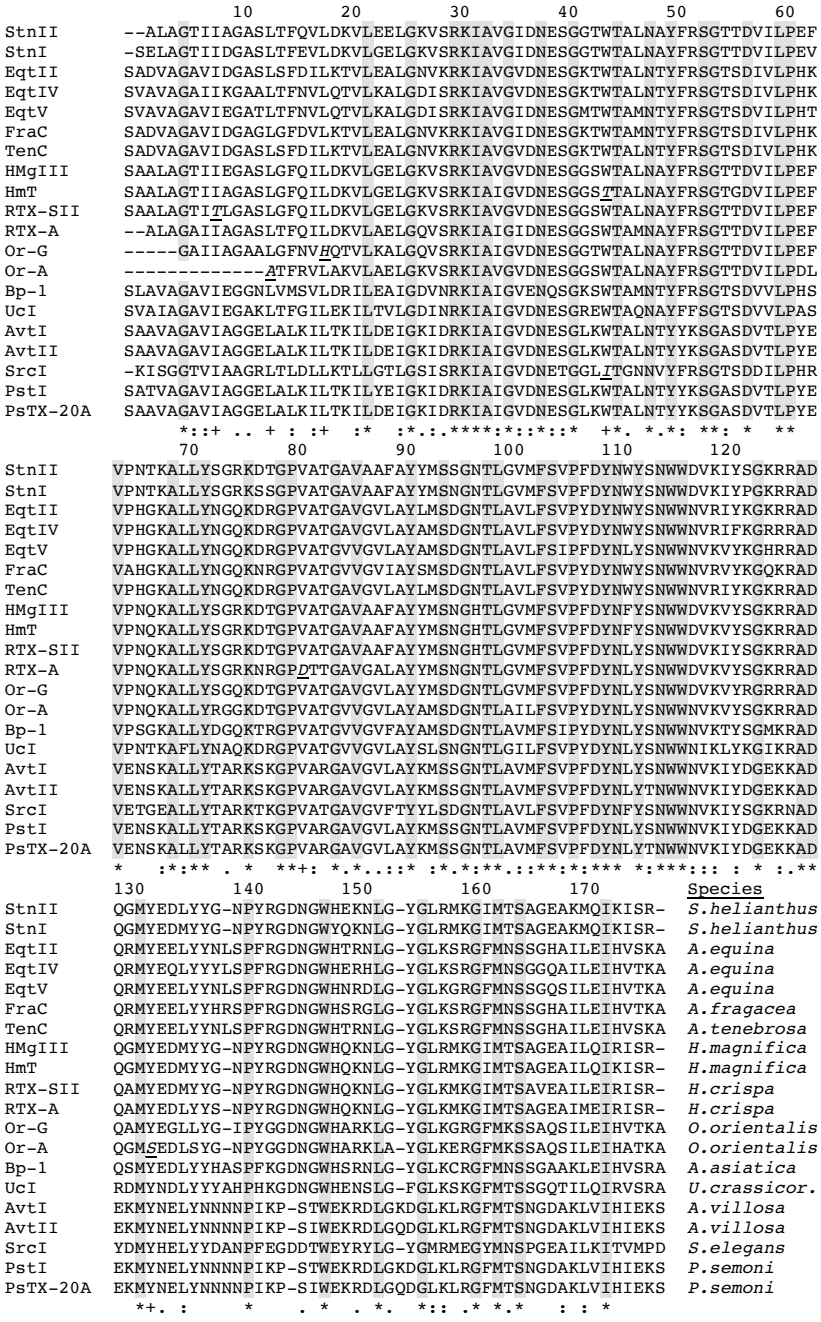

Figure 2. *Sequence alignment of known actinoporin sequences made with ClustalΩ. Consensus, calculated by ClustalΩ using the Gonnet PAM-250 matrix, is indicated in the last line: asterisk (*) indicates total conservation, colon (:), strong conservation of similar properties, and period (.) conservation of weakly similar properties. A plus (+), added afterward, outside of the analysis, indicates that the residue is conserved in all but one or two of the aligned sequences. The numbering is that of StnII.* P. semoni*, which produces the last two proteins, is a stony coral.*

actinoporin fold. The presence of such a protein in a moss appears to have been a result of convergent evolution or horizontal gene transfer [101].

From the sequences, it can be readily observed that actinoporins are cysteinless (all but one in the alignment), with lengths ranging between 165 and 179 residues, with most being closer to the latter number (Figure 2). This is one of the features presented by most of them, along with, in most cases, a basic p*I* [11-13, 85]. The alignment also reveals some sequence motifs. Indicated according to StnII numbering, the most important ones are at positions 29 to 40, at 67 to 71, and the region between residues 92 and 127, in which the P[F/I]DYN[W/L/F]Y[S/T]NWW part (residues 105 to 115) is an essential component of the actinoporin aromatic cluster and is used to identify new possible actinoporins [10, 101]. The high degree of conservation of these residues is indicative of their importance in the folding and function of these proteins, as is pointed out below.

2.3. The structure of sticholysins and the actinoporin fold

The most remarkable ability of these proteins, which is also the basis for their function, is that they are capable of adopting two different folds. One is water-soluble, whereas the other is adopted upon an encounter with a membrane with suitable properties. Most of the three-dimensional structure of actinoporins remains the same in both folds [31, 35]. Nevertheless, nearly 20% of the residues significantly change their relative position upon this structural metamorphosis. Furthermore, a concomitant oligomerization process is started. This is a clear confirmation that the three-dimensional structure adopted by a protein is not only dependent in its sequence, but as well as on the environment that it is exposed to.

To date, the water-soluble structures of StnI, StnII, EqtII, and FraC have been resolved in atomic detail, either by X-ray crystallography or by nuclear magnetic resonance [29-35]. In all cases, this fold consists of a β-sandwich flanked by two α-helices (Figure 3). The α-helices rest on the exterior surface of each of the two β-sheets. The first β-sheet is made up of five to six antiparallel β-strands. The first of those β-strands is just four residues long and a part of the segment of the protein that is eventually responsible of membrane penetration. Likewise, the other β-sheet is also made up of antiparallel β-strands.

From a structural and functional point of view, these proteins have the following four significant regions/features: the N-terminal α-helix, the exposed cluster of aromatic residues, the phosphocholine (POC) binding site, and an array of basic amino acids.

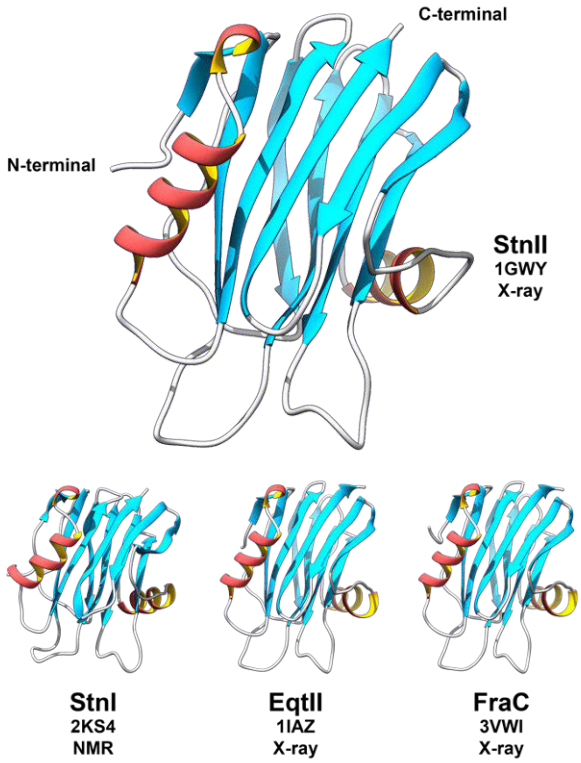

Figure 3. *The three-dimensional structures of actinoporins resolved to date. The name of each protein, along with its PDB accession code and method used to obtain the structure is indicated. The α and 3_{10} helices are depicted in red and yellow. β-strands are in light blue. Regions with non-periodic secondary structures are in light gray. The PDB structure of StnII is used in subsequent figures, unless otherwise indicated. All figures are made with UCSF Chimera, unless otherwise indicated [108].*

2.3.1. The N-terminal α-helix and the β-strands holding it

The first 30 residues of the protein are folded into a short β-strand, followed by a 3_{10} helix and a 10-residue-long α-helix [29, 31, 32, 34, 35, 102, 103]. This stretch has the highest conformational freedom of these proteins. It detaches from the β-sandwich and can fold into an amphipathic α-helix. While the first 30 residues focus most of the variability in these proteins, the β-sheet on which the helix lies in the soluble fold has two of the most conserved sequences: the 29-RKIA[I/V]G[V/I][D/E]N[E/Q][S/T]G-40 and the 67-KA[L/F]LY-71 stretches (Figure 4a). The N-terminal α-helix, by changing its extension and relative orientation to the rest of the protein, is responsible for membrane penetration and lining the pore lumen [102, 104-107].

All actinoporins have polar residues among their first 30 residue stretch. They are sorted so that they face the pore lumen. Their identity, however, is quite varied. In the

first half of this stretch, some present only uncharged polar amino acids, such as Thr and Ser. This is the case with StnII. In turn, StnI, has three acidic residues in addition to the polar amino acids. Thus, its helix has a much more marked negative character [109-111] (Figure 4b). At positions 18 and 19, all actinoporins have polar, complementary residues, most often charged. The sequence in StnI and StnII is Asp-Lys, while in EqtII and FraC it is Lys-Thr. The sidechains of those residues might establish interactions among different subunits to stabilize the final oligomer. Another pair of acid-basic residues appears at positions 22/23 and 26. There is no evidence that these residues interact between them in any of the folds. Nevertheless, it is interesting to note that some actinoporins have a Glu-Lys pair, while others have a Lys-Asp pair, positioned the other way around. In all actinoporins, those two residues have a different charge. These residues might interact with the head groups of lipids in the fenestrations observed in the available pore structures [35].

The hydrophobic residues that form the apolar part of the helix, on the contrary, are, in general, much more conserved, with Leu12 and Phe14 particularly standing out. In fact, they appear to play a double role: they are the part of the helix that stays in contact with the lipids when the helix penetrates the membrane, but they are also responsible, for the most part, for keeping the helix attached to the β-sandwich when the protein is in its soluble form. Phe14 has also been said to be relevant in oligomerization in membranes with tightly packed lipids, such as those with a high Chol content [112].

Residues Arg29 and Lys30 are conserved among all actinoporins as well. In the soluble form of these proteins, Arg29 is likely involved in a cation-π interaction with Phe106 (Tyr in some actinoporins) (Figure 4c) [113]. It is possible that, upon membrane binding, the loop at which Phe106 is located is displaced, releasing the sidechain of Arg29, triggering the deployment of the N-terminal α-helix. Lys30 appears to also play a role in this process. In all resolved structures except that of StnI, Lys30 forms a hydrogen bond with the carbonyl oxygens of Leu21 and Gly25, a residue that is also always conserved (Figure 4c). This hydrogen bond might be affected by Arg29 as part of the mechanisms triggering N-terminal helix deployment.

These last two residues are part of the first significantly conserved segment of the sequence, which expands from positions 29 to 40. Most of this and the following conserved segment (positions 67 to 71) are the part of the β-sandwich responsible for keeping the N-terminal helix attached to the main body of the protein. Ala32 fills a small gap between residues in the helix, and Gly34, in turn, leaves space for the sidechains of Leu12 and Leu17 (Figure 4d). These two Leu residues are also conserved in all but one (different one each) of the proteins shown in the alignment (Figure 2).

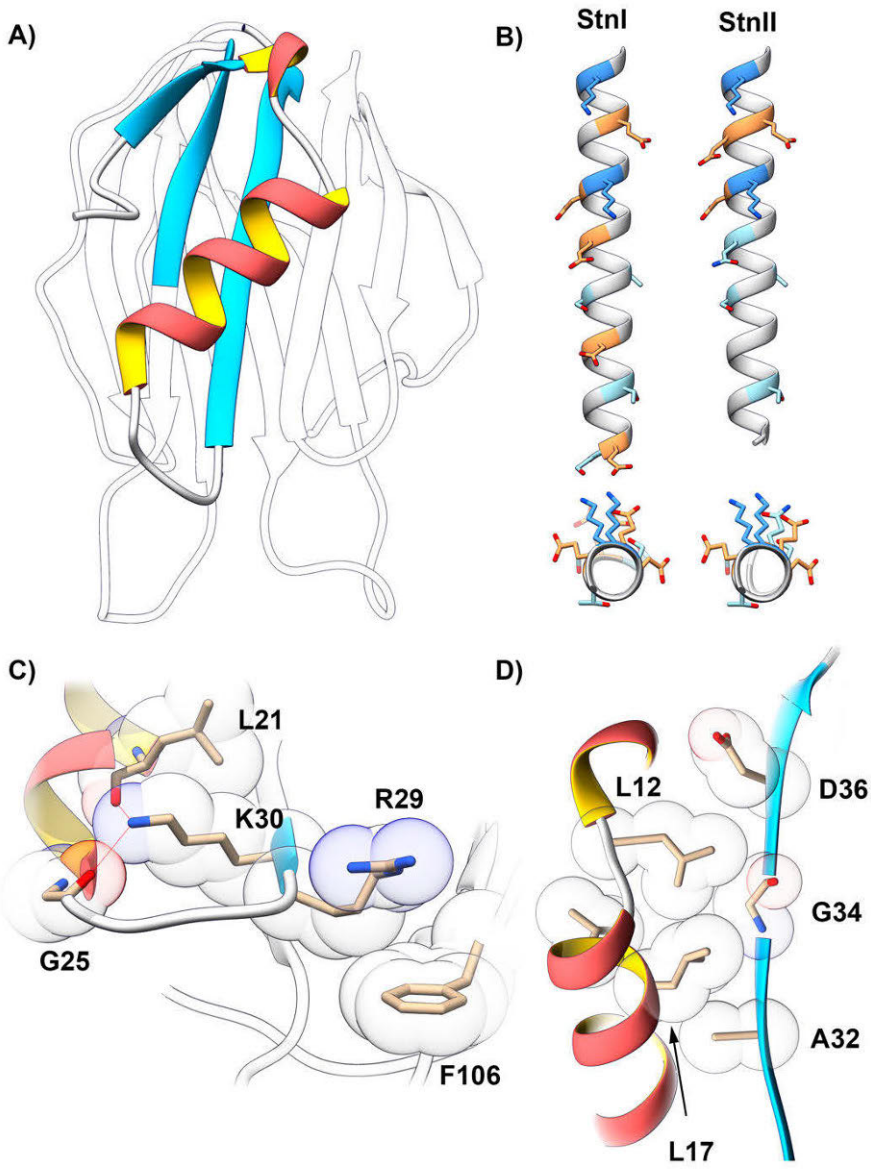

Figure 4. **A)** *N-terminal α-helix and the β-strands that keep it attached to the rest of the protein. Color code as in Fig.3.* **B)** *Top: Stretched helices (C-terminal up) of StnI and StnII, from the N-terminal to V27, made* in silico *with UCSF Chimera using the Richardson rotamer library for the amino acid sidechains. Negatively charged residues in orange, positively charged in blue. Other polar residues, in light blue. Hydrophobics are hidden for clarity. Bottom: C-terminal view of the helices. Note that all polar residues face the same side of the helix.* **C)** *Close up on the structure of StnII. On the right, hydrogen bonds between the carbonyl oxygens of G25 and L21 and the ε-amino group of K30. On the left, R29 is in close range of F106, involved in a cation-π interaction.* **D)** *Close up on StnII showing hydrophobic contacts between the N-terminal α-helix and the first β-strand of the actinoporin fold (see main text for details).*

The residues in between the ones mentioned, whose hydrophobic character and overall volume is conserved, are facing the inside of the β-sandwich and are thus essential for the overall folding of the protein. The remaining residues, from 35 to 40, are also highly conserved, but their roles are more difficult to decipher.

Lys67 has been shown to be related to the hemolytic activity of actinoporins. It can establish a salt bridge with the residue in position 8, as long as it is of acidic nature, as in StnI, but not in StnII. This way, the energy required to release the N-terminal helix is increased by the contribution of this salt bridge. In fact, the StnII mutant A8D, which can form the salt bridge, had its hemolytic activity reduced to that of StnI. Meanwhile, the reverse StnI mutant, D9A, which can no longer form that bond, presented increased hemolytic activity, almost that of StnII [114]. The same effect was observed regarding calcein release [114]. This effect could also explain the differences in hemolytic activity between StnII and FraC and EqtII which, like StnI, have an acidic residue at that position [26]. As in the previous highly conserved section, the next four residues also fulfill folding duties. Ala68 is required to be small and hydrophobic to allow the helix to be properly folded on the surface of the β-sheet. Leu 70 plays an important role in holding the helix folded by filling the void among Leu2, Ile7, Leu12, Val16, and Leu17, giving them a hydrophobic surface to interact with, reducing the likelihood of helix deployment by means of the hydrophobic effect.

It should be noted that the small β-strand at the beginning of the sequence also plays a role in holding the helix folded onto the β-sandwich, by means of being part of that same β-sheet that the helix lies on.

Finally, the first 30-residue stretch of sticholysins has been produced and assayed independently of the whole protein (Figure 4b). The results show that those peptides alone are still able to induce hemolysis [109, 115, 116].

2.3.2. The exposed aromatic cluster

Most of the exposed aromatic cluster is part of the highly conserved sequence between positions 92 and 127, which also contains residues that are included in the other functional regions of these proteins. Briefly, it can be mentioned that most residues in this sequence are conserved, with the remaining being conservatively substituted. This stretch makes up two of the β-strands that constitute the β-sandwich, one of the most exposed and flexible loops in the actinoporin structure, and two other connecting loops. In fact, residues 97 to 104 make the β-strand that is complementary to the aforementioned conserved strand made by the residues 30 to 38 (Figure 5, arrow).

The complete list of residues in the aromatic cluster is: Phe106, Trp110, Trp111, Trp114, Tyr131, Tyr135, and Tyr136 (Figure 5). Amino acids with aromatic

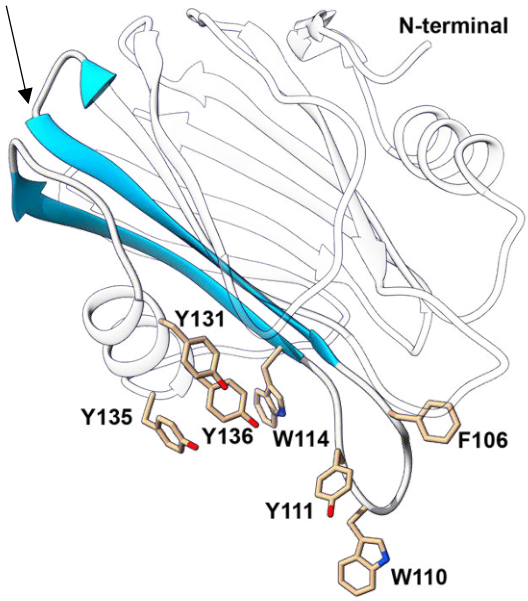

Figure 5. *The exposed aromatic cluster of actinoporins and the conserved sequence between residues 92 and 127. The sidechains of the amino acids that make up the aromatic cluster are shown. Ribbon is shown in color for positions between 92 (arrowhead in blue at the top) and 127 (loop connecting with the second α-helix of the structure). The black arrow is pointing at a β-strand whose role is discussed in the text.*

sidechains in many proteins have been previously shown to be distributed preferentially at the water-membrane interface [117]. The study of several mutants evidenced that the residues in this aromatic cluster were implied in membrane recognition [107, 118].

In EqtII, Trp112, equivalent to Trp110 of StnII, was demonstrated to be key for SM-recognition [119, 120]. However, the residue in this position is only Trp in six of the 20 sequences aligned in Figure 2. In fact, the residue that appears most often in that position is Leu. Nevertheless, the EqtII W112L mutant still retained the specificity for SM [120]. This indicates that that amino acid is only required to have a hydrophobic and large sidechain. The interactions in which it is involved, thus, are presumably not specific.

Phe106, in turn, is much more conserved. The residue in this position is Phe in 13 of the aligned sequences, and Tyr in the remaining ones, denoting that what is important here is the presence of a phenyl-ring. Thus, what seems to be essential is its capability to establish cation-π interactions, such as indicated before with Arg29 (Figure 4d).

In the resolved structures of actinoporins, Tyr111 is always very exposed, not interacting with any other residue in the protein. However, this amino acid is

conserved in all actinoporin sequences. In contrast with most of the residues reviewed this far, Tyr111 does not seem to play a role in protein folding. Instead, it is most likely essential for protein functionality. In fact, when StnII is co-crystallized with POC, Tyr111 is observed to interact with that moiety [29]. Its importance is further highlighted if it is mutated. The mutant Y111N of StnII is essentially incapable of membrane binding [107, 118, 121, 122].

The remaining residues of the exposed aromatic cluster, Trp114, Tyr131, Tyr135, and Tyr136, are conserved in most of the aligned sequences (Trp114 is always conserved). As with Tyr111, it appears that these amino acids are more related to protein functionality than to folding. In fact, all the aforementioned Tyr residues, including Tyr111, play an essential part as constituents of the POC-binding site.

2.3.3. The phosphocholine-binding site

The POC-binding site plays a fundamental role in actinoporin functionality. It is responsible for the direct interaction with the head group of SM [29]. The amino acids that form the site are Arg51, Ser52, Val85, Ser103, Pro105, Tyr111, Tyr131, Tyr135, and Tyr136. Of these, the Tyr residues are also part of the exposed cluster of aromatic residues, and their importance in membrane folding has been discussed above. The remaining amino acids of the POC-binding site, except for Arg51, are conserved in all sequences (Figure 2). Arg51 is preserved in most sequences or conservatively substituted by a Lys residue.

StnII has been co-crystallized with POC (the headgroup of SM), revealing the POC-binding site [29]. Careful inspection of that structure reveals that Tyr111 is involved in a cation-π interaction with the trimethylamine moiety of the POC molecule. Computer simulations have predicted that Tyr111 also interacts with the phosphate moiety of SM via its phenolic hydroxyl group [123]. This residue has been proven to be fundamental for SM recognition regardless of the presence of Chol in the membrane [113].

Similarly, Tyr136 is both predicted and shown to form a hydrogen bond with that same phosphate group [29, 123]. Tyr135 is predicted to interact with the 2NH and 3OH groups of SM, but in the crystal, which does not contain those groups, it helps maintain a network of solvating waters around the POC alongside Arg51, Ser52, Ser103, and Tyr131 [29]. The mutation of Tyr135 showed that this residue is also essential for membrane recognition in the absence of Chol. However, the presence of this sterol seems to compensate for this substitution, both in terms of activity and membrane binding [113]. According to the simulations, the ∂-guanidinium group of Arg51 is predicted to interact with the phosphate moiety as well [123]. This residue

was shown to be, like Tyr111, fundamental for the activity of these proteins [113]. However, it is still capable of binding Chol-containing membranes [113].

The sidechain of Val85 is hydrophobic, whereas that of Pro105 can be considered to be essentially hydrophobic. Both of these residues appear to be in close proximity with the methyl groups of the trimethylamine moiety of POC. In the three-dimensional structure of the StnII-POC complex, there is no major displacement of the sidechains of these amino acids when compared to the orientation they present in the POC-free StnII structure. Nevertheless, it is possible that the interaction with SM does cause a change in the conformation of these residues. This is especially relevant for Pro105 since it is adjacent to Phe106, which was previously mentioned to be involved in a cation-π interaction with Arg29. It is possible that Pro105 acts as the trigger for the deployment of the N-terminal α-helix.

POC binding has been shown to be essential for membrane recognition and binding when facing Chol-lacking bilayers. The presence of Chol compensates for the single substitutions of one of these amino acids. However, even though membrane binding still takes place, Arg29 (which is not part of this site) and Tyr135, and especially Arg51 and Tyr111, are essential for membrane permeabilization [113, 121].

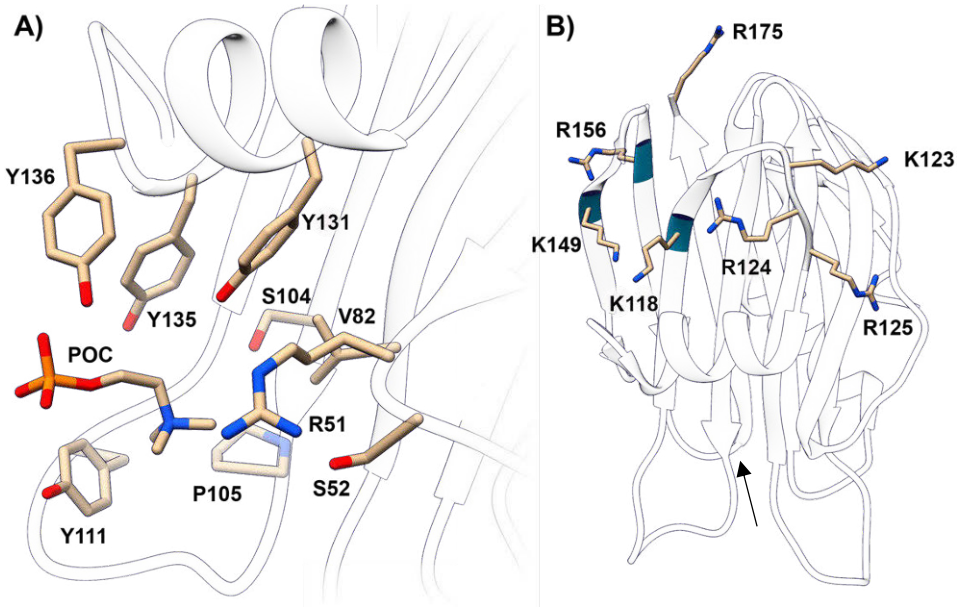

Figure 6. A) *Residues that conform the POC-binding site. Close-up at the structure of StnII complexed with POC (PDB accession code 1O72). All identified hydrogen bonds and solvating waters are omitted for clarity.* **B)** *Positioning of the residues that make up the array of basic amino acids within the complete structure of StnII. The arrow indicates the location of the POC-binding site, shown in* A.

Finally, Arg29, which has already been mentioned to be important for the activity of these proteins (see section 2.3.1), has also been observed to play a role in terms of electrostatic surface potential [122]. The potential of the StnII mutant R29Q is in fact much less positive than that calculated for the wild type (WT) variant of the protein, most likely unpairing the interaction with the phosphate moieties of the lipid in the membrane [122].

2.3.4. The array of basic amino acids

All characterized actinoporins display an array of basic amino acids. These are Lys118, Lys123, Arg124, Arg125, Lys149, Arg156 and Arg175. This array has been shown to be involved in the early steps of membrane recognition in EqtII [32]. In the aligned sequences shown in Figure 2, these residues are conserved or conservatively substituted in most cases. In EqtII, for example, and compared to sticholysins, most of these amino acids are reversed, substituting Lys by Arg and vice versa. It has been hypothesized that this difference could be responsible for the different lipid selectivity displayed by StnII and EqtII [99, 106, 107, 120, 124]. However, it is not clear what the role of these residues is at the detailed molecular level since, though helpful, negatively charged lipids in the membrane are not a strict requirement for actinoporin activity.

2.3.5. Structural differences between StnI and StnII

StnI and StnII are the main actinoporins produced by *S. helianthus* [10]. StnII is made by 175 amino acids, while StnI has an extra residue at the N-terminal. Only 12 amino acids, plus the extra residue at the N-terminal, differ between these two proteins (Figure 7). Of those differences, five are located at the N-terminal α-helix in the part that is exposed in the soluble fold. Two are found in one of the exposed loops that penetrate the membrane upon membrane interaction, and two more are at one side of the structure, which might be involved in monomer-monomer interactions.

In spite of sharing 93.7% sequence identity, the comparative hemolytic activity of these proteins is substantially different [26]. In fact, their membrane binding, as measured by isothermal titration calorimetry (ITC), and their induced calcein release are also unequal and dependent on the membrane composition [26]. Nevertheless, it has been shown that the difference between StnI and StnII at position 8, as mentioned in the section regarding the N-terminal stretch, is responsible, to a very large degree, for the behavior differences between StnI and StnII [114]. The role of the remaining differences is not clear and, so far, it has not been studied systematically. However, it is likely that these residues are responsible for the observed synergy that these two proteins display when assayed together [95].

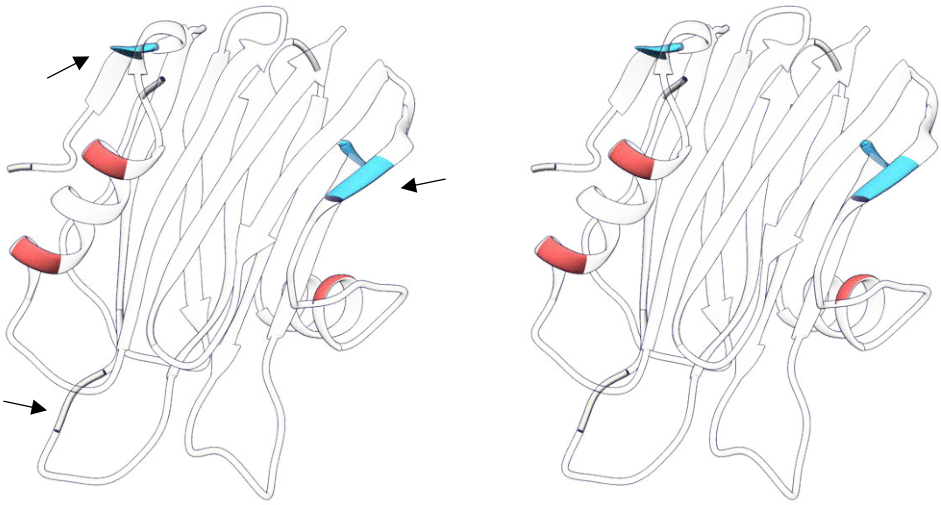

Figure 7. *Cross-eye stereo projection showing the positions differing between StnI and StnII. Arrows point at the residues whose importance is highlighted in the main text, namely position 8 (top left), which is Ala in StnII and Asp in StnI; positions 76 and 77 (lower left), which are Ser-Ser in StnII and Asp-Thr in StnI; and positions 147 and 148 (right), which are His-Glu in StnII and Tyr-Gln in StnI.*

2.4. The target: Lipid bilayers

2.4.1. Biological membranes summarized

Biological membranes are the natural target of actinoporins. They conform the basic compartmentalization structure of all living beings. They determine the extension of the cells, providing the frontier between the self and the non-self, while also supporting all the elements required to maintain the communication and material exchange with the outside world [125]. The fundamental component of biological membranes are lipids. Proteins, fulfilling most of the biological functions, and oligosaccharides, attached to lipid-head groups or to proteins, are also essential from a biological point of view [126]. All lipid bilayers are held together by the hydrophobic effect, which maximizes the entropy of the surrounding water molecules [127, 128]. Nonetheless, the building blocks of membranes are highly varied structurally [128]. These differences cause the membranes to be found in different phase states, which depend on the relative concentration of each of the molecules and on the environment surrounding them [129-135].

The lipids that make up most animal membranes are glycerophospholipids, sphingolipids, and Chol (Figure 8)[136, 137]. Very often the term phospholipid (PL) is used. It refers to phosphate-containing glycerophospholipids and sphingolipids,

such as PC or SM [137]. The structure of PLs and no-PL sphingolipids can be simplified in two parts, the hydrophobic hydrocarbon chains and the hydrophilic head group. [1] The length and degree of unsaturation of the acyl chains is responsible, to a great degree, for the phase behavior of PLs. Briefly, the longer and the more saturated the acyl chains, the more ordered is the phase of a given PL [125]. The head group is exposed to the aqueous phase and has a variety of net charges and sizes [125]. The head group in glycerophospholipids is attached to a glycerol moiety, and to the long sphingoid base in sphingolipids [125]. Although the effect of the head group is more complex than that of the acyl chains [138, 139], the relation between the cross-sectional area of the head group and the hydrophobic moiety can be used to predict which lipid aggregate a lipid will assemble into [140, 141].

The structure and membrane effects of Chol are unlike those of any other lipid (Figure 8) [142]. The hydrophobic part of Chol consists of a sterane moiety with a double bond at position 5 and an isooctyl chain at position 17 [143]. The hydrophilic part is just its 3β-hydroxyl group [143]. Chol has a condensing effect on co-lipids, reducing the average cross-sectional area of their acyl chains by increasing the number of *trans* conformational isomers [144]. Thus, Chol can have a larger number of van der Waals contacts with saturated PLs, interacting preferentially with them [142]. Chol also interacts preferentially with SMs over PCs even if the acyl chains are

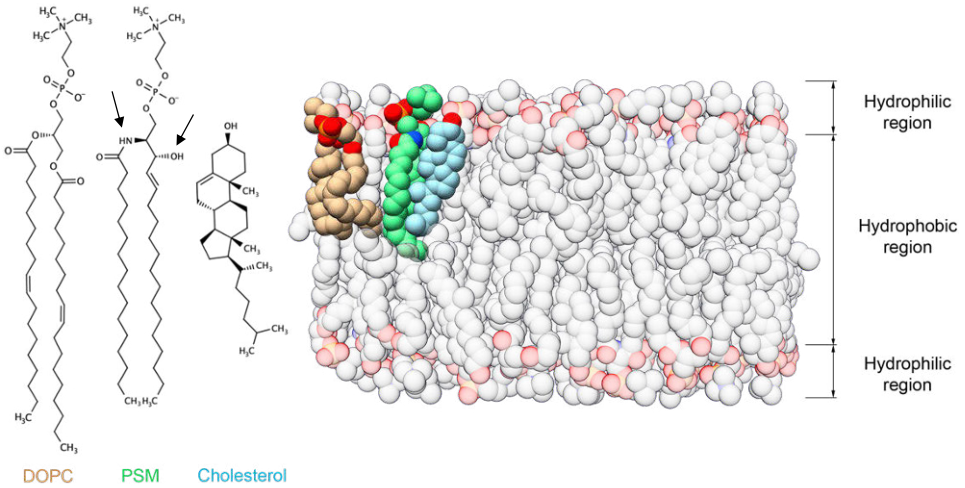

Figure 8. *Left: Schematic representation of the structures of DOPC, PSM and Chol. Arrows point at the 2NH and 3OH groups of PSM, referred in the main text. Schemes made with Marvin Sketch 19.23 (ChemAxon, 2019). Right: space-filling depiction of a lipid bilayer. A molecule of each DOPC, PSM, and Chol is highlighted in the color indicated on the left. Notice Chol's location beneath the head group of PSM.*

[1] Most often, the term *head group* refers to the moiety attached to the phosphate group. Here, *head group* refers to that moiety *plus* the phosphate group.

matched and their order is the same [145]. The presence of hydrogen bond donors and acceptors in the SM structure, namely the 2NH and the 3OH groups, which can form a hydrogen bond network in which Chol can be included, might explain this preference [146, 147]. In contrast, PCs only present donors [147].

Combinations between these molecules can give rise to the most common lipid lamellar phases: solid-ordered phase, commonly called gel phase (S_o), the crystalline phase (L_c), and the liquid crystalline phase ($L_{\alpha'}$), the latter of which is also called the liquid-disordered phase (L_d) [125, 148]. In certain lipid mixtures, and depending on the temperature, these phases can co-exist in a single bilayer, giving rise to lateral segregation [131, 149].

2.4.2. Influence of membrane composition on actinoporin activity

Lipids, and particularly SM, are the only membrane elements that actinoporins require to interact with a membrane. This is clearly shown by their interaction with model membranes that lack non-lipid components and the fact that incubation with SM, or the removal of SM from erythrocytes with sphingomyelinase, inhibits their action [18, 40, 42, 44, 65, 72, 150]. The presence of Chol, membrane phase coexistence, the fluidity and compactness of the bilayer, and the interfacial hydrogen bonding network of SM also affect the activity that actinoporins display when encountering a given membrane [16-19, 21-25, 151, 152]. Since actinoporins present an array of basic amino acids (see section 2.3.4), a preference toward anionic PLs could be expected. However, net charge of the membrane has not been observed to play a significant role in the interaction [102, 120]. In fact, charged residues are essentially absent from the binding site of these toxins, which is mostly unaffected by the overall charge distribution on the protein [120, 153].

The presence of SM in the membrane, however, does not guarantee actinoporin binding to the bilayer, which is largely influenced by the aforementioned phase state of the membrane [18, 24, 25, 44, 65, 72, 150, 153, 154]. If ceramide (Cer) and SM, both fully saturated, are used together, the membrane will contain a highly ordered phase [155-157]. SM and Cer will then partition together, rendering SM out of the actinoporins' reach [23]. Thus, it can be said that the requirement for membrane binding is not just SM presence in the membrane but SM availability.

The SM selectivity displayed by actinoporins happens despite of PC and SM sharing the same head group moiety, POC. Therefore, the capability of discriminating between them must be based on the parts of the molecules that differ between them under the head group [120]. The 2NH and 3OH groups of SM, which constitute the main structural difference between SM and PC, should thus take part in the

interaction with the toxin. Using the analogs of SM that were methylated in either of the groups, it was shown that replacing palmitoyl-SM (PSM) with either of its modified analogs impaired sticholysin activity, as reported by calcein release assays, and membrane binding, as measured by ITC and surface plasmon resonance (SPR), just as if the membrane were made of pure POPC [123]. The residues that take part in this interaction, which have been pointed out previously (see section 2.3.3), also interact with the phosphate moiety of the POC. Just as the 2NH and the 3OH of SM are essential for the interaction, so is the phosphate group, and to a similar level of detail. In fact, it has been shown that the basis for avoiding self-toxicity lies precisely at the head group of SM [158]. This was done studying the activity displayed by the cytolysin of the sea anemone *Phymactis clematis*, which also belongs to the actinoporin family, when it faces *P. clematis* lipids or other exogenous lipids [158-160]. The membrane composition of the sea anemone *P. clematis* does not include SM. Instead, it presents phosphonosphingolipids (PnSL), which are structural analogs of SM. In these molecules, the oxygen atom between the choline moiety and the phosphorus atom is missing, resulting in a direct bond between the phosphorus and the corresponding carbon atom of the choline [158]. Moreover, the degree of methylation of the nitrogen group of the ethanolamine moiety is also different, being mostly unsubstituted or monomethylated, though it can also be found trimethylated [158, 161, 162]. Based on later research, it appears that, while the trimethylation of the nitrogen of choline is likely important in terms of occupancy, the missing oxygen, which never appears in PnSL, is the basis of the selectivity. In fact, the sidechain of Arg51 in StnII is predicted to interact, precisely, with this oxygen [123]. Going back to section 2.3.3, the mutation of Arg51 resulted in a mutant unable to induce calcein release in all instances and in membrane binding in the absence of Chol [113]. The cause would most likely be that the interaction with that oxygen can no longer take place. PnSL have also been observed in other sea anemones, including *S. helianthus*, and, in general, in the Cnidaria phylum [163-166]. This reinforces the hypothesis that these lipids are responsible for the actinoporins' ineffectiveness on the membranes of sea anemones, which can contain 20 mol% of PnSL [166].

Still, some exceptions to the need for SM availability have been observed. In such cases, the vesicles employed were made of PC with significant amounts of Chol, which can induce phase separation [14, 15, 18]. It has also been observed that SM is not enough to ensure pore formation on giant unilamellar vesicles (GUVs), requiring the coexistence of the L_o and L_d phases, with pores being formed at the interface [15]. Nevertheless, it should be pointed out that that last report was made using EqtII mutants labeled with a large, highly hydrophilic fluorophore placed at positions in the N-terminal α-helix that correspond to hydrophobic residues in the WT protein. Back

to phase separation, it has been shown that StnII forms pores on COS-7 cells precisely at the regions of the membrane that are enriched in SM and Chol [151]. Although much more complex than model membranes with L_d and L_o phases, these parts of the cell membrane are also considered to be laterally segregated.

The role played by Chol in the actinoporin-membrane interaction is unclear. For example, pore formation by StnI and StnII is enhanced by the presence of different sterols, regardless of their domain-formation capability [22, 25]. In fact, it was shown that the hydrogen-bond acceptor capability of the sterol 3β-OH and an increase in membrane fluidity were responsible for enhancing the sticholysin-induced release of contents from LUVs, without a concomitant ordering of the SM phase [22, 24, 25]. In a way, this is consistent with the observations that actinoporins preferentially bind at the domain boundaries. These regions and fluid, more disordered membranes are richer in imperfections than the homogeneous, ordered phases. Thus, domain boundaries could facilitate membrane penetration, both increasing the local concentration of toxin and by reducing the energy barrier of the penetration step itself [16]. SM head groups at domain boundaries would be further exposed to the solvent as a consequence of the membrane's imperfections, easing the recognition process. Chol would be responsible for promoting phase separation. Incidentally, Chol is also able to modify the orientation and dynamics of the SM head group, according to the "umbrella hypothesis" (Figure 8) [167, 168]. This can be helpful for actinoporins when it comes to SM recognition [16]. Using an SM analog derivatized with *trans*-parinaric acid (tPa) as its acyl chain (tPa-SM), it was shown that, while including 10 mol% of Chol significantly increased StnII-induced calcein release, the acyl chain order of SM only increased modestly, as shown by the fluorescence anisotropy of tPa, indicating that something else was affected in SM [23].

Chol increasing lipid packing is a consequence of its interaction with the acyl chains of co-lipids, consequently affecting membrane fluidity [169, 170]. Due to Chol's preference for SM, it will mostly affect the acyl chain order of SM when included in a model membrane made of PC-SM as well as the SM hydrogen-bonding network and, overall, the properties of the SM-rich phase [171-173]. The N-terminal α-helix residue Phe16 of FraC (equivalent to Phe14 in StnII) has been proven essential when facing tightly packed membranes, with its substitution resulting in mutants whose ability to induce calcein release is nearly abolished [112].

One of the hypotheses regarding the final configuration of the pore consists of actinoporins bending the membrane so that a toroidal pore is created. The pore walls would then be lined by both the toxins and the polar head groups of lipids [174]. The presence of lipids that induce non-lamellar phases could increase the efficiency of pore

formation. However, no substantial difference was observed when StnII was assayed against model membranes made of SM:Chol:glycerophospholipid in a 50:35:15 ratio, where the glycerophospholipid was PC or phosphatidylethanolamine (PE) [175, 176]. PE induces an inverted hexagonal phase (H_{II}), which is characterized by having a curvature opposite to the one needed [140]. Nevertheless, phosphatidic acid (PA), which also induces the H_{II} phase, has been observed to increase the initial rate of calcein release [140, 150]; perhaps the negative charge of this lipid also played a role in this observation. EqtII has been shown to induce non-lamellar phases which are consistent with toroidal pores [177]. The formation of toroidal pores is also consistent with the observed increased rate of flip-flop induced by sticholysins [150].

Finally, some other potential acceptors for actinoporins have been proposed on the grounds that erythrocytes can be lysed at a comparatively smaller concentrations than those required to induce leakage on model vesicles [11, 65]. Most actinoporins (11 out of the 20 aligned in Figure 2) present an RGD-motif at position 141, which is located at one of the protein sides and, supposedly, close to the membrane in the pore structure. The RGD-motif is involved in the integrins' recognition of fibronectin [178]. It was proposed that this motif could be used by actinoporins to recognize integrins at the cellular surface [97]. However, the mutation of the Gly residue to Ala resulted in mutants whose oligomerization capability was severely restricted [179]. Moreover, it has been proposed that glycolipids could also facilitate actinoporin membrane binding based on the fact that these toxins are eluted later than expected when put through a chromatography on a polysaccharide-based support using a buffer with low ionic strength. Nevertheless, this does not seem to be a specific interaction. Instead, it is probably a consequence of the negative charges displayed by the glycans and the positive charge of the protein [180].

2.5. Pore formation

As PFTs, the ultimate function of actinoporins is to form pores. To do so, actinoporins are required to bind the target membrane and oligomerize. The roles played by different parts of these proteins in the process are understood to quite a high level of detail. Nevertheless, the sequence of events leading to pore formation is still unclear, being a source of controversy in the field.

2.5.1. Membrane binding

In the absence of membranes, actinoporins remain water-soluble. They retain their usual fold, consisting of a β-sandwich flanked by two α-helices. However, when they encounter a membrane with suitable characteristics, they attach themselves to it [181].

The process of membrane binding involves all protein regions mentioned previously (sections 2.3.1 through 2.3.4) [181, 182]. Kinetic measurements made with SPR using EqtII indicate that pore formation is a two-step process [102, 120]. The first step would be membrane binding itself, with the second step comprising oligomerization and actual pore formation (Figure 9).

Membrane binding would be driven mainly by the exposed cluster of aromatic residues, the array of basic amino acids, and the POC-binding site [13, 181, 182]. These elements would provide the required affinity for membrane binding and recognition. The array of basic amino acids and the aromatic cluster would likely be responsible for favoring protein partition to the membrane surface [183]. However, this should not be a strong effect since no binding is observed when vesicles of pure PC are used [120, 123]. The POC-binding site would then provide a firm attachment by recognition of and binding to SM. At this stage, the toxins are unlikely to have undergone significant structural changes other than at the sidechain level.

2.5.2. Oligomerization and membrane penetration

The oligomerization state is at this point of the process not clear nor is whether several degrees of oligomerization are possible at this advanced stage of the mechanism. Though essentially monomeric in solution, there are reports showing that a part of the total population of StnII in solution consists of dimers, trimers, and tetramers, without the need for membrane binding [184]. Thus, it is possible that the oligomerization process starts before encountering a bilayer. Nevertheless, this has not been observed in other actinoporins. As to EqtII, for example, it has been proposed that this difference might lie in the different surface charge distribution of these two proteins [120].

Actinoporins undergo a significant structural change to transition from soluble, monomeric structures to oligomeric, transmembrane ensembles [13, 35, 106, 181, 182]. The biggest alteration of the soluble fold consists in the detachment of the N-terminal α-helix form the β-sandwich. The detachment of the N-terminal α-helix is associated with a conformational change in this segment so that approximately all first 30 residues of the structure adopt an α-helical structure. How these events happen and how membrane penetration occurs is unclear.

Studies on FraC suggest that monomers would serve as the membrane-binding unit, increasing the local concentration of toxin at the water-membrane interface (Figure 9). After that, dimerization would occur (Figure 9B) [35]. The sidechain of Phe16 of FraC (Phe14 in StnII; highly conserved among actinoporins) would be displaced by the sidechain of Val60 (Val62 of StnII; conserved in all sequences in

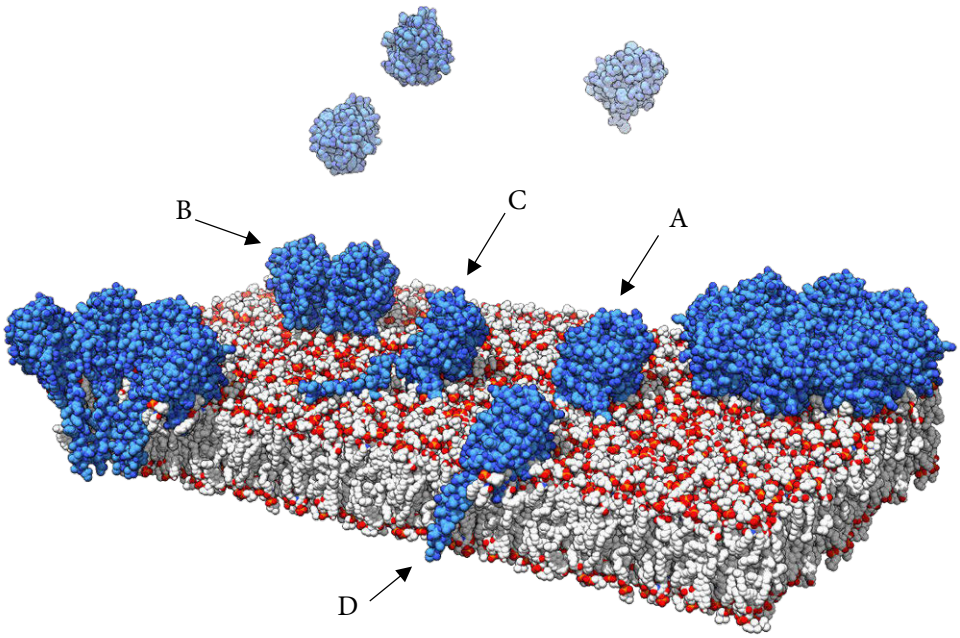

Figure 9. *Artistic all-atom representation of the process of pore formation by actinoporins, including some hypothetical intermediates. Lipids in white (carbon atoms), red (oxygen atoms), and orange (phosphorus atoms). Actinoporins in light blue (carbon atoms) and, for simplicity, dark blue (heteroatoms). Soluble monomers (top) would bind the membrane as monomers (A) or higher-order oligomers (dimers in B). Then the helix would be deployed, lying on the surface of the membrane (C). Eventually, the helix would penetrate the bilayer (D) causing a perturbation on membrane continuity (not shown). Finally, the monomers would assemble into the final pores (left, showing the transitable channel, and right).*

Figure 2) of the other subunit of the dimer, causing a partial unfolding of the N-terminal α-helix. In this case, it is proposed that further oligomerization would lead to the formation of a pre-pore ensemble, which would transition directly into the final pore [35, 185]. According to this model, helix-detachment would be mediated and induced by oligomerization. The existence of a pre-pore is highly controversial since some claim that it might not be large enough to allow the extension of the helices and their subsequent insertion in the bilayer.

However, it is also possible that helix-deployment occurs before, being triggered, as presented in sections 2.3.1 and 2.3.3, by SM binding. SM binding would be the only requirement in that scenario. After being released from the β-sandwich, the N-terminal α-helix would lie on the surface of the membrane, due to its amphipathic character (Figure 9C) [13]. Then, at some point, it would break the energy barrier and penetrate the bilayer (Figure 9D). Some results indicate that the membrane insertion of the helix takes place just after membrane binding [186]. Since no other monomers would be required to detach the helix, it is possible that oligomerization takes place

before helix detachment, while the helix lies on the membrane surface, once it has penetrated the membrane, or under any of the listed circumstances (Figure 9B). Helix insertion prior to oligomerization implies that the pre-pore state would not be required [186]. EqtII single-molecule live-imaging and subsequent analysis indicated that, as proposed for FraC, the pores would be formed by the condensation of dimeric intermediates [187]. This is also supported by the observation that preassembled StnI dimers cross-linked by disulfide bridges at the N-terminal end appear to improve pore formation [188].

2.5.3. The pore

The final structure and stoichiometry of the pore, as with the oligomerization process, remains unclear. Over the years, several different views and models of the structure have been obtained, with different degrees of acceptance in the scientific community.

The first direct observations of actinoporin pores, as mentioned in section 2.1 (see Figure 1), were electron micrographs of ferritin-labeled sticholysin, obtained in 1977 [42]. Much later, StnII was crystallized on egg-PC and DOPC monolayers [29, 189]. The volumes obtained could be used to fit the previously obtained soluble structures, including some modifications. The result was a tetrameric ensemble in which the contacts between the monomers would be minor, between the N-terminal α-helix and the C-termini of the neighboring monomer. The monomers would induce the formation of toroidal pores. The height of the complex was 43 Å, with its outer diameter being 110 Å and the inner diameter being 50 Å. These dimensions could be considered surprising since functional assays performed previously indicated that the hydrodynamic diameter of the sticholysins pore ranged between 6 and 12 Å [18, 86].

Years later, a crystal structure of FraC complexed with detergents was obtained [34]. This structure was that of a potential pre-pore ensemble, in which the sidechains of the aromatic residues are in contact with the molecules of detergent. Whether the pre-pore complex was or was not induced by the methodology can be considered controversial. In addition, some low-resolution volumes of FraC pores on LUVs were obtained. These two results were combined to obtain a structure of the pore consisting of nine subunits. In this structure, the N-terminal α-helices line the wall of the pore all by themselves. This time, the narrower constriction of the pore, at the tip of the α-helices, had a diameter of 15 Å, much closer to the aforementioned functionally predicted values for sticholysin. The outer vestibule of the complex was 50 Å wide, with the outer diameter of the whole structure being 130 Å.

In 2015, a new FraC complex was obtained [35]. This time, the structure, of 3.2 Å resolution, was composed of eight subunits, with the lumen of the pore being lined by

both the N-terminal α-helices and lipids. The α-helices of the different subunits are in contact with those of the adjacent monomer, helping stabilize the structure. They are also in contact with the corresponding intercalated lipid. There are three lipid molecules per toxin monomer. One is bound at the POC-binding site though with its head group adopting the inverse orientation to that of the POC shown in Figure 6a. Another one is sitting on top of Trp112 (Trp110 in StnII), surrounding it with its acyl chains, while its head group is engaged in a cation-π interaction with Trp116 (Trp114 in StnII) in what could be a non-canonical binding site for SM. The last lipid is the one that is exposed to the lumen of the pore. Strikingly, the parts of the lipid that are exposed to the lumen of the pore, and consequently to the solvent, are acyl chains. In this case, the head group is sitting between two toxin subunits involved in a cation-π interaction with Tyr110 (Tyr108 of StnII) of one subunit and the phosphate moiety being stabilized by Arg79 (which in StnII is T77) of the other. In spite of being an octameric structure instead of nonameric, the diameters are very similar. The narrowest pass in the lumen is 16 Å, while the distance between the highest points in the structure (using the theoretical position of the membrane as reference) is 60 Å. The total width and height of the structure are 110 and 70 Å respectively, with the part of the β-sandwich core being approximately 45 Å.

At this point, it is noticeable that the stoichiometry of the actinoporin pore is not clear. However, it is worth mentioning that all complexes have very similar dimensions. In fact, if the low-resolution volume used to fit sticholysin into a tetramer complex is inspected carefully, ignoring its four larger bumps, eight smaller, symmetrically-disposed bumps can be observed (see Figure 5b of ref. [29]). It could be said that the FraC octamer fits in that volume except for the N-terminal α-helices. Regardless of the stoichiometry, the retention of the β-sandwich fold and the extension of the N-terminal α-helix are common features of all the models. These features are supported by the characterization of a wide variety of mutants. For example, using EqtII, it was shown that the N-terminal region was required to be flexible while the β-sandwich could not be substantially perturbed if activity was to be maintained [105]. Similarly, covalently attaching the N-terminal region to the protein core or introducing a Pro residue in what would become the transmembrane α-helical segment significantly reduced the hemolytic activity of EqtII and StnII respectively [102, 107].

A widely accepted model in the field is that of a toroidal pore in which the lumen is lined by both the proteins and the head groups of PLs, with the pores having a small range of stoichiometries [186, 187, 190-192]. Besides a hydrodynamic size of ~10 Å, functional experiments have also shown that, at least for EqtII and sticholysins, the

pores are cation-selective [17, 18, 65, 66, 72]. This would be controlled by the character of the residues facing the lumen [65, 72, 104, 193]. It has also been observed that the presence of anionic lipids such as PA enhances the selectivity for cations, supporting the exposure of the lipid head groups to the pore lumen [177]. There are many observations showing that the conductance of the pores varies over time, which is indicative of the small size and dynamic nature of the pores [17, 193]. In spite of this, the average aperture of the pores appears to be concentration-independent [86]. In fact, experimental results indicate that a small number of monomers is enough to achieve the formation of functional pores [72, 190].

3. AIMS OF THE PRESENT STUDIES

The general aim of these studies was to better understand the functionality of sticholysins. With that purpose, several aspects of the interaction between actinoporins and suitable model lipid bilayers were examined. A wide variety of methods, such as fluorescence spectroscopy, isothermal titration calorimetry, and SPR, were used. When required, sticholysins mutants were designed and produced as well.

In **paper I**, the aim was to study the influence of bilayer thickness in the activity of sticholysins. Different functional assays were used to compare the behavior of sticholysins when facing model membranes of different thicknesses. Chol was included to examine its effect on each of the situations.

In **paper II**, the aim was to delve into the effect that StnII, SM, and Chol have on each other when they interact. Several Trp mutants of StnII were used in combination with two fluorescent derivates of Chol and SM, cholestatrienol (CTL) and pyrene-SM (pyr-SM). Fluorescence quenching and FRET involving CTL as well as excimer formation by pyrene were used to clarify their interactions.

In **paper III**, the aim was to better understand sticholysin-induced permeability. Probes with different structural and electrostatic features were selected to evaluate their release from model lipid vesicles as induced by sticholysin. NDB-labeled lipids were used to study the steady-state permeability of StnII pores in combination with dithionite.

In **paper IV**, the aim was to test the stoichiometry of sticholysin pores directly on model membranes, using as few perturbations as possible. With this purpose, single cysteine mutants of sticholysin were produced and labeled with ATTO-probes. Resonance energy transfer was used to evaluate the oligomerization of sticholysins in solution and the stoichiometry of the pores of StnI and StnI with StnII on membranes containing and lacking cholesterol.

4. MATERIALS AND METHODS

4.1. Materials

Lipids, lipid-precursors, and NBD-labeled POPE were purchased from Avanti Polar Lipids (Alabaster, AL, USA) or Sigma-Aldrich (St. Louis, MO, USA). Calcein, Rhodamine 6G, terbium chloride, dextran-labeled fluorescein, Triton X-100, octaethylene glycol monododecyl ether ($C_{12}E_8$), and bovine serum albumin were obtained from Sigma-Aldrich. 14:0-SM, pyr-SM, OCer, and CTL were synthesized and purified in house according to published procedures [194, 195]. PSM was purified from egg-SM using preparative high-performance liquid chromatography, as described in [196]. ATTO-labels were from ATTO-Tec GmbH (Siegen, Germany).

Mutant and WT variants of StnI and StnII were produced in *Escherichia coli*, strand RB791, and purified to homogeneity as previously described [197, 198].

4.2. Methods

Table 1. *Analytical methods used in the publications.*

	Publication			
Technique	I	II	III	IV
Steady state fluorescence anisotropy	X			X
Release of aqueous contents from LUVs	X	X	X	
Excimer/monomer (E/M) ratio of pyr-SM		X		
CTL emission in presence of quencher		X		
Intrinsic steady state fluorescence of proteins		X		
Förster Resonance Energy Transfer (FRET)		X		X
Quenching of NBD-labeled lipids			X	
Time-resolved anisotropy				X
Surface Plasmon Resonance (SPR)	X			
Isothermal Titration Calorimetry (ITC)	X			

4.2.1. Mutant production and protein purification

Mutants were produced using site-directed mutagenesis by overlap extension using polymerase chain reaction (PCR) [199]. Cell transformation, using competent *E. coli* cells (strand RB791), was performed with a procedure of thermal shock at 37 °C for 4 minutes. Transformed cells were selected with ampicillin at 10 mg/mL in a lysogeny

broth (LB) medium at 37 °C. Cells were grown, first in plaque and then in a liquid medium. Protein production was induced with 1 mM isopropyl β-D-1-thiogalactopyranoside when the culture reached an optical density of 1.0 at 600 nm. Production lasted 4 hours. Then, it was stopped by centrifugation at 6000 g for 30 minutes at room temperature. The pellet was frozen at -80 °C until the procedure could be continued.

The cell pellet was then resuspended in 50 mM TRIS containing 1% (v/v) Tween 20 and lysed by staff sonication. Soluble fraction was recovered by centrifugation at 40000 g for 30 minutes at 4 °C. The next step of protein purification was ion-exchange chromatography (carboxymethyl cellulose), eluted using a linear gradient of NaCl. Starting from 0 M NaCl, the upper limit of the gradient was 0.3 M NaCl for StnI and 0.5 M NaCl for StnII. The gradient for mutant purification was selected based on the similarity of their p*I* to that of StnI and StnII. Since sticholysins display no enzymatic activity, fractions were selected according to absorbance at 280 nm. Selected fractions were then applied to a size exclusion chromatography column (Biogel P-2). In the column, the buffer was changed to 50 mM NH_4HCO_3, pH 7.0. The selected fractions were lyophilized for long-term storage at -20 °C.

The amino acid composition of the purified proteins was analyzed for all purified protein batches. The analysis was performed on a Biochrom 20 automated analyzer (Pharmacia). The results allowed the calculation of the molar extinction coefficient of the proteins. The proper folding of resuspended proteins was ascertained using absorbance spectra, fluorescence emission, far- and near-UV circular dichroism, and thermostability analysis, performed by monitoring circular dichroism at 215 nm.

4.2.2. Vesicle preparation

Lipid vesicles were prepared by mixing organic solutions of the desired lipids to the desired final lipid molar ratio, followed by evaporation of the solvent at 40 °C under nitrogen flow and then by 1–2 hours in vacuum to ensure total elimination of the organic solvent. The dried lipid films were then hydrated 30–60 minutes in a water bath at a temperature higher than the melting temperature of the lipid mixture. The buffer used for hydration was 10 mM TRIS, 140 mM NaCl, pH 7.4. The buffer was argon-purged if required by the subsequent measurements. The prepared vesicles were then extruded, passing them at least 14 times through polycarbonate filters at the same temperature as that of hydration, to obtain LUV populations of the desired average vesicle diameter. In cases where steady-state fluorescence anisotropy measurements were aimed to measure membrane order, extrusion was substituted by water-bath sonication for 10 minutes at hydration temperature. In cases where

experiments on the release of aqueous contents were to be performed, the vesicles were freeze-thawed 10 times prior to extrusion using liquid nitrogen. Then, the vesicles were separated from the non-encapsulated dye by centrifugation-assisted filtration on Sephacryl-S200HR. Dye-loaded vesicles were used for permeabilization studies within the day.

4.2.3. Fluorescence spectroscopy

Two spectrofluorimeter models were used to measure steady-state fluorescence—SLM Aminco 8000 spectrofluorimeter (Aminco International, Inc., Rochester, NY, USA), and PTI Quanta-Master spectrofluorimeter (Photon Technology International, Lawrenceville, NJ, USA)—both operating in L- or T-format, depending on the experimental requirements. A FluoTime100 spectrofluorimeter, equipped with a PicoHarp300E time-correlated single photon-counting module (PicoQuant GmbH, Berlin, Germany) was used to perform time-resolved lifetime measurements. All fluorescence experiments were performed under constant stirring, with the temperature controlled by a Peltier element. To avoid inner filter effects, the optical density (OD) at the excitation wavelength was always such that $OD_{l/2} < 0.05$.

4.2.3.1. Steady-state fluorescence anisotropy

The steady-state anisotropy of fluorescence was measured and calculated according to Lakowicz [200]. The probe in the lipid samples contained diphenylhexatriene (DPH) in 1 mol%. The temperature was controlled by a Peltier element, with a probe submerged in a reference cell. When required, the temperature was increased at a rate of 1 °C /min.

The anisotropy of proteins in solution was also measured to see whether it was affected by the degree of labeling of the protein, as could be expected for an oligomerizing protein, according to [201, 202]. In such case, the label was ATTO-488. The excitation anisotropy spectrum of ATTO-488 was also recorded to measure the fundamental anisotropy of the probe at each wavelength (see appendix Figure A1). For this, maleimide-modified ATTO-488 was diluted at 250 nM in an 87% (v/v) glycerol solution to minimize molecular motions. With the spectra, the results from the steady-state and time-resolved experiments could be compared properly, since different wavelengths had to be used due to laser availability and signal sensitivity. The probe was excited at its maximum absorption in the steady-state experiments, at 500 ± 2 nm. In all, polarizers were used as needed.

4.2.3.2. Release of aqueous contents from LUVs

These experiments were carried out in the steady-state spectrofluorimeters using dye-loaded LUVs. Excitation and emission wavelengths were selected according to the spectral properties of the dye in use. The sample was measured prior to toxin addition to ensure a steady signal level. The release curve was followed until a steady plateau was reached or for a maximum of 13 minutes. Then, Triton X-100, or $C_{12}E_8$ if Triton X-100 had been observed to quench the dye in use, was added to obtain the fluorescence intensity corresponding to the maximum release. In publications I and II, only calcein was employed. In publication III, rhodamine 6G (R6G), Tb^{3+}, and H^+ were also used as probes. The use of these different probes required changes from the standard calcein protocol. For further details on the calcein method, see papers I and II. Please refer to paper III for details on the methods using other probes. The Tb^{3+} release assay is described in ref. [203], and was used with only minor modifications regarding lipid concentrations. Lipid concentration in sample was determined *a posteriori* using Rouser's method of phosphorous determination [204]. The quantitation of the lipid in the samples was done in this manner for all methods.

4.2.3.3. Time-dependent modeling of dye release

In paper III, a model that accounts for dye release upon membrane-perturbation was fitted to the kinetic data. The model is

$$\frac{F_{obs}(t)}{F_{max}} = 1 - \exp\left(J_2\left(e^{-\nu_{relax}t} - 1\right)\right), \qquad \textit{Eq. 1}$$

as defined by Andersson *et al.* [205]. It describes the fluorescent trace recorded for the membrane perturbation-induced release of fluorescent dyes. Once equilibrium is reached, perturbations cease, and leakage stops.

The model has two parameters, J_2 and ν_{relax}. J_2 is proportional to the intensity of the perturbations and, if a good fit is obtained, it can be obtained from $J_2 = -\ln|1-L_{max}|$, where L_{max} is the value of the final maximum release. The parameter ν_{relax} is related to the lifetime of the perturbations. The derivation of Eq. 1 with respect to t can be used to show that the product $J_2 \cdot \nu_{relax}$ is equal to the slope of the release curve at $t = 0$.

4.2.3.4. Measurement of the E/M ratio of pyrene-labelled SM

E/M ratio measurements were performed using LUVs with a composition consisting of POPC:PSM:pyr-SM:X, in a molar ratio of 5:3:2:1, in which X could be Chol, OCer, or nothing. Pyrene was excited using 345 nm. The E/M ratio was calculated from the steady-state fluorescence intensities corresponding to pyrene-monomer at 392 nm and pyrene-excimer emission at 480 nm. When the effect of sticholysin was analyzed,

the E/M ratio continuously followed, and the final value was determined 10 minutes after protein addition to ensure the system had reached equilibrium.

4.2.3.5. CTL emission in the presence of a phase-selective quencher

CTL emission was monitored on LUVs containing 7-SLPC, which has a doxyl-group in the *sn*-2 acyl chain. This group acts as a collisional quencher of CTL while also precluding 7-SLPC from the ordered domains due to its bulkiness. The membrane compositions used were POPC:7-SLPC:PSM:CTL in molar ratios of 50:30:20:5 and 30:20:50:5. These constituted the F samples. Emission in the absence of a quencher, that is, F_0 samples, was measured replacing 7-SLPC with POPC. CTL content was kept below 5 mol% to avoid self-quenching [206]. The sample was excited at 310 nm to avoid significant contribution of Trp emission from StnII. Still, Trp contribution was subtracted from the final signal. Emission was collected at 400 nm. Different toxin amounts, duplicated for the F and F_0 samples, were added after 100 seconds of steady levels of the CTL signal were recorded. Toxin contributions, though small, were quantified and subtracted from the raw fluorescence signal. Toxin effect on CTL emission was quantified as $\Delta(F/F_0)$, that is, the actinoporin-induced increment of CTL quantum yield when comparing samples with and without the quencher.

4.2.3.6. Intrinsic steady-state fluorescence of proteins

The emission spectra of the intrinsic fluorescence of StnII and StnII mutants were recorded between 280 and 500 nm using 260 nm for excitation. Wavelengths were selected so that CTL contribution, which was present in subsequent experiments, was minimized. Protein concentration was 200 nM. In cases where lipid vesicles were present, emission spectra were recorded once the system had reached equilibrium. Lipid titration of the proteins was performed by the addition of 1.3 μM increments of lipid to a final lipid concentration of 18.5 μM, that is, a 92.6 L/P molar ratio, to ensure that all proteins were bound to the bilayer. Toxin-free samples with the same lipid amount were used to correct for light scattering contributions. The lipid composition was DOPC:eSM:Chol, in a 1:1:1 molar ratio (eSM being egg-SM). Relative quantum yields were calculated using the numerically integrated areas of the emission spectra.

4.2.3.7. Förster Resonance Energy Transfer (FRET) measurements

FRET efficiencies were calculated fitting the donor spectra in the absence of the acceptor to that recorded in the presence of the acceptor, using nonlinear least-squares in the spectral region free of contributions other than that of the donor. The spectra were always corrected for dilution effects and scattering and non-sensitized acceptor contributions. When of interest, the acceptor-sensitized emission was obtained by the subtraction of the fitted donor-alone spectra from those in the presence of the

acceptor. Experimental FRET efficiency data were later used in combination with theoretical models to draw further conclusions.

In all cases where FRET was used, the Förster distance (R_0) of the employed donor-acceptor pair was calculated directly in Å as

$$R_0 = 0.2108\sqrt[6]{\kappa^2 n^{-4} Q_D J(\lambda)}, \qquad \textit{Eq. 2}$$

where κ^2 is the orientation factor, usually set to 2/3, representing the dynamic isotropic limit; n is the refractive index of the medium, set to 1.33 for water and 1.39, the average between n_{water} and n_{membrane}, when energy transfer occurred between fluorophores in different phases; Q_D is the quantum yield of the donor; and $J(\lambda)$ is the overlap integral between the emission spectra of the donor and the absorption spectra of the acceptor. This is calculated as

$$J(\lambda) = \int_0^\infty F_D(\lambda)\varepsilon_A(\lambda)\lambda^4 \, d\lambda \,, \qquad \textit{Eq. 3}$$

where $F_D(\lambda)$ is the emission spectra of the donor with its area normalized to 1, and $\varepsilon_A(\lambda)$ is the acceptor spectra in M^{-1} cm^{-1} units.

FRET from Trp in StnII to CTL (R_0 = 22.9 Å) was used in paper II to determine which Trp residues in StnII are located closer to sterols in the membrane and to discover whether sterols are preferentially distributed near StnII when the toxin is bound to the bilayer. FRET efficiencies were calculated at high L/P molar ratios to ensure that all proteins were bound to the bilayer in order to avoid contributions from toxin subunits in an acceptor-free environment.

The distribution was estimated with the aid of a model that calculates the theoretical FRET efficiency that is to be expected for an unlinked donor-acceptor pair in which each class of molecules diffuses randomly in a separate plane. The basis of the model was derived by Davenport *et al.* [207]. Specifically, the model calculates the time-dependent probability of the donor decay of remaining unquenched as a function of the spectral properties of both fluorophores and the range of available distances, expressed as

$$\rho_{cis'}(t) = \exp\left(-2\pi h^2 m \int_0^\omega \left\{1 - \exp\left[-\left(\frac{R_0}{R_e}\right)^6 \times \left(\frac{t}{\langle\tau\rangle}\right)\alpha^6\right]\right\}\alpha^{-3} d\alpha\right), \qquad \textit{Eq. 4}$$

where h is the distance between the diffusion planes, m is the surface density of the acceptor, R_e is the exclusion radius between the donor and the projection of the

acceptor in the donor diffusion plane, and $\langle\tau\rangle$ is the average lifetime of the donor. The parameter α is defined as $\alpha = h/\sqrt{h^2 + r^2}$, where *r* is the distance between the donor and the projection of the acceptor in the donor's diffusion plane. The parameter ω represents the maximum value of α, achieved at the particular case at which $r = R_e$. The expected fluorescent decay of the donor in the presence of randomly distributed acceptors is then obtained as $I_{DA}(t) = I_D(t)\rho_{cis'}(t)$. The theoretical FRET efficiency is calculated as

$$E = 1 - \frac{\int_0^\infty I_D(t)\rho_{cis'}(t)\,dt}{\int_0^\infty I_D(t)\,dt}, \qquad \textit{Eq. 5}$$

where $I_D(t)$ is the decay of the donor in the absence of the acceptor. From the results, it can be concluded that the acceptor is preferentially, randomly distributed near the acceptor or excluded from its vicinity as the experimental efficiency values are higher, equal, or smaller than those predicted, respectively.

In paper IV, FRET between labels attached at a specific position in the structure of sticholysins was used to delve into the process of oligomerization. The mutant used was StnIT43C. Its design takes advantage of the lack of Cys residues of actinoporins, which enables labeling them specifically at a convenient position, safe from the point of view of functionality. The labels used were ATTO-488 and ATTO-542. The R_0 for the self-transfer of ATTO-488 was calculated to be 49.3 Å, whereas the R_0 for the ATTO-488/ATTO-542 FRET pair was 63.8 Å.

The mutant StnI-T43C was characterized structurally and functionally using circular dichroism, intrinsic fluorescence emission, and hemolytic assays, as previously described [113, 114] (Figure A2). Its hemolytic activity was the same as that of StnI-WT, indicating the unaffected functionality of the protein. Labeling was performed using maleimide-modified ATTO probes (5-8 molar excess) O/N after a previous two-day incubation with TCEP (50:1 molar excess) in a phosphate buffer (140 mM NaCl, 10 mM phosphate), pH 7.4. The excess of label was removed using Pierce™ dye removal columns (ThermoFisher), following manufacturer specifications. The degree of labeling varied between 17 and 25%. This was calculated using the absorption spectra of each sample, using extinction coefficients of ε = 49450 M^{-1} cm^{-1} for the mutant StnI-T43C at 280 nm, ε = 9.0 x 10^4 M^{-1} cm^{-1} at 500 nm for ATTO-488, and ε = 1.2 x 10^5 M^{-1} cm^{-1} at 542 nm for ATTO-542. Corrections for label contributions at 280 nm were made using the corresponding correction factors provided by the manufacturer, which are 0.09 and 0.08 for ATTO-488 and ATTO-542, respectively. These factors represent the fraction of the absorbance of the label at 280 nm relative to their absorbance at the maximum. Protein mixtures assayed were

made by a combination of aliquots of WT (StnI and StnII, as indicated) and labeled StnI-T43C (with donor or acceptor) stocks. Fractional amounts were calculated according to the corresponding fractional labeling and concentration of the stocks. StnI-WT was added last, if needed, to adjust the overall fraction of labeling of the final mixtures. StnI-WT and StnI-T43C have been considered to be equal in terms of activity and structure, as evidenced by their structural and functional characterization by circular dichroism and hemolysis rates, respectively (Figure A2).

A model was constructed to calculate the FRET efficiencies for each possible stoichiometry in a way that was dependent on the fraction of acceptor-labelled toxin in the sample, keeping the fraction of donor constant. Using single-point mutants allowed the assumption that the fluorophores were distributed as the vertices of regular polygons. Distance from the center of each protein to the center of the polygon is

$$r_c = \frac{r_{mm}}{2\sin\left(\frac{\pi}{N}\right)}, \qquad \textit{Eq. 6}$$

where r_c is the radius of the polygon, r_{mm} is the distance between fluorophores on adjacent subunits, and N is the number of subunits per pore. The value used for r_{mm} was 29.0 Å since that was the measured diameter of a sticholysin subunit (see below, section 4.2.3.9). However, r_c cannot be used directly. Instead, the offset of the fluorophore relative to the center of the protein has to be taken into account. The distance to the center of the polygon to the fluorophore is then

$$r_{cf} = \sqrt{\left(r_c + r_f\cos(\omega)\right)^2 + \left(r_f\sin(\omega)\right)^2}, \qquad \textit{Eq. 7}$$

where r_f is the distance from the mass center of the protein to the labelled position as observed from a top view (distance in the z axis is ignored), and ω is the angle between the line that joints them and the prolongation of the line that unites the center of the monomer and the center of the oligomer. r_f and ω were 10 Å and 66 º, respectively, based on the position of the residue Thr43 on the available structure of StnI (PDB ID: 2KS4).

Once r_{cf} is known, the distance between any two subunits can be calculated using the following equation:

$$r_{ij} = 2r_{cf}\sin\left(\frac{\pi(i-j)}{N}\right), \qquad \textit{Eq. 8}$$

where *i* and *j* are the indices of the subunits of interest. Usually, it is easiest to assume $j = 1$, as will be done onwards (subscript *j* is thus omitted), so that Eq. 8 yields the distance between the selected (number 1) and the i^{th} subunit. The obtained values for the distances were then used to calculate the corresponding rates of energy transfer according to

$$k_T(r_i) = \frac{1}{\tau_D}\left(\frac{R_0}{r_i}\right)^6, \qquad \textit{Eq. 9}$$

where τ_D is the lifetime of the donor. In our case, ATTO-488 acted as donor. Its fluorescence lifetime was measured to be 4.09 ± 0.05 ns, in good agreement with the value provided by the manufacturer (4.1 ns).

Next, to have the highest precision, all possible arrangements of all possible combinations of unlabeled and donor- and acceptor-labeled subunits were calculated for each of the stoichiometries considered, assuming that monomer associations were random and unbiased by the labeling, using a Python program made by the author (attached as Appendix 4 to this thesis; the program also performs all other calculations indicated here except for the calculation of the RMSD of the experimental values when compared to the predictions). The arrangements of the subunits were made so that possible redundancies due to rotational symmetry were avoided. In all cases, it must be maintained that $N_D+N_A+N_U = N$, that is, the sum of unlabeled (N_U) and donor- (N_D) and acceptor-labeled (N_A) subunits must equal the total number of subunits.

The expected FRET efficiency was then calculated for each of the possible arrangements, using the additive property of rates [200], as

$$E_{Nqv} = \frac{\sum_{i=2}^{N} k_T(r_i)}{\frac{1}{\tau_D} + \sum_{i=2}^{N} k_T(r_i)}, \qquad \textit{Eq. 10}$$

where E_{Nqv} denotes that that is the FRET efficiency for a stoichiometry of *N* subunits (for example, $N = 8$), a combination *q* of unlabeled and donor- and acceptor-labeled subunits (for example, $N_D = 1$, $N_A = 3$, and $N_U = 4$), in a particular arrangement *v*. For each arrangement, *E* will depend on the order of the subunits. However, since we assumed that monomer associations were random and unaffected by the labeling, the observed FRET efficiency for each combination *q* will be the average of the *E* values for all the possible arrangements since it is assumed that they are all equally likely within each combination.

The final FRET efficiency to be observed would then depend on the fraction of toxins labeled with acceptor or donor in the sample (f_A and f_D, respectively). These

fractions determine which combinations are more likely to happen. In this case, the respective fractions of the labeled and unlabeled subunits must sum to one, that is, $f_A+f_D+f_U = 1$. The probability of each combination, including all its possible arrangements, is then calculated as

$$P(N_D, N_A, N_U, f_D, f_A, f_U) = \frac{(N-1)!}{(N_D-1)!\,N_A!\,N_U!} f_D^{N_D-1} f_A^{N_A} f_U^{N_U}, \qquad \textit{Eq. 11}$$

which is a version of the trinomial distribution adapted to rule out redundancies due to rotational symmetries. The sum of all probabilities calculated in this manner must sum to one. This probability is used to weight the energy transfer efficiencies of each combination so that the final result yields the expected FRET efficiency for a given stoichiometry and fraction of labeling.

A comparison of the experimental data with the model using root minimum squared deviations (RMSD) allowed the estimation of the stoichiometry of the pores of actinoporins. The errors on the measurements were used to weight the importance of each experimental value so that those with the smallest error were more significant to the final RMSD value. FRET efficiencies were measured in a large L/P molar ratio to avoid energy transfer between different pore complexes. The estimation of the right L/P ratio was done as $r_{av} = \sqrt{1/\sigma}/2$, where r_{av} is the average distance between oligomers, and σ is the surface density of the complexes [202]. Lipid contributions were measured separately and subtracted to avoid scattering contributions to the final fluorescence signal. Accordingly, assuming that the stoichiometry was eight, the average separation between complexes would be ~$3R_0$. Even if the stoichiometry was equal to four, the average separation would be ~$2R_0$, at which E is < 2%. Ideal L/P molar ratios, which would be even larger, could not be used due to experimental limitations, namely, light scattering by LUVs, lack of availability of materials, and instrumental sensitivity.

4.2.3.8. Quenching of NBD-labeled lipids

The quenching of NBD-labeled lipids assay is also termed the equilibrium pore assay. LUVs containing 1 mol% of NBD-POPE were employed. A freshly prepared solution of 0.6 M sodium dithionite in 1.0 M sodium phosphate buffer, at pH 10, was used to quench NBD emission. The excitation wavelength was 470 nm. Fluorescence emission was recorded at 520 nm. Dithionite was added to a final concentration of 55 mM. LUVs were disintegrated using Triton X-100. For further details, please see paper III and ref. [203].

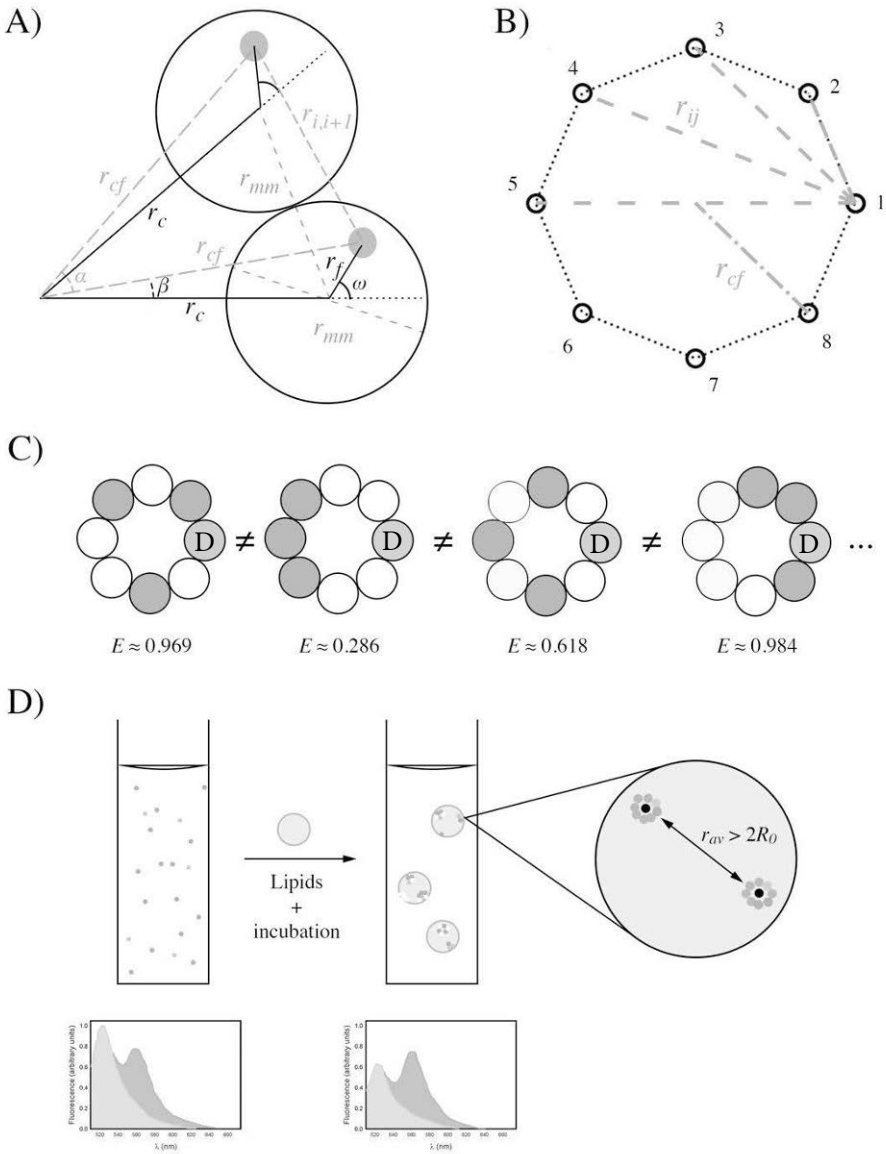

Figure 10. A) *Representation of the geometrical arrangement of two adjacent labeled proteins in a given* n*-mer (only two subunits are shown). Fluorophores are depicted as solid gray circles. Parameters shown are those in Eqs. 6 to 8. The value of* r_{mm}*, the distance between the centers of two adjacent subunits, is the same as the diameter of one subunit. This rule cannot be applied to the position of the fluorophores since they are not at the center of the protein (given a top-down projection). Their offset,* r_j*, by an angle* ω*, has to be taken into account. Consequently,* $r_{mm} \neq r_{i,i+1}$*. This is solved by using Eq. 7, which enables the calculation of* r_{cf}*, and with that* $r_{i,j}$*. Angle* α *has a value of* $2\pi/N$ *radians,* N *being the number of subunits in the oligomer. Angle* β *represents the offset of* r_{cf} *relative to* r_c*, and is a function of* r_c*,* r_f*, and* ω*. It is a consequence of this that* r_{mm} *and* $r_{i,i+1}$ *are not parallel to one another. This scheme is valid for any* n*-mer.* **B)** *Representation of an exemplary oligomer, an octamer. Circles represent the fluorophores in oligomerizing proteins (omitted)(cont.)*

4.2.3.9. Time-resolved measurements

Lifetime decays of fluorescence were recorded using suitable excitation LED-lasers (Pico-Quant, Berlin, Germany) and cut-off and bandpass filters, according to the photophysical characteristics of the fluorophores used. If lifetime decays were to be studied directly, these were recorded in the absence of polarizers until the channel with the maximum counts reached 10000 counts. If anisotropy decays were to be obtained, the corresponding lifetime decays were recorded for 200 seconds using polarizers. If needed, neutral density filters were used to attenuate the excitation intensity, to avoid artificial shortening of the lifetime due to artifacts caused by excessive input signal. The instrument response function (IRF) was recorded in the absence of colored filters using buffer up to 10,000 counts. For measurements with ATTO-488, a 457 ± 15 nm pulsed diode laser was used for excitation. Emission was collected though a long-pass filter (> 480 nm). If Trp fluorescent decays were recorded, a 297 ± 10 nm pulsed diode laser was used. Emission was collected with a long-pass filter (> 350 nm).

The decays were analyzed using the FluoFit Pro software from PicoQuant. In the case of lifetime decays, the multiple exponential model was used for fitting. Fluorescence anisotropy decays were fitted using a sum of discrete exponential terms. In both cases, the number of exponential components used was the smallest required to obtain a satisfactory fit as judged from the fitting parameters, the trace of residuals, and the autocorrelation plot. Errors in the values of the obtained parameters were obtained performing bootstrap analysis. To simplify, if the upper and lower error values obtained were approximately symmetrical relative to the value of the parameter, they were averaged so that the final value could be indicated as value ± average of errors.

(cont.) The parameter $r_{i,j}$ *is presented as dashed lines, some of which are omitted for clarity.* **C)** *Following the example in B) of eight subunits, we can assume* $N_D = 1$ *(light grey, with a "D"),* $N_A = 3$ *(dark gray), and* $N_U = 4$ *(white), we have that those can assemble into 35 possible arrangements (discarding those that differ only by circular symmetries). Four of those possible arrangements are shown in the figure. In the model, the assumption is made that the probability of those subunits (*$N_D = 1$*,* $N_A = 3$*, and* $N_U = 4$*) assembling into any of the 35 possible arrangements is the same. The FRET that a donor experiences from being at each arrangement, however, is different (see figure), hence the need to average them. Then, those averages need to be weighted since the probability of an assembly as those considered (regardless of the arrangement) is different from that of those with a different composition (say,* $N_D = 1$*,* $N_A = 1$*, and* $N_U = 6$*). These probabilities depend on the fractional population of donor- and acceptor-labeled proteins in the sample.* **D)** *Scheme of the experimental design. Non-labeled toxins, together with donor- and acceptor-labeled toxins, are placed in a cuvette, and the emission is registered (light gray for donor, darker gray for acceptors). After that, lipids are added. The sample is left for a few minutes to ensure that binding is complete. After that, emission is registered again, revealing the FRET from a diminished donor emission. The L/P ratio is such that the average distance,* r_{av}*, between oligomers is, at least, larger than* $2R_0$*.*

Molecular diameters were calculated from the correlation times obtained from the time-resolved anisotropy decays using the following equation:

$$\emptyset(\text{Å}) = 20\sqrt[3]{\frac{\theta RT}{\eta N_A} 10^{27} \frac{3}{4\pi}}, \qquad \textit{Eq. 12}$$

which derives from the Perrin equation [200], and then was modified to yield the molecular diameter directly in Å. In the equation, θ is the correlation time of the rotating unit in s; R is the ideal gas constant, with a value of 8.314 m^3 Pa mol^{-1} K^{-1}; T is the temperature in K; η is the viscosity of the solvent, used as 0.94 x 10^{-3} Pa s; and N_A is Avogadro's constant. The numeric constants that appear in the equation transform the values from m to nm and then to Å and from radius to diameter. The cubic root and the 3/(4π) factor transform the volume of the molecule into its radius, assuming its overall shape is that of a sphere, as expected for molecules that display a single correlation time.

4.2.4. Molecular Adsorption from Surface Plasmon Resonance (SPR)

SPR experiments were conducted on a BioNavis SPR Navi 200 instrument (BioNavis Ltd. Tampere, Finland). Gold chips were activated with *N*-hydroxysuccinimide and *N*-ethyl-*N*'-(dimethylaminopropyl)-carbodiimide and then coated with a layer of carboxymethylated dextran, competent for capturing LUVs of the appropriate composition. All solutions applied to the instrument were previously filtered through 0.2 μM membrane filters and degassed using bath sonication. Protein solutions, which cannot be sonicated, were degassed by centrifugation. The flow rate of the buffer was 5 μL/min. The chip surface was first washed with two injections of 10 mM 3-[(3-cholamidopropyl)-dimethylammonio]-1-propanesulfonate (CHAPS). LUVs were then applied to the surface at 0.5 mM lipid concentration with a 10-minute injection. The excess was removed by a 50 mM NaOH injection (2 min). A 2-minute injection of bovine serum albumin at 0.1 mg/mL was used to confirm total chip coverage with LUVs. The selected toxin was then applied at 4.0 μM for 10 minutes. The buffer was then applied to induce protein dissociation for 2 minutes. The chip was regenerated with CHAPS. The assay was performed at 25 °C.

Association and dissociation constants could not be calculated since sticholysins could not be substantially removed from the LUVs. Instead, the L/P molar ratio of the chip-bound LUV-protein complexes could be calculated based on the ng/cm^2 values of the sensograms once they reached a steady signal, given that the M_w of the proteins and the average values of the lipid mixtures are known.

4.2.5. Isothermal Titration Calorimetry (ITC)

The interaction of the toxins with LUVs was studied by ITC using a VP-ITC calorimeter (Malvern MicroCal, Worcestershire, U.K.). Briefly, 1.4 mL protein solutions, at concentrations between 0.7 and 4.0 μM, were titrated with 20 μL injections of lipid suspensions at concentrations ranging between 0.5 and 2.0 mM. The temperature was kept constant at 25 °C. The buffer employed consisted of 10 mM TRIS, 100 mM NaCl, and 1 mM EDTA at pH 7.4. The thermodynamic parameters of the interaction were obtained from data analysis in Origin using the "one set of identical sites" model, which is applicable to situations such as the one at hand, in which a protein binds the membrane. The situation is considered to be a protein binding a "binding-site" at the membrane, each of these consisting of n lipids [107, 208-210]. In all cases, the parameter c, which is defined as $K_b[P]_{cell}$, had values between 1 and 1,000, a range permitting the correct calculation of the value of K_b [107, 210].

5. RESULTS

5.1. Effect of membrane thickness on sticholysin activity

Results from publication I

The activity of sticholysins, and actinoporins in general, has been characterized by a wide variety of membranes with varying compositions and physicochemical properties [18, 21-25, 40, 42, 44, 72, 102, 120, 123, 150, 153]. However, the effect of membrane thickness on the activity of these toxins had not previously been studied with any actinoporin.

For this first study, a series of PC species was used. Each PC had acyl chains with different lengths, from 14 to 22 carbon atoms per chain, in intervals of two. In all cases, both acyl chains were equal and presented a double bond to *a priori* ensure that all membranes used were fluid at the experimental temperature of 25 °C. The position of the double bond was Δ^9, except for di-20:1-PC and di-22:1-PC, in which it was Δ^{11} and Δ^{13}, respectively. 14:0-SM was used instead of PSM, eSM, or brain-SM, as it has a shorter acyl chain than other SMs, displaying a smaller tendency to form ordered domains at the selected experimental temperature. Finally, Chol was included to study its influence in the systems. The lipid mixtures that StnI and StnII were assayed against were made of di-X:1-PC:14:0-SM:Chol in a molar ratio of 4:1:0 (no Chol) or 4:1:0.5.

5.1.1. Bilayer characterization

To rule out the presence of gel phases in any of the lipid mixtures, temperature-dependent DPH anisotropy measurements were performed. The plot of anisotropy as a function of temperature showed a smooth curvature in all cases, indicating that no phase transition occurred in the assayed temperature interval (Figure 11). A plot of the anisotropy values at 25 °C as a function of acyl chain showed that, in the absence of Chol, the membrane order varied linearly (inset in Figure 11). Chol slightly increased anisotropy values in all membrane systems. The increment was larger in the bilayers in which the PC had shorter acyl chains (insets in Figure 11).

5.1.2. Sticholysin-induced calcein release

Sticholysin-induced calcein release was measured for both StnI and StnII on all membrane systems. The initial rate of calcein release, that is, the slope of the release curves, was used as more representative parameter than the final release since the final release did not show any clear trend when plotted as a function of bilayer thickness.

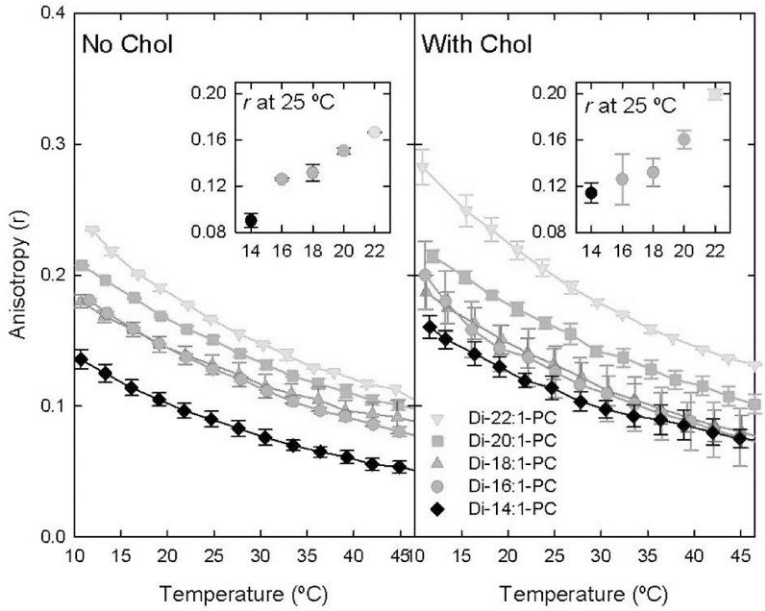

Figure 11. *Temperature-dependent DPH anisotropy measurements of membranes with compositions of di-X:1-PC:14:0-SM:Chol in molar ratios of 4:1:0 (left panel) and 4:1:0.5 (right panel). Each value is average ± standard error of the mean (SEM) of n = 2.* Insets*: DPH anisotropy values measured at 25 °C plotted as a function of the number of carbons in the acyl chains of the PC species present in each bilayer. Modified from publication I.*

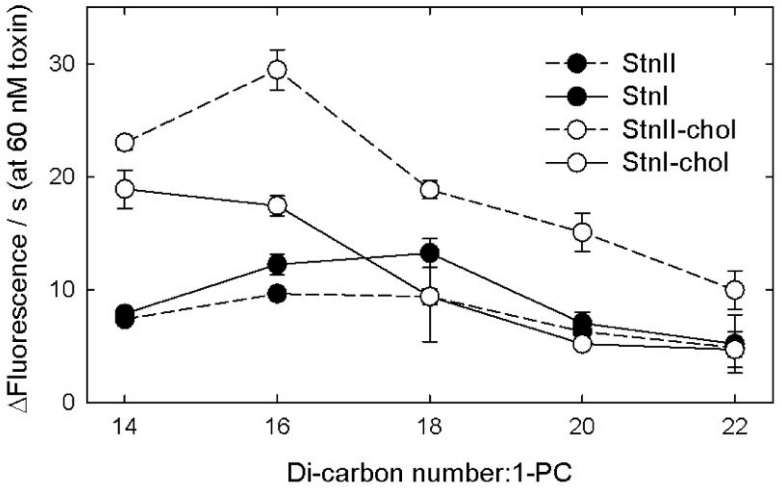

Figure 12. *Initial rates of calcein release measured for an L/P molar ratio of 42:1, i.e., 60 nM toxin. Lipid concentrations were 2.5 μM in all experiments. Composition of LUVs was di-X:1-PC:14:0-SM:Chol at molar ratios of 4:1:0 or 4:1:0.5. Values were calculated as normalized fluorescence units per second. Values are average ± SEM of n = 2. Modified from publication I.*

At an L/P molar ratio of 42/1, the results showed that, in the absence of Chol, both sticholysins were most active versus bilayers whose main component was di-16:1-PC or di-18:1-PC, with StnI being somewhat faster than StnII (Figure 12). A similar trend, with faster values, was observed in the presence of Chol. The trend was shifted toward bilayers with shorter acyl chains (Figure 12). In this case, and as previously observed [26], StnII was proven faster than StnI but, overall, induced calcein release was faster for both proteins as compared to the no-Chol situation.

5.1.3. Sticholysin association to LUVs as measured by SPR

Equal coverage of the chip by all membrane systems was ascertained comparing the theoretical mass ratio of the sticholysin-free vesicles with the ratio of the masses measured on the chip for the sticholysin-free LUVs, possible thanks to the SPR signal being in ng/cm^2 (see Table S1 of paper I). The results agreed with the expected values, confirming that all situations were comparable.

LUV-coated gold chips were then exposed to either sticholysin. The signal was registered as a function of time and the acyl chain length of the PC species and reached saturation after 100 to 200 seconds after toxin injection except for StnI and the bilayers containing di-14:1-PC, which were slightly delayed. The signal of the sensograms, given that the M_w of the proteins and the lipid mixtures were known, could be used to calculate the L/P molar ratios of the LUV-protein complexes at saturation. These data indicate that maximum binding was achieved to LUVs with the shortest acyl chain lipids (Figure 13). Binding was then reduced (higher L/P ratio) as the acyl chain increased. The behavior observed for both StnI and StnII was very similar. In either

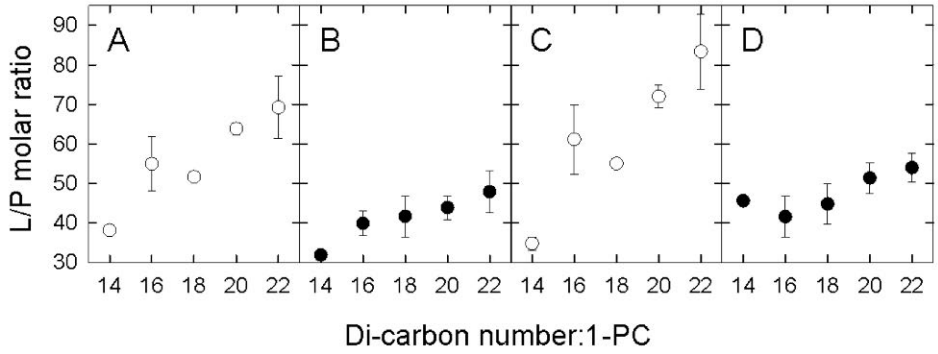

Figure 13. *SPR data for sticholysin binding to supported LUVs. The calculated L/P ratios are plotted as a function of the acyl chain length of the PC species making up each membrane. Values were calculated once SPR signal reached steady levels (500 s and 580 s after LUVs and toxin application). Panels* **A** *and* **B** *show StnI data. Panels* **C** *and* **D** *show StnII data. Filled symbols indicate lipid mixtures that include Chol. Since lipid concentration is constant, lower L/P ratio indicates higher binding. Modified from publication I.*

case Chol increased membrane binding (lower L/P ratio) and reduced the differences between all membranes, while maintaining the overall trend.

5.1.4. The interaction measured by ITC

The interaction of sticholysins with LUVs of varying bilayer thicknesses was also analyzed by means of ITC. Solutions of either sticholysin were titrated with a suspension of LUVs with selected composition until saturation was reached. The analysis of the thermograms allowed the determination of the values of the association constant (K_a), and the entropy (ΔS) and enthalpy (ΔH) of the interaction.

A plot of K_a values as a function of acyl chain length revealed that, in the absence of Chol, StnI presented a higher affinity toward membranes with di-14:1-PC, which was higher than for membranes with longer acyl chains (Figure 14). In fact, the heat change induced by the interaction of StnI with membranes composed of di-22:1-PC was beyond the detection limit of the instrument. StnII, however, presents higher affinity for membranes with intermediate thicknesses, between di-16:1-PC and di-22:1-PC, and similar to that of StnI in the same cases. The values of ΔH essentially followed the same trend as K_a. This was also true for ΔS except reversed, being less favorable when ΔH and K_a were more favorable.

The inclusion of Chol in the membranes drastically increased the affinity of the proteins toward the vesicles, especially in the case of StnI. The presence of Chol highlights the preference of both toxins for membranes with relative intermediate thicknesses, namely, those including di-18:1-PC and di-16:1-PC.

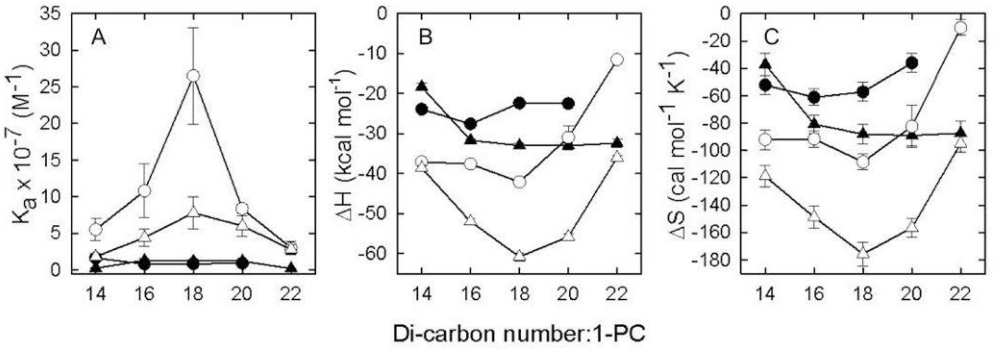

Figure 14. **Panel A**: *K_a values obtained from the ITC measurements.* **Panel B**: *enthalpy of the interaction between sticholysins and LUVs of varying bilayer thickness.* **Panel C**: *entropy of the same interactions. Open symbols depict experiments in absence of Chol. Circles and triangles are for StnI and StnII, respectively. Values are average ± SEM of n = 3. Modified from publication I.*

5.2. The tripartite interaction of sticholysins, SM, and Chol

Results from publication II

The results of the previous study brought up some standing questions of the field. One such question was what the effect of Chol's presence in the membrane was on the activity of sticholysins.

A fluorescently labeled SM analog, pyr-SM, and a fluorescent analog of Chol, CTL, were used to address this issue. OCer, a ceramide species that is unable to induce gel phase due to its oleoyl acyl chain, was used to compare its effect to that of Chol, with which it shares both the tendency to interact with SM and a hydroxyl moiety for a head group. The inability of OCer to induce gel phase formation was essential since the gel phase is known to hinder sticholysin activity [23]. CTL was used in combination with 7-SLPC, a phase-selective quencher, to better appreciate the effect of StnII on the membrane distribution of sterols. Finally, a series of StnII Trp-to-Phe mutants, available from a previous study [198], allowed detailed Trp-CTL FRET studies, to investigate the distribution of CTL near membrane-bound StnII.

5.2.1. SM-SM acyl chain contacts in the presence of OCer, Chol, and StnII

Pyrene molecules can form excited-state dimers (abbreviated excimers) if two of them are properly oriented and within close range of each other during the lifetime of their excited state. Pyrene emission, which regularly displays three peaks, becomes unstructured and red-shifted when excimers are formed [200]. Thus, the labeling of lipid acyl chains with pyrene can be used to detect lipid clustering by measuring the relative emission of the monomer and excimer species of pyrene, that is, the E/M ratio [211-213].

SM is known to cluster in membranes in which POPC is present in equimolar amounts [214]. Consistent with that, the highest E/M ratio observed (3.45 ± 0.09) was in membranes composed of POPC:PSM:pyr-SM in a 5:3:2 molar ratio (Figure 15, open circles at P/L ratio = 0). The inclusion of OCer or Chol (final composition POPC:PSM:pyr-SM:X, 5:3:2:1 molar ratio, where X is OCer or Chol) resulted, in both cases, in a reduction of the E/M ratio to 2.78 ± 0.03 and 2.38 ± 0.12, respectively (Figure 15, solid triangles and circles at P/L ratio = 0). The reported reduction of the acyl chain contacts of SM is a clear indication that OCer, and Chol, are interspersed between SM molecules. For this reason, these two lipids will be referred to, hereafter, as *intercalators*.

The E/M ratio was monitored after the addition of different StnII amounts to each of the membrane systems. The final values, determined at equilibrium, showed that

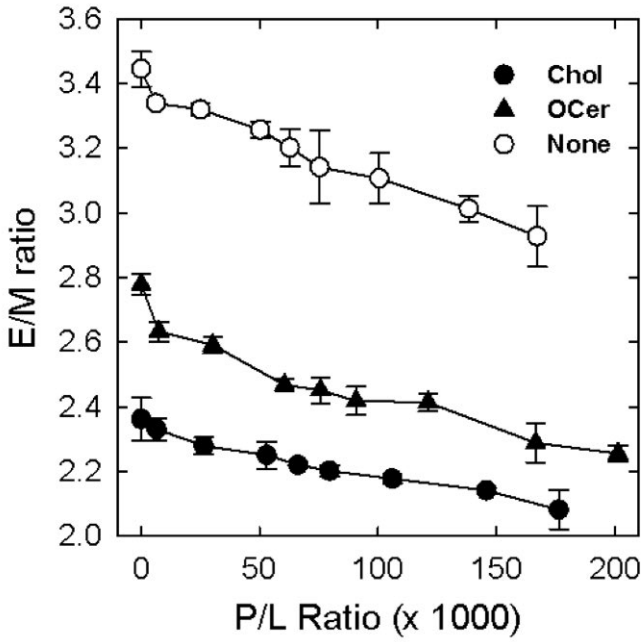

Figure 15. *Measured values of the E/M ratio of pyr-SM as a function of StnII concentration in bilayers composed of POPC:PSM:pyr-SM (5:3:2) (open circles), POPC:PSM:pyr-SM:Chol (5:3:2:1) (solid circles), or POPC:PSM:pyrSM:OCer (5:3:2:1) (solid triangles). Lipid concentration was ~1 μM (measured afterward). Stable E/M ratio values were determined 10 min following toxin addition. Each value is average ± SEM of n = 2-3. Adapted from publication II.*

StnII further reduced the acyl chain contacts between SM molecules. The slope was essentially independent of the presence or absence of OCer and Chol (Figure 15).

5.2.2. Dependence of StnII activity on Chol and OCer presence

Then, the effect of Chol and OCer on the activity of StnII was evaluated. For this, calcein release experiments were used. The assays were performed with DOPC:SM:Y (80:20:X molar ratio) LUVs, in which Y is OCer or Chol, and X ranged from 0 up to 30. The P/L molar ratio (equal to 0.09) was kept constant in all release experiments.

The results showed that Chol greatly increased the calcein release rates even when present in very low amounts (Figure 16). The effect was noticeable even at molar fractions of Chol below the limit required for the formation of Chol-induced domains [129]. Regarding OCer, inclusion was observed to enhance the activity of StnII. However, its effect was much less pronounced than that of Chol. In both cases, the effect of the intercalator lipid was stabilized at ~7 mol%. It is interesting to note that Chol presence at amounts over 20 mol%, at which L_d/S_o phase separation is induced by Chol itself, did not promote StnII activity any further.

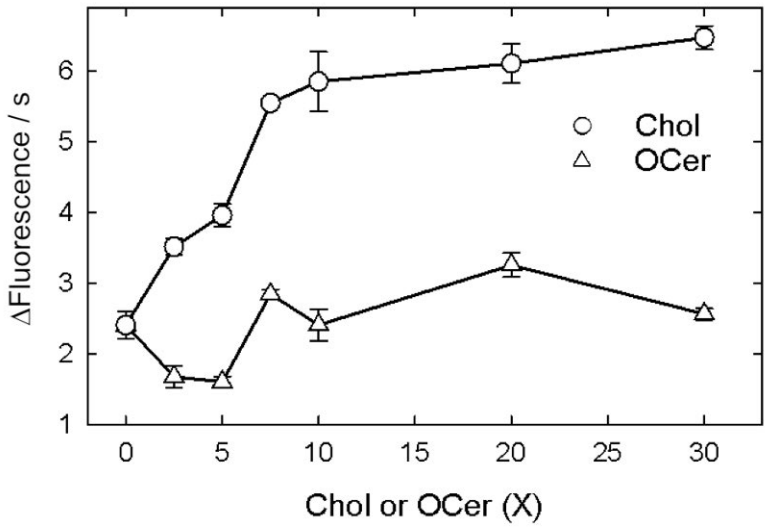

Figure 16. *Initial rates of StnII-induced calcein release from LUVs composed of DOPC:SM:Y, where Y is Chol or OCer, in a molar ratio of 80:20:X, plotted as a function of intercalator content (X). Values were normalized according to fluorescence corresponding to complete dye release, achieved by addition of Triton X-100. Values are average ± SEM (n = 3). Modified from publication II.*

5.2.3. Effect of StnII on the microenvironment of CTL

To study the effect of StnII on the microenvironment of Chol, CTL, a fluorescent analog of Chol, was used as a probe [130, 195, 206]. The relative location of the probe within the membrane could be estimated by means of a quencher, 7-SLPC, which is known to partition selectively in the L_d phase [215, 216]. Thus, the variation on the fluorescence signal of CTL allowed ascertaining whether StnII changed the distribution of CTL between the fluid, PC-rich regions of the membrane and the more ordered, SM-rich domains.

The signal was first compared between membranes that contained the quencher (F samples) and those in which it was replaced by POPC (F_0 samples). The F/F_0 value for the membranes with ~20 mol% PSM was 0.27, indicating a large exposure of CTL to the quencher. In the membranes with nearly 50 mol% PSM, the F/F_0 value was 0.78, consistent with a reduced exposure of CTL to the quencher. Since sterols are known to associate with SM [145], this effect could be expected upon the increment of PSM content in the bilayer. The addition of different amounts of StnII resulted in an increase in the F/F_0 value in a dose-dependent manner. The magnitude of the increments is shown in Figure 17. Though qualitatively the same, StnII-induced protection of CTL from the quencher was larger in membranes with lower SM mol%. This could be explained by CTL being already shielded from the quencher, in the PSM-rich phase, in the membranes with higher PSM content.

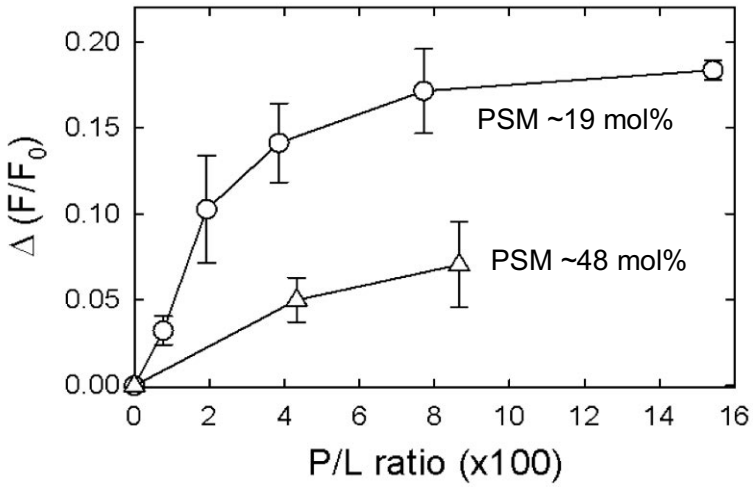

Figure 17. *Dose-dependent effect of StnII on the 7-SLPC-quenched quantum yield of CTL embedded in membranes composed of POPC:7-SLPC:PSM:CTL (50:30:20:5) (open circles) or POPC:7-SLPC:PSM:CTL (30:20:50:5) (open triangles). Bilayers in which 7-SLPC was replaced by POPC were used as reference (F_0 sample) in order to rule out direct effect of StnII. Each value is average ± SEM (n = 2). Modified from publication III.*

5.2.4. Membrane interaction of the Trp residues of StnII

To delve into a potential closeness of Chol and StnII, a FRET approach was chosen. This was possible thanks to the respective photophysical characteristics of CTL and Trp. Prior to the FRET assays, however, the effect of membrane binding on Trp emission from StnII was studied using the five Trp-to-Phe mutants available. Besides the WT protein, the proteins included the single mutant W43F, double mutants W43/110F and W43/114F, and triple and quadruple mutants W43/110/114F and W43/110/114/115F (Figure 18). The last mutant was particularly interesting because only a single Trp residue was left in its structure, W146.

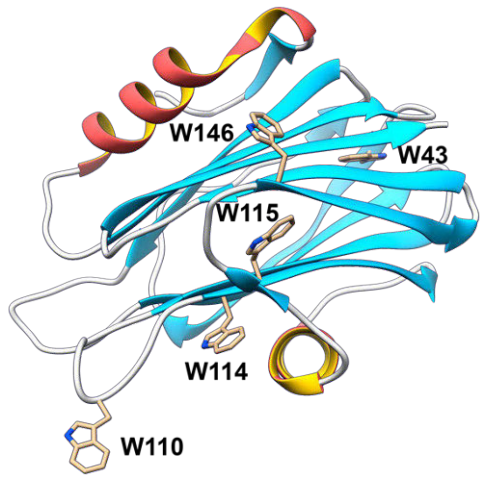

Figure 18. *The Trp residues on the structure of StnII. In the mutants available, all these residues, except for Trp146, have been replaced by Phe.*

All listed proteins were titrated with DOPC:eSM:Chol (1:1:1 molar ratio) LUVs. This composition was required to ensure membrane binding by some of the mutants [198]. In all cases, an increase in the quantum yield of Trp was observed (Figure 19).

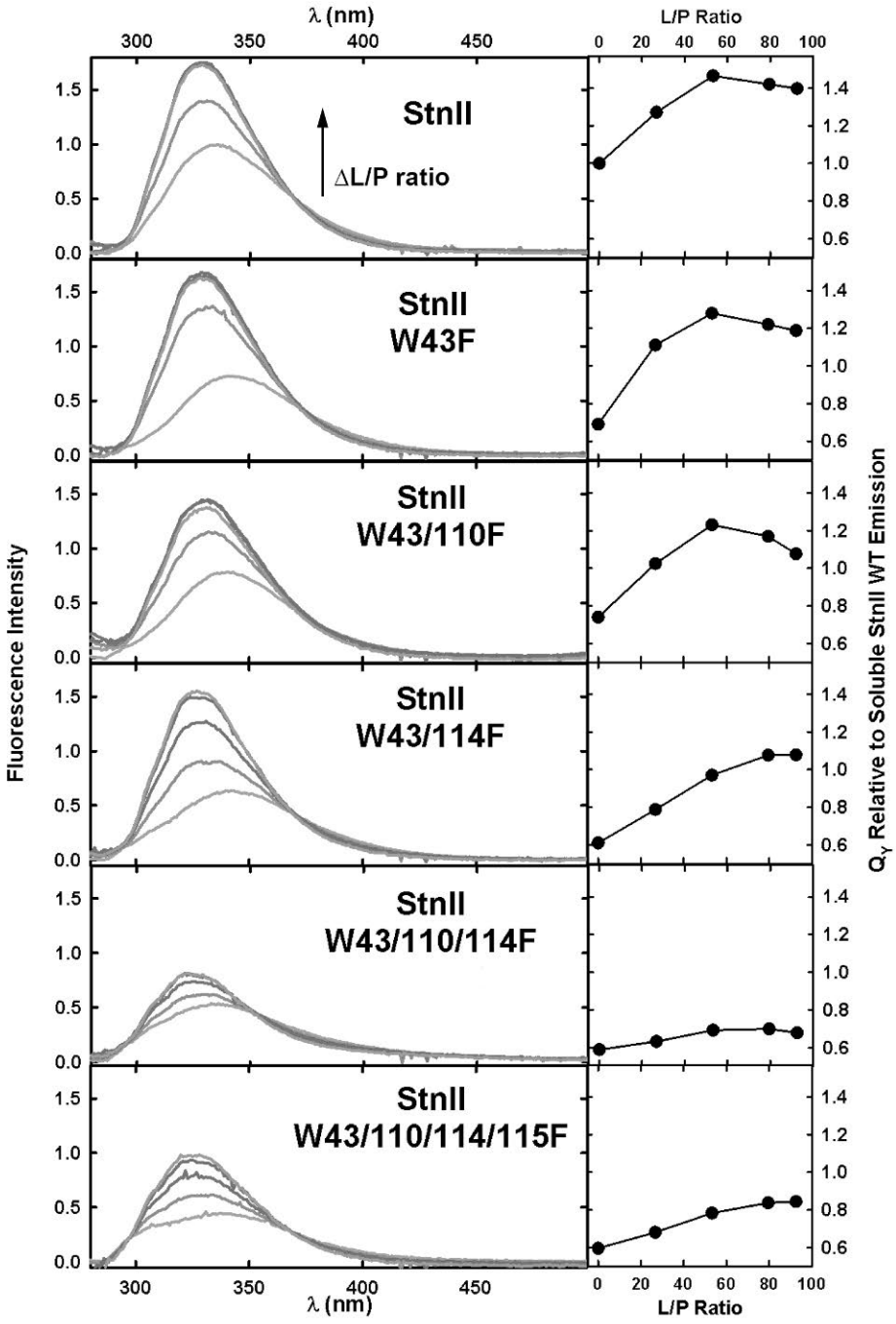

Figure 19. *Fluorescence spectra of StnII WT and its different Trp mutants as recorded while titrating with DOPC:eSM:Chol (1:1:1) LUVs. Arrow on top left panel indicates progression of the spectra as L/P ratio was increased. Panels on the right represent the change in the relative quantum yield of each protein as a function of the L/P ratio. Emission of soluble StnII WT as reference. Protein concentration was 200 nM. Adapted from publication II.*

Concomitant with the increase in quantum yield, spectral narrowing and blue-shifting were also observed. These effects are expected for Trp residues transitioning to an environment that is more hydrophobic. The results pointed W110 and W114 as the two residues whose environment is affected the most by membrane binding.

5.2.5. Location of CTL relative to Trp residues of StnII

A new titration was performed using StnII and the Trp-to-Phe mutants. This time, the vesicles were made of DOPC:eSM:sterol in a 1:1:1 molar ratio. Sterol content included CTL to a final amount of 5 mol%, with Chol being the remainder. To properly measure transfer efficiency, FRET should be quantified using quenched donor emission. However, these toxins all have several Trp residues, complicating the analysis. Hence, sensitized CTL emission was used instead since no further calculations were to be made using these data. This methodology provided a straightforward way of visualizing and comparing the contributions of each Trp residue to the total FRET observed for each toxin variant.

The results showed that the energy transfer from the Trp residues to CTL was taking place (Figure 20). As could be expected from the results above, the removal of

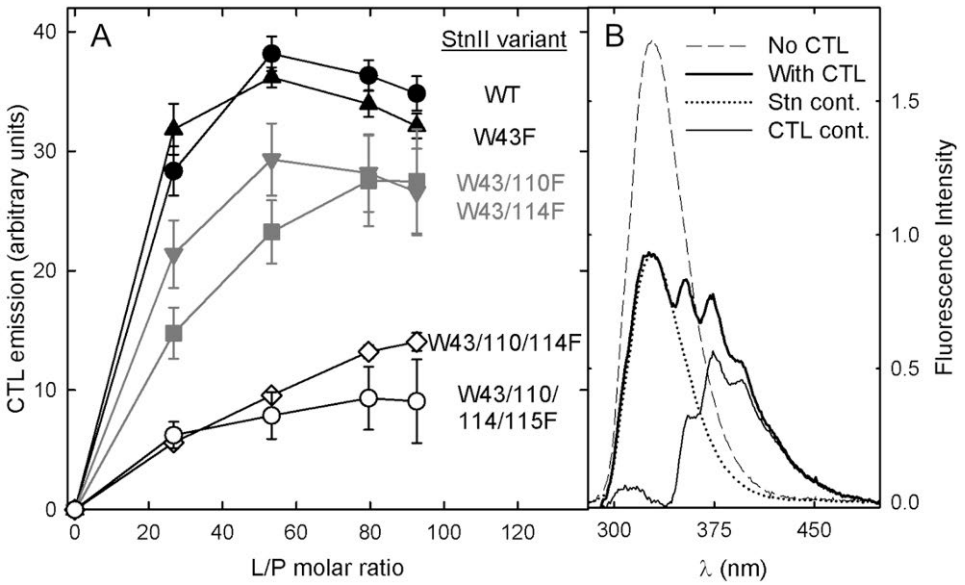

Figure 20. A*: Sensitized emission of CTL as measured when the indicated StnII variant was titrated using DOPC:eSM:Chol:CTL (33:33:28:5) LUVs. Each value is average ± SEM (n = 3).* **B***: Example (at 93 L/P molar ratio) showing how CTL emission was quantified. Protein emission in presence of CTL-lacking LUVs (dashed line) was fitted (dotted line) to total emission (thick solid line) using the range between 325 and 340 nm (only Trp emission). CTL emission (thin solid line) was obtained by subtraction of the corresponding spectra. CTL emission was quantified by numerical integration from 340 nm. The small bump centered at 320 nm corresponds to unquenched Tyr emission. Modified from publication II.*

W110 and W114 greatly diminished the observed transfer efficiency and, hence, sensitized CTL emission. This effect is not observed when other Trp residues are replaced by Phe. Therefore, CTL can be said to be closest to Trp residues 110 and 114 (Figure 18).

5.2.6. Chol distribution around StnII

Previous results indicated that CTL was in close proximity to W110 and W114. However, given that StnII and CTL were both in the membrane, it was possible that the observed proximity happened by chance thanks to both the orientation of StnII relative to the membrane and CTL being at high enough local concentrations.

To resolve whether CTL was randomly distributed around StnII, the FRET efficiency from Trp to CTL was measured using the single Trp mutant of StnII. This mutant, which has only W146, was titrated with vesicles with increasing amounts of acceptor (CTL) in the membrane. Then, the experimental FRET efficiencies, calculated using quench donor emission, were compared to those expected for a pair of fluorophores randomly distributed in two parallel diffusion planes, namely, the *cis* leaflet of the membrane, and the plane at which W146 is located (Figure 21). The expected values were calculated using a modified version of a previous approach [207, 217]. Experimental results were always above the calculated values for random distributions even with different limiting parameters (Figure 21), indicating that CTL is preferentially distributed near StnII when this protein is bound to the membrane.

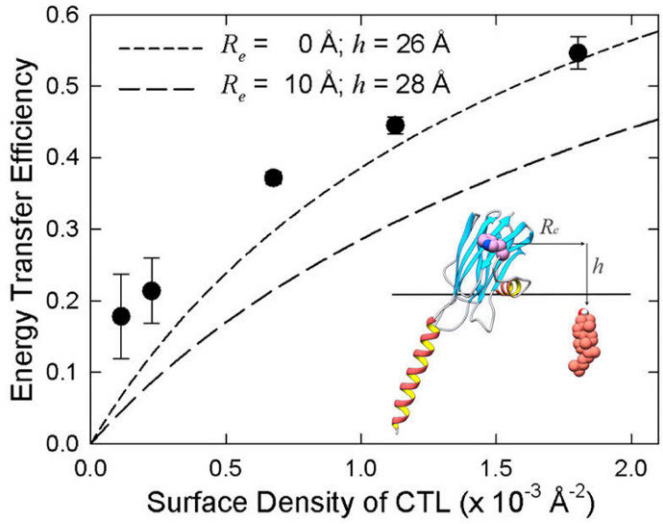

Figure 21. *Experimental Trp-to-CTL FRET efficiencies of the single Trp mutant of StnII (circles) as a function of CTL surface density, compared to the theoretically expected values for the indicated values of the parameters* R_e *and* h. *The scheme on the lower right of the figure depicts StnII, CTL and the model parameters* R_e *and* h. *Modified form publication II.*

5.3. Details of sticholysin-induced membrane permeability

Results from publication III

In the previous studies, the activity of sticholysins was evaluated based on their ability to induce the release of aqueous contents from vesicles of varied composition. In all cases, calcein was used as the probe. Always, the leakage trace reached a plateau before the complete release of the probe was reached, as shown by the maximum induced by Triton X-100. This brought up the following question: if actinoporins make holes in membranes, how was it possible that calcein stopped flowing to the outside of the vesicles?

To clarify this issue, a series of different assays were performed. These consisted in variations on the experiment of the release of aqueous contents. Some of the variations came from the literature, and some were developed in house. In the assays, a variety of probes were used. The probes were selected according to their charge and size in order to see how these two parameters affected sticholysin-induced permeability.

5.3.1. Calcein release

First, calcein release experiments were performed using StnII and vesicles composed of DOPC:eSM:Chol in a 1:1:1 molar ratio. These assays were used as the reference to which all later release experiments were compared. The addition of StnII to the LUVs of the aforementioned composition (2.5 μM) in a series of different P/L molar ratios yielded the results shown in Figure 22. In all cases, calcein release stabilized once it reached ~60% of the final possible release (Figure 22a), measured by applying Triton X-100. The LC_{50} value, calculated as the protein concentration required to induce 50% of the maximum possible protein-induced release, was 52 pM (Table 2).

The final release values can be reached relatively easy with a small concentration of protein, concealing otherwise differences that could otherwise be significant at those concentrations [26]. Thus, the initial rate of release, quantified as the slope of the leakage trace just after toxin addition to the cuvette was also measured (Figure 22b). The values obtained at 20 nM toxin, corresponding to a L/P molar ratio of 125 (a saturating concentration) were selected as representative from all experiments. In this case, a value of 0.061 ΔF units/s was obtained (Table 2).

5.3.2. Release of rhodamine 6G

Next, the release assay was performed by replacing calcein with R6G, while maintaining the lipid composition of the vesicles. The final release values plateaued at ~60%, as with calcein (Figure 22a). However, the LC_{50} was approximately six-fold

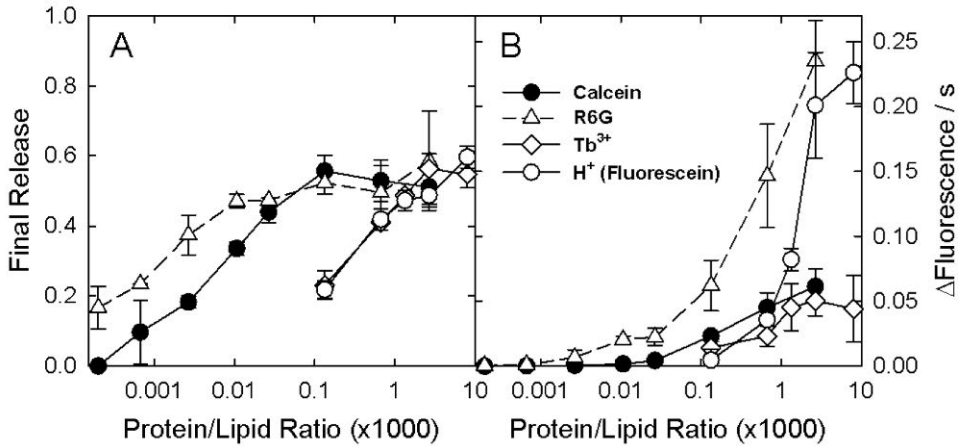

Figure 22. A: *Fraction of final release 5 min after toxin addition to dye-loaded LUVs composed of DOPC:SM/Chol (1:1:1) at different P/L molar ratios. Suitable detergents were added the samples to induce total release of the dye in order to register maximal fluorescence used to normalize each of the traces.* **B**: *Initial rates of dye release for the experiments in* A. *Ions used were calcein (solid circles), R6G (open triangles), Tb^{3+} (open diamonds), and H^+ (fluorescein (open circles). Values are average ± SEM of n = 2-3. Modified from publication III.*

Table 2. *Parameters obtained from each of the leakage assays.*

Assay	LC_{50} (nM)	Release rate at 20 nM (ΔF/s)	Saturation (% of release)
Calcein	0.052	0.061	53.2
R6G	0.009	0.235	53.5
Tb^{3+}	1.990	0.051	55.1
H^+ (fluorescein)	2.880	0.201	62.5

lower than when calcein was used (Table 2). Likewise, the rate at 125 L/P molar ratio was 0.235 ΔF units/s, faster than that observed when using calcein (Figure 22b and Table 2).

5.3.3. Release of cations (Tb^{3+} and H^+)

The permeability of StnII pores to small cations was evaluated using Tb^{3+} and H^+. In either case, and as in previous assays, the release never exceeded ~60% (Figure 22a). The measured LC_{50} values were 1.99 and 2.88 nM respectively (Table 2). The initial rate of release differed significantly between both approaches. For Tb^{3+}, the rate at 125 L/P molar ratio was slower than that observed for calcein (Table 2 and Figure 22). The leakage of H^+ was shown to be faster but only at high protein concentrations (Table 2 and Figure 22).

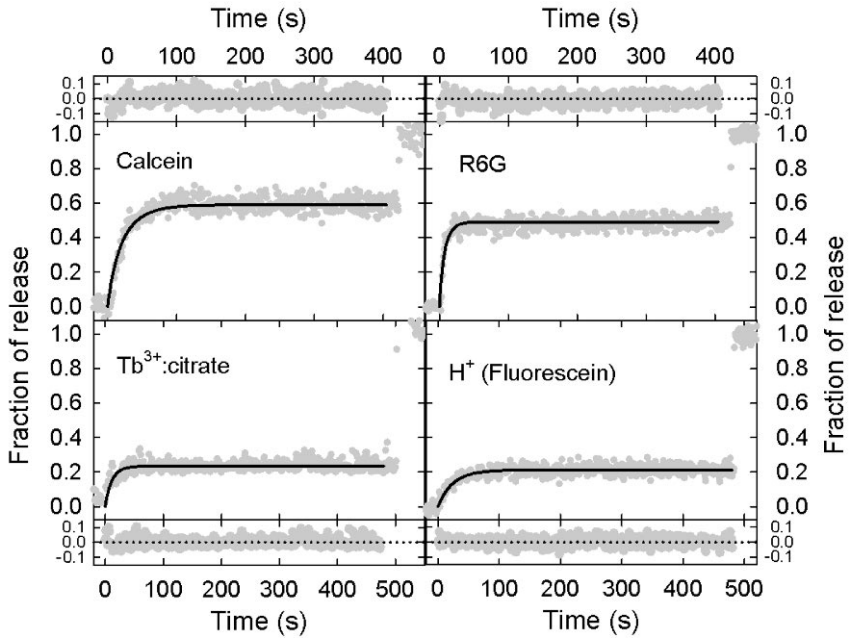

Figure 23. *Representative data from release experiments using calcein, R6G, Tb^{3+}, and H^+ (fluorescein), acquired using 1 nM StnII in all shown cases. Solid lines are fits of the perturbation model. Small panels show the residuals of each fit. Adapted from publication III.*

5.3.4. Agreement with kinetic models

The release traces form the above experiments were used to fit the perturbation model (see section 4.2.3.3) [205]. In all cases, the model provided very good fits (Figure 23), indicating agreement of the experimental results with the model's theoretical basis.

5.3.5. Equilibrium pore assay

In all previous assays, the probe was encapsulated in the LUVs and then freed by the action of StnII. Those experiments cannot differentiate between leakage induced by membrane perturbation and leakage through the stable pore lumen.

To reveal whether sticholysin pores were permeable once stabilized, LUVs made of DOPC:eSM:Chol (1:1:1 molar ratio) were prepared, including 1 mol% of POPE-NBD. NBD emission was quenched using sodium dithionite. The advantage of this assay is that dithionite can be applied to the sample *before* or *after* pore formation by StnII, that is, exposure of the LUVs to the toxin. Therefore, it allows the evaluation of dithionite's ability to pass through already-established pores.

The incubation of intact LUVs with dithionite resulted in a ~40% decrease in the observed NBD emission (Figure 24a), indicating that the employed vesicles were

impermeable to dithionite, at least at the time scale of these experiments. Triton X-100 was used to obtain the emission of fully exposed NBD, which should then be quenched completely, inducing a decrease in the fluorescence of the remaining 60%.

Once the LUVs were proven impermeable, dithionite was applied to LUVs that had been previously incubated at various StnII concentrations. This time, NBD's emission underwent a much more significant decrease (Figure 24b). The magnitude of the decrease was dependent of the concentration of toxin to which the LUVs had been exposed. The addition of Triton X-100 caused a modest reduction in NBD emission.

Finally, different amounts of StnII were added to the LUVs that had been exposed to dithionite (Figure 24c). NBD emission, which was already reduced by 40%, was further diminished by StnII addition in a dose-dependent manner.

Altogether, these results indicate that the stable pores of StnII are indeed open, and permeable, at least to dithionite. We observed that Triton X-100 distorted NBD emission. Although we were not able to correct the signal for that effect, we believe that the effect of Triton X-100 accounts for the deviation from the 50% quenching that should be observed due to the first dithionite addition. Nevertheless, this is not relevant to the conclusion obtained from these experiments since the larger decrease observed due to preincubation with StnII is sufficient to conclude that dithionite can pass through thermodynamically stable StnII pores.

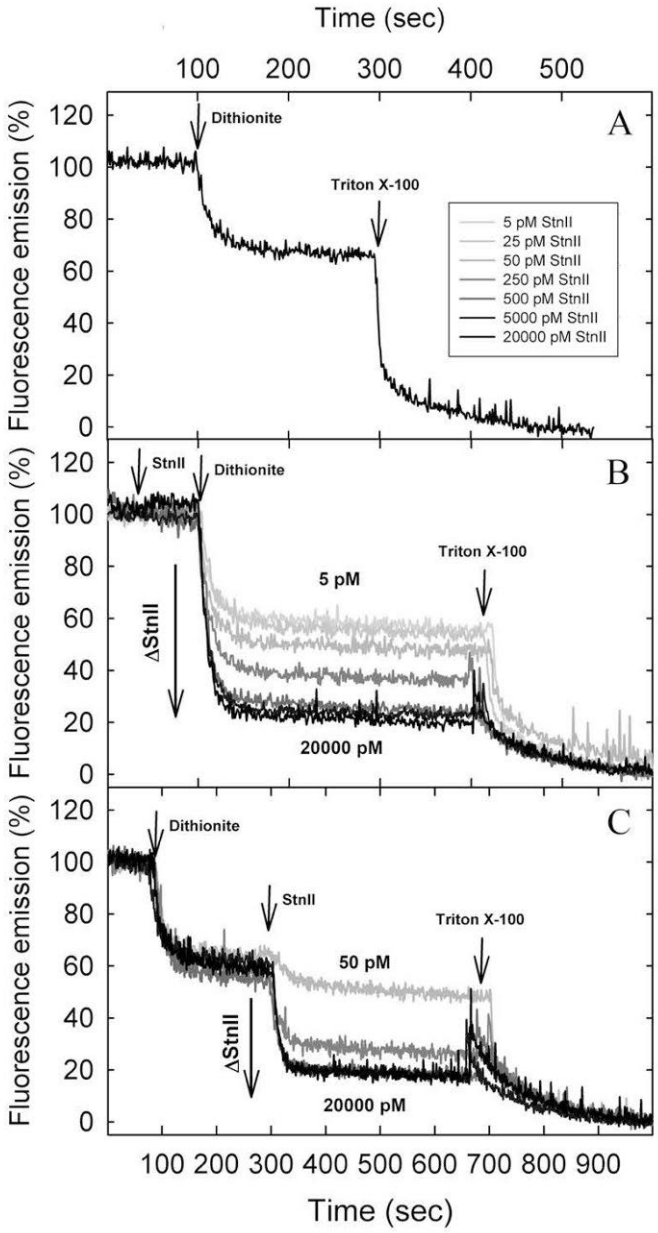

Figure 24. *Equilibrium pore assays. Sodium dithionite (final conc. 55 mM) was added to LUVs of DOPC:eSM:Chol (1:1:1) with 1 mol% POPE-NBD.* **A***: LUVs were first exposed to dithionite, then to Triton X-100 (final conc. 0.045% v/v) was applied to achieve complete vesicle disruption.* **B***: the procedure in* A *was repeated with LUVs that were preincubated with different amounts of StnII, which greatly increased LUVs permeability to dithionite.* **C***: StnII was added after dithionite addition to the sample. As in the previous experiments, LUVs were disintegrated with Triton X-100. Adapted from publication III.*

5.4. Oligomerization of sticholysins from Förster resonance energy transfer

Results from publication IV

The stoichiometry of the actinoporin pores has been long debated in the field. Several different structures of the final pore have been published so far [29, 34, 35, 189]. However, due to the difficulty of isolating the pore structure in a way that was suitable for analysis, such as X-ray crystallography or nuclear magnetic resonance, different methods, which involved non-native conditions, had to be used.

Our goal was to develop an approach that enabled us to determine the stoichiometry of these pores directly on model membranes with the least perturbation possible of the system. For this, a single Cys-mutant of StnI was produced. This mutant, which was essentially identical to StnI-WT from a structural and functional point of view (Figure A2), could be labeled at a specific position that was not expected to interfere either with protein-protein interactions or with membrane recognition and binding (Figure A3). This approach allowed the estimation of the stoichiometry of the complexes, while permitting us to delve into other details on the behavior of these toxins, such as the association in solution and the cooperativity of StnI with StnII.

5.4.1. Motions of sticholysins in solution and on membranes

StnI-T43C was first labeled with ATTO-488. The time-resolved anisotropy decays of the toxin as well as of the free label were recorded using solutions in which only 2% of the total sticholysin was labeled (Figure 25). For the free label, whose anisotropy rapidly decayed to zero, only a single, very short correlation time (0.2 ns) could be resolved. The toxin displayed two correlation times. The fast one was ~0.3 ns, very close to that of the free label, accounting for the segmental motions of the probe itself. The slower one was ~2.95 ns and corresponded to the rotational motions of the proteins within the solvent (Table 3). This correlation time could be used, with Eq. 12, to estimate the molecular diameter of sticholysins. The value obtained, 29.0 ± 1.3 Å, agreed with the molecular structures available, as evidenced when placing a sphere of that size at the mass center of those structures (not shown). The time-dependent anisotropy did not decay to zero, displaying a limiting anisotropy value of ~0.014.

Next, the same anisotropy decays were recorded in the presence of LUVs, composed of DOPC:eSM:Chol (1:1:1 molar ratio) and, separately, POPC:PSM (4:1 molar ratio). Energy transfer is a phenomenon that is known to reduce anisotropy [200, 202]. Hence, the fractional labeling of sticholysins was kept low, at 2% in

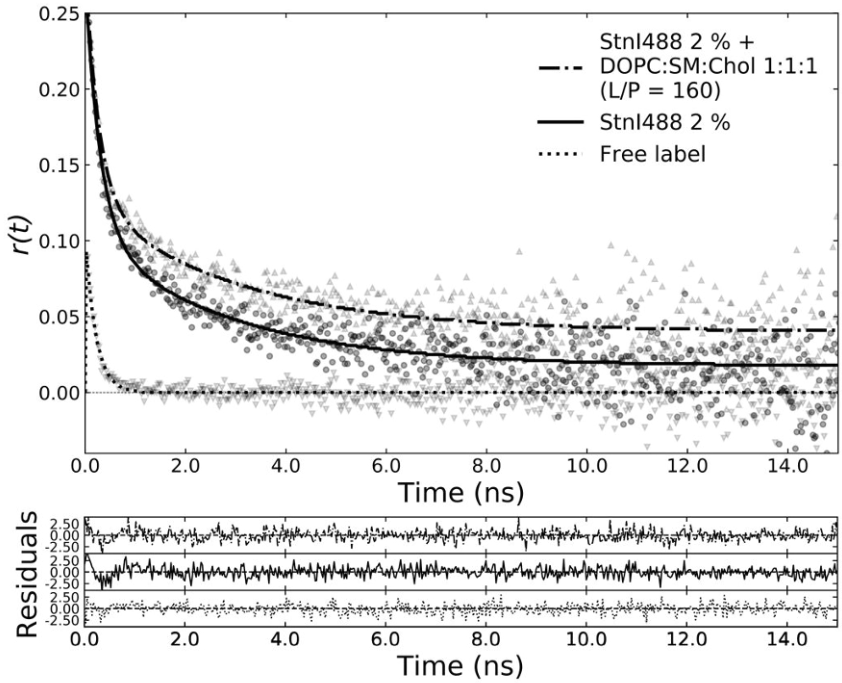

Figure 25. *Time-dependent anisotropy decays of StnI labeled with ATTO-488 free in solution (degree of labeling = 2%; solid line) or in presence of DOPC:eSM:Chol (1:1:1) membranes (L/P molar ratio = 160; dash-dot line). The decay of the free ATTO-488 label was also recorded (dotted line). Traces of residuals for each of the fits are shown below. The order of the graphs of the residuals is the same as that of the legend. Modified from publication IV.*

presence of Chol and 5% when it was absent, to minimize potential energy transfer between neighboring subunits in the pores. Not only that but the L/P molar ratio was also high, beyond saturation, so that energy transfer between the subunits of different pores was unlikely while also achieving maximum possible binding of the available toxin. The observed fast correlation time did not vary from the previously measured one, whereas the slow correlation time was slightly increased for StnI and reduced by ~0.6 ns for StnII. The limiting anisotropy was larger in both cases, with values of ~0.04, indicating a restricted mobility of the membrane-bound proteins (Table 3). This time, the correlation times could not be used to calculate molecular sizes due to the complex environment surrounding the toxins, and the unevenly restricted mobility of the complexes due to their very structure and the restrictions imposed by the membrane.

5.4.2. Oligomerization in solution

It has been shown that StnII is able to oligomerize in solution [184]. Hence, energy transfer could be expected to occur even in solution, at least to some extent, without the need for pore formation on membranes. As a first approach, steady-state

Table 3. *Parameters of the anisotropy decays of ATTO-488, StnI (degree of labeling = 2%) in absence and presence of lipids (DOPC:eSM:Chol 1:1:1 in L/P molar ratio = 160; POPC:PSM 4:1 in L/P molar ratio = 160). Indicated are the initial anisotropies (r_i) and correlation times (θ_i) of each component and the limiting anisotropy (r_∞). Values were obtained from fitting, errors from bootstrap analysis.*

	r_1	θ_1 (ns)	r_2	θ_2 (ns)	r_∞
ATTO-488	0.125 ± 0.005	0.228 ± 0.012	-	-	0.000 ± 0.0004
ATTO-488 + DOPC:eSM:Chol	0.135 ± 0.006	0.232 ± 0.012	-	-	0.001 ± 0.0004
StnI	0.200 ± 0.008	0.299 ± 0.030	0.089 ± 0.006	2.851 ± 0.530	0.014 ± 0.002
StnI + DOPC:eSM:Chol	0.195 ± 0.009	0.267 ± 0.034	0.088 ± 0.004	2.979 ± 0.587	0.040 ± 0.003
StnI + POPC:PSM	0.157 ± 0.007	0.224 ± 0.020	0.103 ± 0.005	2.273 ± 0.170	0.031 ± 0.002

anisotropy, which is affected by energy transfer, was measured. Anisotropy is expected to diminish as a consequence of energy transfer [202, 218]. Hence, the steady-state anisotropy of ATTO-488-labeled StnI in solution was measured at increasing degrees of labeling (DoL). The anisotropy appeared to decrease only slightly, not significantly, at high DoL values.

Thus, to increase the resolution, a sample of ATTO-488-labelled StnI-T43C (hereafter StnI-488 or donor) was titrated with ATTO-542-labelled StnI-T43C (hereafter StnI-542 or acceptor). The R_0 of this FRET pair is significantly larger than the distance over which the previous approach is effective (only at $r < 0.8R_0$ [218]). The titration was performed in the presence of WT StnI to properly control the relative amounts of donor and acceptor in the sample. The fraction of both the donor and the acceptor in the sample varied as a consequence of the titration process. The measured FRET efficiencies were plotted as a function of the acceptor fraction, which was deemed more representative (solid line in Figure 27). A small increase in the values of E was observed, indicating the presence of StnI oligomers in solution.

Incidentally, it has been shown that a minimal amount of StnII, just 1%, is able to significantly enhance the hemolytic activity of StnI, presumably by facilitating the membrane-binding step of the process of pore formation [95]. In such case, StnII could foreseeably oligomerize with StnI in solution. This could be revealed with the present FRET approach. The titration of StnI-488 with StnI-542 in the presence of WT StnII showed an increased FRET efficiency compared to the previous experiments in which WT StnI was used (dashed line in Figure 27).

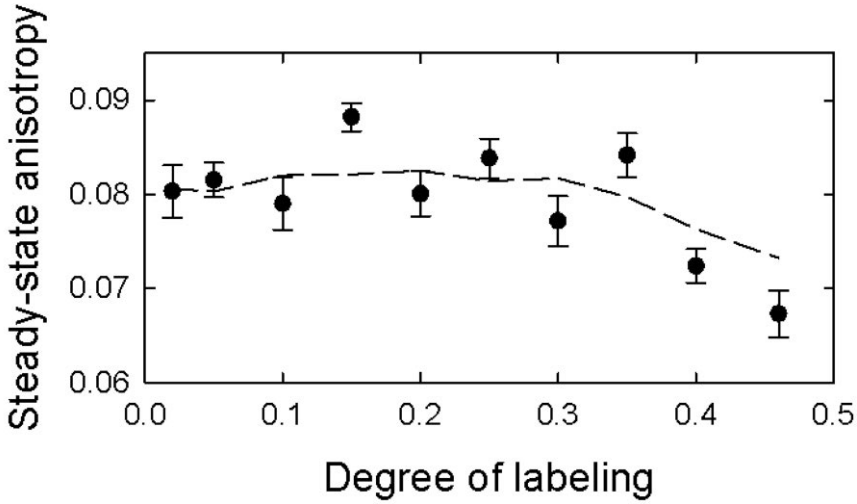

Figure 26. *Steady-state anisotropy dependence on the degree of labeling of StnI in solution. The dashed line is only a guide to the eye. Modified from publication IV.*

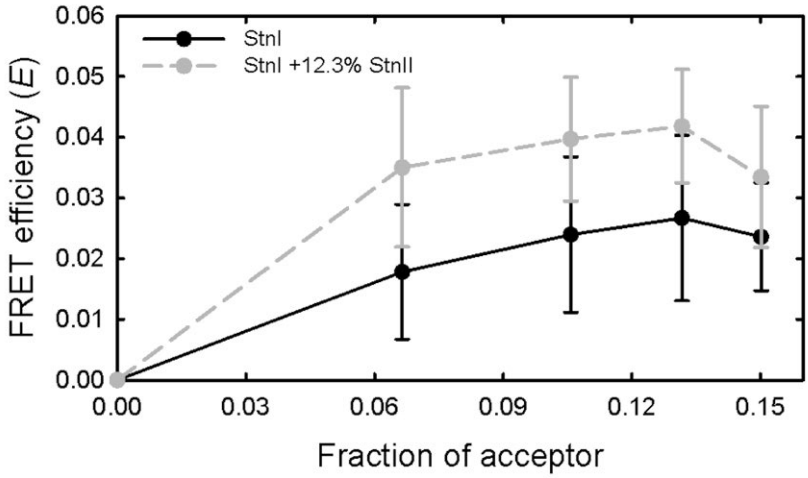

Figure 27. *FRET efficiencies observed for donor-labeled StnI with WT StnI (solid black trace) or with WT StnII (dashed gray trace) titrated with acceptor-labeled StnI to a final composition of 5% donor, 15% acceptor, and 12.3% of the corresponding WT sticholysin variant. Modified from publication IV.*

5.4.3. Stoichiometry of StnI on DOPC:eSM:Chol membranes

Energy transfer efficiency values were obtained from steady-state data using quenched donor emission from the deconvoluted sample emission.[2] Lipids were directly added to a 100 nM solution of StnI, with a fraction of 0.05 donor and the selected fraction of acceptor (up to 0.15), to a final L/P molar ratio of 160. The obtained *E* values were plotted as a function of the acceptor fraction in the sample and compared to the theoretical predictions (Figure 28, left panel). RMSD calculations showed that an octameric ensemble would be in best agreement with the observed signal obtained in the presence of DOPC:eSM:Chol (1:1:1 molar ratio) membranes (Figure 28, right panel). Nevertheless, this result should be taken cautiously due to the limited resolution of the model for large complexes. Based solely on this, it can be concluded that sticholysin pores are heptamers or larger structures.

5.4.4. Is the stoichiometry of StnI pores different in POPC:PSM 4:1?

The procedure in the previous section was repeated for StnI in combination with POPC:PSM (4:1 molar ratio) vesicles. The L/P molar ratio was increased to 320 this time, in spite of increased lipid-induced light-scattering, to ensure complete binding. This was necessary due to the smaller affinity of StnI for Chol-lacking membranes. Unexpectedly, the signal from StnI did not follow the trend expected from any of the theoretical predictions (Figure 29).

5.4.5. Inclusion of StnII does not affect stoichiometry

Once more, the procedure was repeated but this time including 12.3% of WT StnII in all samples to evaluate the effect the inclusion of StnII had on the stoichiometry of StnI pores. This was the result in both cases, when Chol and Chol-lacking membranes were used. The distribution of the RMSD values in the experiment including Chol closely resembles that observed for StnI alone (Figure 30). In the absence of Chol, the experimental FRET efficiency values also present the same trend as in the absence of StnII, again not following the predictions (Figure 31).

[2] This same procedure was also used in paper II. For more details, see Figure 20b and papers II and IV.

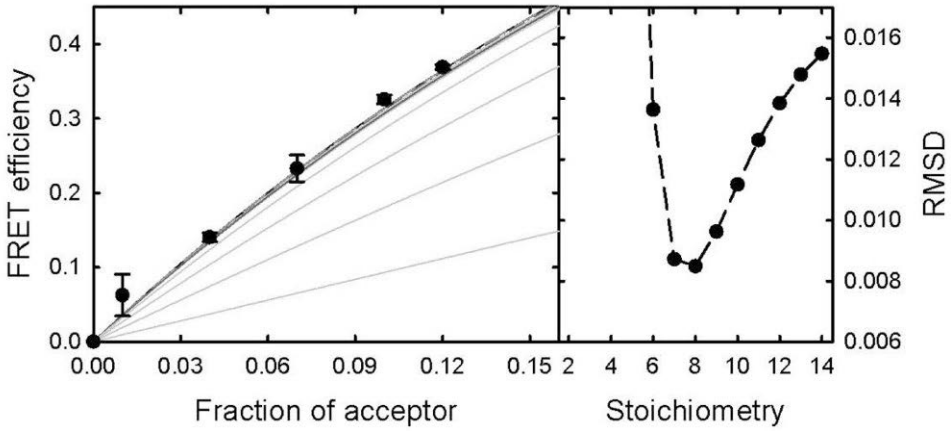

Figure 28. Left: *experimental FRET efficiency values (solid dots) using labeled StnI in combination with DOPC:eSM:Chol 1:1:1 molar ratio membranes plotted with the theoretical predictions made for stoichiometries from 2 to 10 (11 to 14 were removed for clarity). From bottom to top, predictions for 2, 3, 4, 5, and so on. Predictions from 6 on are hardly distinguishable at this scale. With the conditions considered, maximum FRET efficiency is reached for heptamers, being slowly reduced for higher values (see supplementary figure 2).* **Right**: *root mean squared distances (RMSD) obtained for the experimental values on the left compared relative to each of the predictions. Adapted from publication IV.*

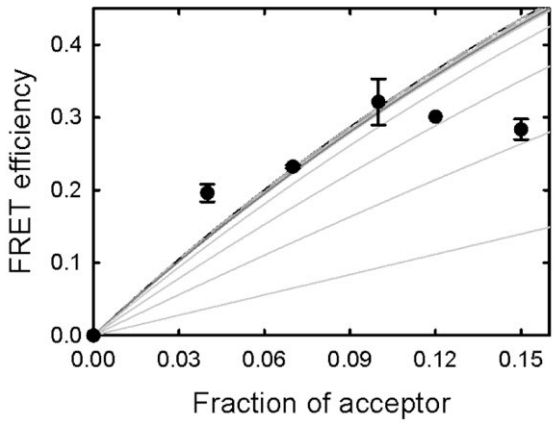

Figure 29. *FRET efficiency values observed for labeled StnI in combination with LUVs composed of POPC:PSM 4:1 molar ratio. Notice that experimental results do not agree with predictions as in the previous case. Adapted from publication IV.*

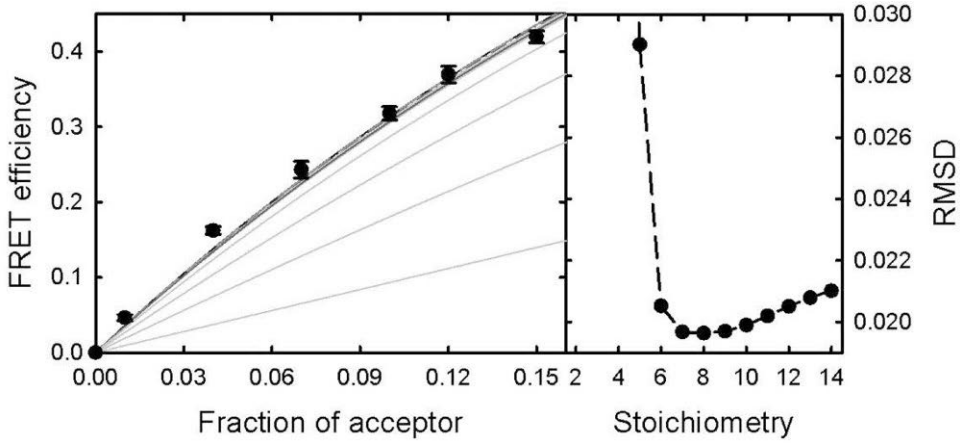

Figure 30. Left: *experimental FRET efficiency values (solid dots) obtained using labeled StnI with 12.3% StnII in combination with DOPC:eSM:Chol 1:1:1 molar ratio membranes plotted with the theoretical predictions as in Figure 28.* **Right**: *RMSD values for each of the predictions. In this case, the difference observed between the stoichiometries is reduced compared to the previous result in absence of StnII. Adapted from publication IV.*

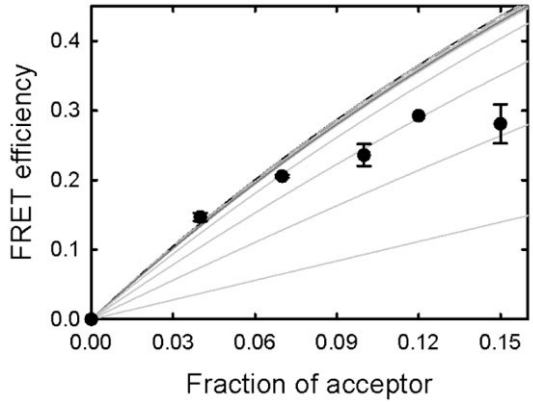

Figure 31. *FRET efficiency values observed for labeled StnI in presence of 12.3% StnII in combination with POPC:PSM 4:1 molar ratio LUVs. Again, the experimental values do not follow the expected trends. Adapted from publication IV.*

5.4.6. Pores of sticholysins are not remodeled once formed

Electrophysiological measurements have suggested that sticholysins pores might be unstable given the level of conductance noise they yield compared to those observed for β-pore-forming toxins [219]. This noisiness could be just a consequence of the thermal oscillations of the system given the characteristics of these pores, whose lumen would be lined by both the N-terminal α-helices of sticholysins and lipids. However, it has also been proposed that, once formed, the pores would be under continuous remodeling, with monomers transiting from one complex to another.

To test this idea, StnI or StnII, to a final increment of 57 nM, was added to 100 nM StnI already including 5% donor and 15% acceptor preincubated with lipids. The initial L/P molar ration was 240. This way, the final L/P molar ratio was 160, comparable to the results of the aforementioned assays. In both cases, the observed FRET efficiency was maintained after the addition of the extra amount of protein, regardless of it being StnI or StnII (Figure 32). These results indicate that already-formed pores could not be affected by the toxin supplied afterward.

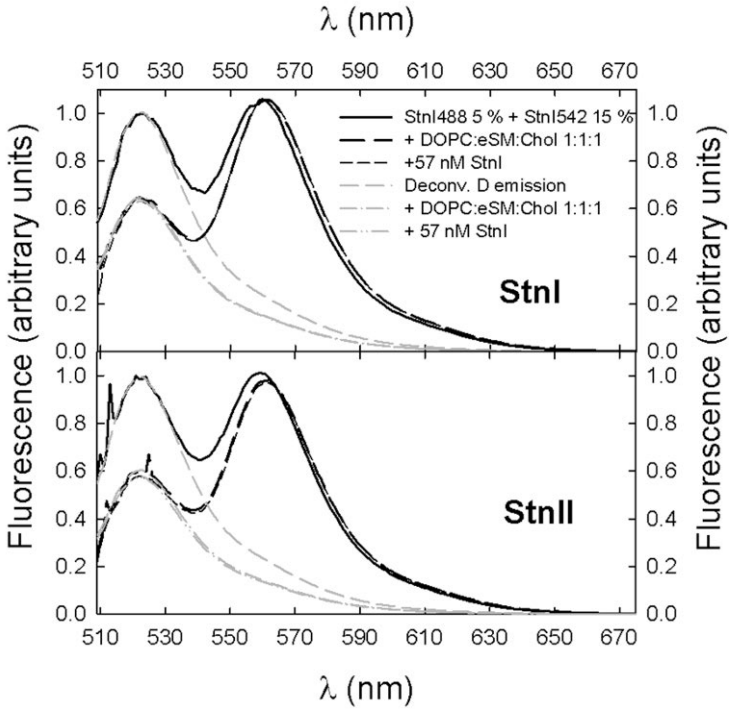

Figure 32. Top panel: *Emission spectra of StnI with 5% donor labeling and 15% acceptor labeling in solution (solid black line), with DOPC:eSM:Chol 1:1:1 (long dashed black line) and after addition of extra 57 nM unlabeled StnI (short dashed black line). Deconvoluted donor emission is also shown in gray. The later addition of StnI did not affect FRET efficiency, indicating that pores are not remodeled.* **Bottom panel:** *same as top, but the addition of WT StnI was replaced by WT StnII. Modified from publication IV.*

6. DISCUSSION

6.1. Sticholysins prefer bilayers of intermediate thicknesses

6.1.1. Properties of membranes differing in thickness

To understand the interaction between sticholysins and membranes of different thicknesses, it is essential to understand which membrane properties vary as acyl chain length is increased. Bilayer thickness has been shown to depend linearly on acyl chain length [220]. As membrane thickness is increased, so does acyl chain order (see Figure 11), thanks to the increased possibility of van der Waals interactions. In our membrane systems, the position of the unsaturations in the acyl chains (see section 5.1) might also play a role since the double bond distance from the water-membrane interface is known to result in higher order in the part of the acyl chains closer to the lipid head group [221, 222]. Taking all into account, we can say that the membrane surface is quite similar for all bilayers, which only differ in membrane thickness and essentially vary in packing, as shown from anisotropy measurements (Figure 11).

In general, the inclusion of Chol also increases acyl chain order [223]. This is a consequence of Chol's nearly perfectly planar phenanthrene surface, which forces a *trans*-gauche configuration on the single bonds of the neighboring lipids. For the same reason, Chol is also responsible for increasing bilayer thickness [224]. Generally, Chol is preferentially associated with SM molecules [145]. Thus, in our system, Chol is likely distributed with 14:0-SM, though some would remain with the PC molecules, increasing membrane thickness and, as observed for most cases (see Figure 11), acyl chain order.

6.1.2. Dependence of sticholysin activity on bilayer thickness

Sticholysin-induced calcein release experiments were used to test the activity of StnI and StnII when facing membranes with different bilayer thicknesses. In all cases, a final total release between 60 and 80% was reached in 15-minute experiments though saturation was reached in a much shorter time. In the absence of Chol, the fastest calcein release was observed for membranes with average thickness, in which the main component was di-16:1-PC or di-18:1-PC (Figure 12). When Chol was included, calcein release became faster for both toxins, with the maximum shifted towards bilayers whose main components were di-14:1-PC and di-16:1-PC (Figure 12).

Since the trend observed for calcein release in each case does not correlate with the observed acyl chain order, it can be assumed that bilayer thickness, rather than acyl

chain order, is a more important parameter from the point of view of the insertion of the N-terminal α-helix of sticholysins. The effect of the inclusion of Chol, in terms of increased release rates, is likely related to the observation in EqtII that Chol is required for complete helix insertion in the membrane [27]. The observed shift is probably related to the predicted Chol-induced increase of bilayer thickness.

6.1.3. SPR binding data

When sticholysin-to-LUV binding was measured using SPR, a linear dependence of bilayer thickness was observed. The trend showed that higher acyl chain order and thickness hindered membrane binding (Figure 13).

This is not consistent with the results from the calcein release assays. However, calcein is a functional assay, whereas SPR is not. Due to the conditions used in the SPR assay, these experiments report maximal protein association to LUVs. In fact, since LUVs are immobilized on the chip surface, they might behave differently from freely diffusing LUVs as LUVs are in the rest of the experiments, possibly explaining the different acyl chain-dependence levels observed in this assay.

6.1.4. Thermodynamic parameters of the interaction

In all cases, the interaction between the toxins and the membrane was enthalpy-driven. The entropy of the interaction was non-favorable but always compensated by enthalpy. Though this might seem surprising for an interaction that is essentially hydrophobic, this has been observed for many proteins that penetrate membranes, including actinoporins [107, 225]. The explanation assigns the favorable ΔH to the van der Waals energy of the interaction between the hydrophobic moieties, with contributions of protein-protein interactions. The non-favorable ΔS would then be a consequence of the ordering of water solvating the newly exposed surfaces.

It is noticeable that ITC results present a very similar trend to that of calcein release assays. Probably, as mentioned in the previous section, the difference from SPR results is due to LUVs being freely diffusing. In the absence and presence of Chol, sticholysins presented the highest values of K_a for vesicles with intermediate bilayer thickness (Figure 14a). The values were much higher when Chol was included, especially for membranes with di-16:1-PC and di-18:1-PC. Nevertheless, the trend remained unchanged. The effect of Chol, which does not seem to be related to membrane thickness or acyl chain order, might instead be related to specific effects that Chol might have on the membrane or on the recognition of SM by sticholysins [22, 25, 26].

6.1.5. A simple model to explain the thickness-dependence of sticholysins' activity

Calcein release was observed for all combinations of membrane systems and toxins. Release was membrane thickness-dependent, indicating that either oligomerization, final pore structure, or membrane penetration was affected by bilayer thickness.

To explain the observed membrane thickness effect, a very simple model was constructed (Figure 33). Using the membrane thickness values previously reported for bilayers composed of pure di-X:1-PC [220], the angle θ formed by the N-terminal α-helix with respect to the bilayer normal was estimated. For this, we considered that the first 30 residue stretch of the N-terminal formed into a 45 Å-long (1.5 Å/residue x 30 residues) α-helix. This parameter (length of the helix) will be referred to as *l*. Thus, the value of θ can be calculated as $\theta = \arccos(h/l)$, where *h* is the bilayer thickness. Once known, the angle was used to calculate the expected inner radius of the pore, *r*', in each of the membranes as $r' = \sin(\theta) \times (l + l')$, where $l + l'$ is the distance from the N-terminal to half the height of the β-barrel. This was 57.8 Å, as measured on the FraC pore crystal structure (PDB code 4STY) using UCSF Chimera [108]. Monomer width, *w*, was measured to be 25.8 Å at that position. The value of *r*' was used to calculate the circumference along which the monomers would be located. Then, the number of monomers per pore was calculated dividing the calculated circumference over *w*.

The results of the model predict that, for membranes composed of di-18:1-PC, the angle θ would be 32.4º, and the pores would consist of 7.5 monomers each. These two values are consistent with previous reports. The angle of the N-terminal helix of StnII was measured previously to be ~31º on DOPC:SM:Chol 1:1:1 membranes using infrared spectroscopy [106], while the most accepted stoichiometry is eight monomers per pore, as shown in the FraC structure obtained through crystallization [35]. In membranes of different thicknesses, it is possible for the pore's structure to be slightly different in terms of the angle of the α-helix, stoichiometry, or overall pore conformation. This could result in less favorable and effective assemblies, as suggested by our results.

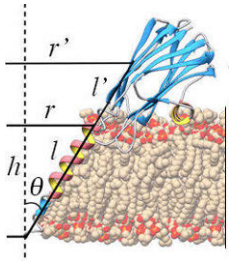

Pure lipid	Experimental *h* (Å)	Theoretical θ	Estimated *r*' (Å)	Estimated nº of monomers/pore
Di-14:1-PC	31.00	46.46	41.9	10.2
Di-16:1-PC	34.50	39.94	37.1	9.0
Di-18:1-PC	38.00	32.39	30.9	7.5
Di-20:1-PC	41.50	22.75	22.3	5.4
Di-22:1-PC	45.00	0.00	0.0	0.0

Figure 33. *Theoretical estimation of potentially bilayer thickness-dependent pore parameters. Parameters in the scheme and values in the table are explained in the main text. Adapted from publication I.*

6.2. Chol is preferentially distributed near StnII

6.2.1. StnII induces declustering of pyr-SM regardless of OCer or Chol presence

Sterols, regardless of the details of their structure, have been observed to enhance sticholysin activity [25]. We wondered if the interfacial hydroxyl group, shared by all of the assayed sterols, could be enough to explain their effect. Hence, OCer, which also presents an interfacial hydroxyl group, was selected. OCer was particularly convenient because, like Chol, it tends to associate with SM [156, 226, 227], but it does not induce gel phase formation, which hinders sticholysin activity [23].

First, the effect of OCer and Chol on SM was evaluated. As expected, if OCer and Chol partition preferentially in the SM-rich phase, the inclusion of either of them in the membranes used resulted in a significant reduction of acyl chain contacts between SM molecules, as reported by the E/M ratio of pyrene (Figure 15). The effect of Chol was larger than that of OCer, proving it a better intercalator.

However, the observed dose-dependent effect of StnII was nearly the same in all situations (Figure 15). The toxin also reduced SM-SM acyl chain contacts but independently of the presence of lipids that prefer the SM-rich phase. The effect of StnII could have two different, non-mutually excluding explanations. On one hand, the protein itself could be able to stand between the acyl chains of SM, reducing their contacts. On the other hand, it could promote a different lipid distribution in the membrane, somehow diluting SM molecules, either by driving them into the SM-poor domain or taking other lipids into the SM-rich phase.

6.2.2. Chol is a better enhancer of the activity of StnII than OCer

Since no significant difference had been observed in terms of StnII effect on SM contacts, we proceeded to compare the effect that the presence of OCer or Chol in the membrane had on the activity of StnII. For this, calcein release assays were chosen. While Chol has been long known to be a great enhancer of actinoporin activity [15, 19, 21-23, 25-28, 113], OCer had not been used in combination with StnII.

Chol proved itself a much better promotor of StnII activity when compared to OCer (Figure 16), revealing that having an interfacial hydroxyl group is not enough to enhance the activity of StnII. The effect of Chol was significantly larger than that of OCer even at Chol concentrations that do not promote phase separation [129]. Therefore, the improvement induced by Chol could not be solely attributed to its hydroxyl group. Instead, its overall structure, and the way it interacts with SM, which was shown to be different than that of OCer, could explain Chol's enhancing effect.

6.2.3. CTL microenvironment changes upon StnII binding

Using CTL in combination with a phase-selective quencher revealed that StnII binding to the membrane significantly altered the microenvironment surrounding CTL. CTL emission in the F_0 samples (no quencher) was already enhanced upon sticholysin addition (not shown), indicating that, at least, the toxin was able to improve CTL shielding from the water. However, the increase in the quantum yield of CTL compared to the situation of toxin absence, was much larger in the F samples. This difference was highlighted by the F/F_0 ratio. If water shielding was the only effect exerted by sticholysin, the F/F_0 ratio would have been constant and toxin-independent. Instead, a significant increase, quantified as $\Delta F/F_0$, was observed (Figure 17). This increment revealed that StnII not only shielded CTL from water, but it also protected it from 7-SLPC, that is, it changed the neighboring lipids of CTL. This was further clarified thanks to the samples in which the SM mol% was larger. In these, the effect of StnII was qualitatively equal but of much smaller amplitude. This was likely a consequence of most CTL being already protected from the quencher by preferentially partitioning in the SM-rich domains. Taken together, it could be said that StnII favored SM-Chol interactions since it appeared to drive CTL from SM-poor regions to SM-rich domains.

6.2.4. The fluorescent emission of the Trp residues of StnII

The intrinsic fluorescence emission of StnII-WT and Trp-to-Phe mutants (Figure 19) was recorded while titrating with LUVs using 260 nm excitation.[3] Fluorescence emission spectra showed that W110 and W114 were the two Trp residues whose environment was modified the most upon toxin binding to the membrane. These two residues appear to be highly similar in terms of solvent exposure and membrane penetration. This is consistent with their exposure in the soluble fold of the protein (Figure 18) and crucial role in membrane binding (see section 2.3.2), which implies the insertion of both in the hydrophobic region of the membrane.

Though not relevant regarding a potential interaction with Chol, an inspection of the emission spectra revealed some other details regarding Trp emission. First, W43 is the Trp residue with the highest quantum yield in the WT StnII. This could be expected from its location in the three-dimensional structure of StnII, buried and

[3] Tyr contributions could have been avoided by using 295 nm excitation instead of 260 nm. Regardless, they were very small in most cases (see main text). Excitation at 260 nm was used because it provided the highest Trp excitation while keeping direct CTL excitation at a minimum. It was selected so that the results were comparable with later experiments that included CTL as a FRET acceptor.

protected within the β-sandwich. For the triple and quadruple mutants, Tyr contribution is higher due to the absence of Trp residues that quench Tyr emission acting as acceptors (see refs. [198, 200] for further details). The emission of the triple and quadruple mutants in solution is, in spite of their one Trp difference, nearly the same. This can be clarified by their respective fluorescence spectrum in the presence of vesicles. The Trp emission of the quadruple mutant is increased more than that of the triple mutant (Figure 19). Apparently, when present, W115 acts as very low quantum yield acceptor for W146. This—which might seem surprising at first given that W146 is relatively exposed to the solvent, while W115 is completely buried inside the β-barrel—is explained by the presence of three Met sidechains in close contact with W115. The sidechain of Met is known to be an efficient Trp quencher [200, 228]. Finally, the increased quantum yield of W146, which is not expected to go into the membrane, is consistent with it playing an important role in oligomerization. Instead, it would be shielded from the solvent by the neighboring pore subunit, as reported previously for FraC [35, 229].

6.2.5. CTL is located close to the Trp residues 110 and 114 of StnII

FRET from the Trp residues to CTL was measured for StnII WT and the Trp mutants. The quantification of the sensitized emission of CTL was consistent with the results of the previous section. The substitution of W110 or W114, and especially both of them, resulted in a significant decrease in sensitized CTL emission (Figure 20a), indicating that W110 and W114 are the two residues closest to CTL in the membrane. Though W110 and W114 are the two Trp residues that are closest to CTL, the remaining Trp residues were close enough to CTL such that energy transfer occurred (Figure 20a).

6.2.6. Sterols are preferentially distributed close to StnII

In spite of StnII driving Chol and SM together, the observed toxin closeness to CTL could be a consequence of random motions in the membrane. To ascertain whether this was the case, the quadruple mutant, StnII W43/110/114/115F, was used. This protein has only W146, which was highly useful to avoid complications in subsequent calculations.

To predict the energy transfer efficiency between randomly distributed StnII and CTL, two situations were considered. In the less favorable one, the distance between the diffusion planes was considered to be 28 Å (based on the octameric crystal structure of FraC [35]), with CTL being unable to go closer than 10 Å to the projection of W146 in the membrane. In this case, CTL was considered to be excluded from that

area by the protein itself or other protein-bound lipids. In the other situation, the diffusion planes would be separated by 26 Å, and CTL would be able to go right beneath W146. In neither case the calculation took into account that membrane-bound sticholysins are forming pores. This is relevant because the predictions assume that all the area beneath the protein, and its surroundings, is available for acceptor diffusion. In this case, there is a large part of that area that is excluded for CTL since it is the lumen of the pore (Figure 34). Thus, in all considered situations, the predicted values were overestimations.

Even though the predictions overestimated the expected FRET efficiency, the experimental results were always higher than the predicted values (Figure 21). This shows that CTL is preferentially distributed close to StnII in membranes. In fact, given that previous studies revealed no difference between the enhancing capabilities of sterols on sticholysin activity [25], we can conclude that Chol is also preferentially distributed close to StnII.

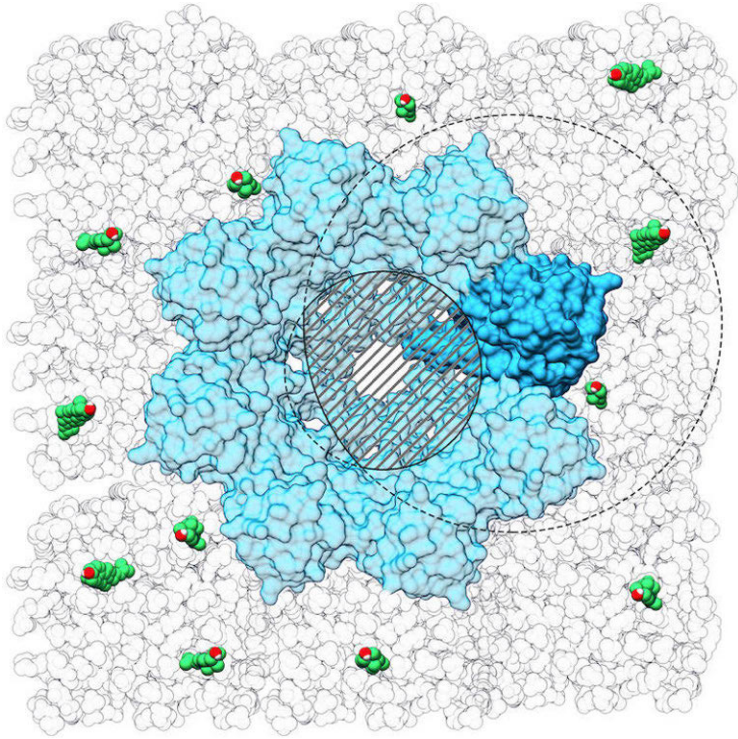

Figure 34. *Schematic illustration showing the expected situation of sticholysins in the membrane. A given monomer (darker one in the pore structure) can transfer energy to CTL molecules (highlighted lipids) within the larger dashed circle (not to scale). The model used assumed that the whole circle was accessible for CTL. However, since these proteins form pores, the lumen (smaller circle) is not accessible. Hence, the model overestimated the expected FRET for a random distribution by a factor that would be proportional to the overlapping area (striped area in the figure).*

6.3. Actinoporin pores are still open even if release traces show plateaus

Traditionally, two assays have been used to evaluate the activity of actinoporins: hemolysis and release of aqueous contents [18, 24-26, 60, 65, 84, 114, 123]. Hemolysis can be used, for example, to compare actinoporin mutants between them, since bilayer composition is equal in all cases [113, 114]. The experiment of release of aqueous contents, which can also be used to the same end, is especially useful when it comes to evaluating the effect of membrane composition on actinoporin activity since it is performed using model bilayers [23, 25, 123].

In the hemolysis experiments, the light scattering due to erythrocytes, and particularly the decrease due to the actinoporin-induced disruption of these cells, is the measured parameter. When using model vesicles, however, actinoporins do not induce vesicle breakage. In the experiments of release of aqueous contents, the measured parameter is the increase in fluorescence due to the dequenching caused by actinoporin-induced dye dilution (when released from the vesicles). This assay has been performed, traditionally, using calcein [18, 24-26, 60, 65, 84, 114, 123] or carboxyfluorescein [230-234]. However, the release traces always plateaued before reaching 100% release. This was surprising considering that, if actinoporin pores were permeable, the dye should keep leaking out of the vesicles until an equilibrium between the inside and outside concentrations of dye was reached. To delve into this issue, a series of probes was selected (Figure 35), first according to their charge and later to their size (Table 4).

6.3.1. The importance of charge

Actinoporin pores had been shown to be cation-selective using electrophysiological measurements [11, 17, 43, 64]. However, calcein and carboxyfluorescein, the probes used most often, are both negatively charged at the pH used in the experiments, as is the lumen of the pore. Based on this, the following working hypothesis was proposed: negatively charged probes would not be able to pass through the pore due to electric repulsion once the pore structure is stabilized. Instead, leakage would occur though membrane imperfections caused by the process of pore formation.

To test this hypothesis, R6G was used. R6G is a high quantum yield fluorescent probe that is positively charged at the pH used in these experiments. Due to its charge,

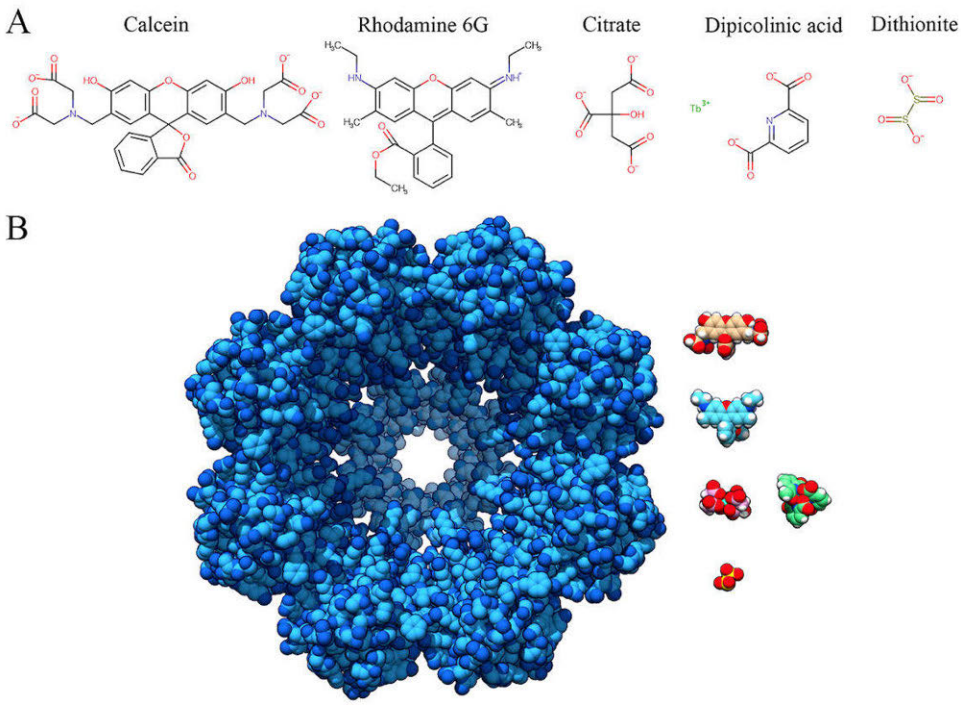

Figure 35. A: *Chemical structures of the probes used in this work to measure the rates and extent of release induced by actinoporins' pores. Citrate and DPA are shown because they are the chelating agents that keep* Tb^{3+} *in solution. Formulas were made using the Marvin 19.22 (2019) software by ChemAxon.* **B**: *Illustration showing the relative sizes of the complexes formed by the structures above, as compared to the StnII pore, based on that of FraC [35], using CPK representations.* Tb^{3+} *is depicted in a 1:2 complex with citrate (pink) and in a 1:3 complex with DPA (green). Adapted from publication III.*

Table 4. *Estimated radii of the probes used in this study.*

Probe	Calcein	R6G	Tb^{3+}	H^+	Dithionite
Estimated radius (nm)	0.74	0.59	0.12	0.10[a]	0.20[b]

[a] *[235]*

[b] *Estimated for dithionite. For comparison, the ionic radius of sulfate is 0.26 nm.*

it should be able to transit through the stable pores, being selectively allowed to pass. Hence, complete release was expected. The experiments showed that the rate of release was much faster than that measured for calcein (Figure 22b), indicating that probe charge is in fact relevant for actinoporin-induced membrane permeability. However, a plateau was still observed when using R6G (Figure 22a). Thus, as for calcein, StnII failed to induce complete release of R6G.

6.3.2. First attempts to show the relevance of size

In light of the results obtained with R6G, the working hypothesis was updated. Although charge had been shown to be important for the rate of release, it was possible that the probes employed were too large for actinoporin pores. In fact, the radius of these pores has been estimated to range between 1–2 nm [18, 29, 34, 35, 104, 236]. The hydrodynamic radii of calcein, carboxyfluorescein, and R6G is 0.74, 0.50, and 0.59 nm, respectively [237-239]. Hence, the probe diameters are very close to the estimated width of the pore's lumen, and that is without taking into account the potential size effect of the hydration layer surrounding both the probe and the pore walls. Thus, it appears that size, rather than charge, is what ultimately prevents complete leakage from taking place. In fact, the radii of Ca^{2+} and K^{+}, the two cations that are supposed to transit through the pores in natural circumstances [17, 43, 240], are about 0.10 and 0.14 nm, respectively—much smaller than those of the probes employed so far. Nevertheless, it should be pointed out that charge does help, as observed for R6G. We can speculate that this is due to R6G having a little longer time to transit through membrane imperfections since it would not be repelled by the StnII α-helices delimiting the zones of transient membrane disruption.

To test the influence of size, Tb^{3+} was the first probe selected. This fluorescent lanthanide, which is positively charged and has a diameter of ~0.12 nm, seemed like the perfect candidate. The results obtained, though valid, were poor in terms of rate and final release (Figure 22). The explanation may lie in the fact that Tb^{3+} is, by itself, insoluble. In order to remain in solution, it needs to be chelated (Figure 35b). When encapsulated, each Tb^{3+} atom was chelated with two citrate molecules. A citrate molecule displays three negatively charged groups at the experimental pH, thus rendering complexes that had a net charge of -3. Therefore, the situation would be essentially that of calcein since the complex would be larger than Tb^{3+} on its own, and negatively charged, both of which hinder the transit of the complex through the pore. Moreover, Ni^{2+} has been observed to inhibit EqtII action [66, 236]. This might have also played a role in the slow release observed for Tb^{3+}.

Given that Tb^{3+} did not result as expected, an experiment was designed in order to track proton release, the smallest possible cation. For this, fluorescein, a probe that displays a pH-dependent absorption maximum, was encapsulated at pH 4.2 coupled with 3,000 Da dextran. Dextran of that size is not released from LUVs upon sticholysin activity [18]. Thus, coupling of fluorescein with dextran prevented it from leaking out. This was essential in order to measure proton efflux to the outside of the vesicles, where the pH was kept at 7.2. Unfortunately, the fluorescent traces indicated that proton release was also slow and only noticeable at high protein concentrations within

the range used (Figure 22). This could be caused by StnII being less selective to cations at the pH found inside the vesicles [17], to which it would be suddenly exposed once it interacts with the membrane. In fact, the pK_a of the titratable groups was ~5.0 [17]. Hence, this assay would reflect pH influence on pore selectivity rather than proton permeability. It should be mentioned that cation flux through actinoporin pores has been shown to be favored asymmetrically [11] and that experiments using model vesicles such as those described so far would measure passage in the less favorable direction.

6.3.3. Results indicate release by transient membrane perturbations

Given the observed results, all assays so far could be said to be measuring leakage induced through transient membrane perturbation. The time-dependent traces of all experiments were used to fit the membrane perturbation model by Andersson *et al.* [205] (see section 4.2.3.3). In all cases, the model succeeded in describing the data (Figure 23), supporting that, in fact, the probe release observed in these assays occurs due to StnII-induced membrane perturbations, as hypothesized. Many proteins and peptides have been observed to use this mechanism to induce cell damage [241, 242]. It can be speculated that membrane perturbation during membrane penetration can also be useful for actinoporins.

6.3.4. StnII pores can be impermeable to calcein and still be open

Tb^{3+} and proton assays did not result as expected. As with calcein and R6G, the release traces reached plateaus, indicating that complete release was not possible with those probes. Thus, a new procedure was set up to clarify whether StnII-induced leakage was solely caused by transient permeation, or whether it could also occur through thermodynamically stable, open pores. This new approach consisted of measuring quenching of membrane-bound POPE-NBD using sodium dithionite, as described by Wimley [203].

LUVs were made including 1 mol% POPE-NBD, randomly distributed between both leaflets. The addition of dithionite to the vesicles resulted in the quenching of ~40% of the available NBD (Figure 24a). However, when the vesicles were preincubated with StnII, the addition of NBD resulted in a much larger decrease in NBD's emission (Figure 24b), indicating that the NBD on both leaflets was available for dithionite. The reverse experiment, in which StnII was added after dithionite had quenched all NBD available in the outer leaflet, was used as a control and showed that dithionite was still able to go into the LUVs, quenching the remaining NBD emission.

Therefore, these results allow the conclusion that StnII pores and, presumably, those formed by any actinoporin are indeed open after they stabilize. These proteins have been shown to also be able to induce membrane permeability during their process of pore formation. In fact, it was this effect, rather than pore-induced conductivity, that had been observed by calcein release assays. The calcein release results from papers I and II, which have been interpreted in terms of sticholysin activity, are actually consistent with this conclusion. According to this interpretation, calcein release is proportional to the number of pore formation events, and, undoubtedly, the toxin would be more active on those membranes upon which it is more prone to form pores.

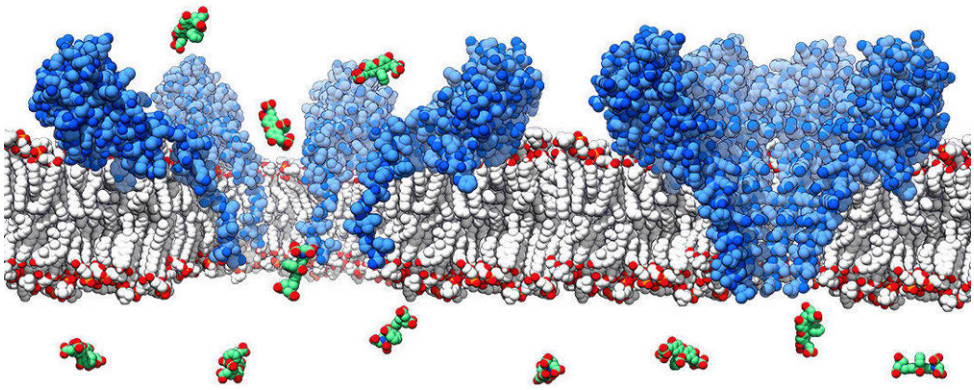

Figure 36. *Cartoon illustrating the conclusion regarding the calcein release assay. While a pore acquires its final conformation (right), membrane disruption would be large enough to allow calcein molecules to pass through. However, once the structure stabilizes (left), it would not permit passage anymore. Adapted from publication III.*

6.4. Oligomerization and stoichiometry of sticholysins

Many aspects of the behavior of actinoporins, such as SM-selectivity, the role of Trp residues, Chol's enhancing effect on the activity, and the importance of the N-terminal segment of these toxins during the process of pore formation have been resolved [18, 23, 44, 65, 72, 102, 104-107, 150, 198]. However, the oligomerization process and the final stoichiometry of the pores, two of the most relevant aspects of the behavior of any pore-forming toxin, have remained elusive for years. Important advances have been made using other actinoporins, such as FraC, which revealed that dimerization might be a step required for membrane binding while also showing that FraC forms octameric pores [35]. However, in order to do so, detergents had to be used to isolate and purify the mentioned intermediates. In our case, using a FRET-based approach,

we have shed some light onto the problem with a system that causes the least perturbation possible on the proteins.

6.4.1. Sticholysin size and mobility

The labelling of the single Cys-mutant with ATTO-488 allowed measurement of the anisotropy decay of StnI in both the presence and absence of membranes. In all cases, the decays could be fitted using just two components, accounting for the segmental motions of the label and the overall rotational motions of the protein itself (Table 3). The anisotropy did not decay to zero in either case, only when the decay of the probe free in solution was measured (Figure 25 and Table 3).

The slow correlation time enabled us to calculate the molecular diameter of these proteins. The result, 29.0 ± 1.2 Å, agrees with the molecular structures obtained using X-ray diffraction and nuclear magnetic resonance [29, 30]. Based on this alone, it could be said that the monomer is the fundamental organization unit for sticholysins when in solution. However, the fact that the limiting anisotropy did not decay completely even when the correlation time was shorter than the lifetime of the excited state of the probe (4.1 ns) could indicate the presence of yet slower correlation times, not resolvable, which would account for higher-order oligomers in solution. The existence of such complexes, which, apparently, would not be very abundant, is consistent with previous reports indicating that sticholysins can oligomerize in solution [184].

The addition of LUVs to these solutions resulted in a significant increase in the slow correlation time and the limiting anisotropy for StnI (Table 3), revealing the reduced mobility of the proteins as a consequence of membrane binding and oligomerization. The segmental motions of the label, whose situation had not changed significantly, remain the same (Table 3).

6.4.2. StnI oligomerizes in solution alone and with StnII

Time-resolved anisotropy results suggested that oligomers were present when StnI was in solution in the absence of membranes. This behavior had been described before for StnII using analytical ultracentrifugation [184]. To delve into this, StnI T43C was also labeled with ATTO-542, which would act as an acceptor of ATTO-488 (donor). The titration of donor-labeled StnI with the acceptor-labeled toxin revealed that energy transfer was taking place (Figure 27), indicating the presence of StnI oligomers in solution, as had been observed for StnII.

StnII has been observed to increase the activity of StnI, presumably by promoting the binding step of the pore-formation process [95]. Consequently, it could be

expected that StnII oligomerized with StnI while in solution. Indeed, the increase in the FRET signal when the previous experiment was repeated in the presence of StnII confirmed that not only the number, but also the size of the oligomers were increased (Figure 27). This conclusion can be achieved simply due to the increased signal and because, given that StnII was not labeled, it had to couple labeled StnI subunits in order to promote energy transfer, thus inducing the formation of, at least, trimeric ensembles.

6.4.3. Stoichiometry of sticholysin pores in DOPC:eSM:Chol membranes

The FRET approach was taken one step further in order to resolve the stoichiometry of StnI pores directly on model membranes. Again, the same StnI mutant, T43C, was used with the same labels previously specified, acting as FRET donor and acceptor.

The experimental values of energy transfer efficiency obtained using StnI with its labeled mutant were compared to those predicted taking into account the size of the proteins, the position of the label within the structure of the proteins, and the photophysical properties of the probes. The RMSD values exclude stoichiometries of five or fewer subunits (Figure 28). In fact, the results agree best with the signal expected for an octameric ensemble. However, the resolution of the predictions (Figure 37) does not allow for ruling out stoichiometries consisting of seven or more

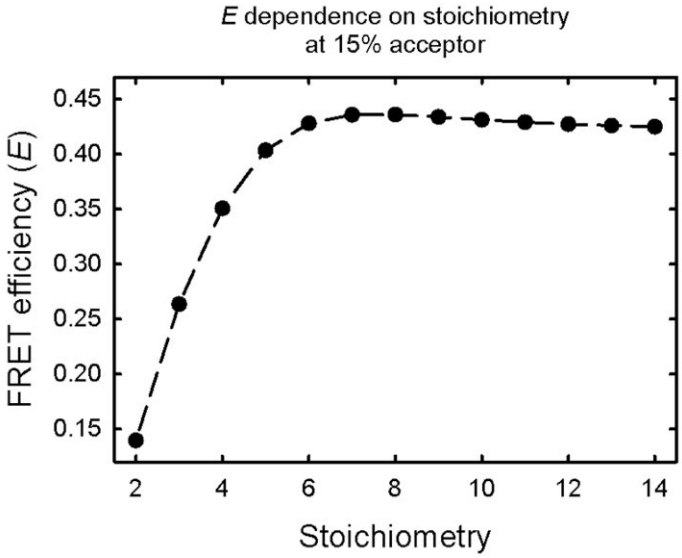

Figure 37. *Theoretical variation of the FRET efficiency at a fixed acceptor content in the sample o 15% as a function of the stoichiometry of the complexes, according to the physical restrictions imposed by the size of sticholysins, the position of the label in their structure, and the photophysical characteristics of the labels used. The differences in the predictions are further reduced as the acceptor content in the sample is increased. Modified from publication IV.*

subunits. It must be mentioned that the results are also compatible with the presence of several different stoichiometries simultaneously, which would yield the same final signal as if they were all octamers.

When the experiment was repeated in the presence of StnII (12.3%), the results were essentially the same. In fact, the distribution of the RMSD values was also maintained albeit with the differences between heptamers and higher-order oligomers somewhat reduced (Figure 30). It could be argued that the same stoichiometry is observed because StnI and StnII do not form heteropores. However, despite present (Figure 30) and previous evidence indicating otherwise [95], if this were the case, the observed signal should be higher than observed, since, in practice, the degree of the labeling of the StnI pores would be higher than assumed if StnII was collaborating in the formation of heteropores.

It is interesting to remember that oligomerization was observed to be promoted by the presence of StnII. Two of the 12 residues that differ between StnI and StnII are precisely located at the presumed protein-protein interfaces or very close to them. These two residues are Tyr148 and Gln149 in StnI and His147 and Glu148 in StnII. The properties of the residue are overall conserved: a hydrogen-bonding-capable aromatic residue (Tyr/His) followed by another relatively long-chained amino acid that is also capable of hydrogen bonding (Gln/Glu). Based on these properties, we can predict the properties of the complementary residues as being also capable of hydrogen-bonding, one of them probably cationic, in order to establish a potential cation-π interaction with the aromatic rings of Tyr/His. An inspection of the three-dimensional structures of StnI and StnII reveals that there are, in fact, two residues appropriately placed and oriented in both their structures. These are Arg126 and Lys124 in StnI and Arg125 and Lys123 in StnII (Figure 38). The difference in activity between StnI and StnII has been attributed, mostly, to the different attachment strength of the N-terminal α-helix to the β-sandwich [114]. Nevertheless, this does not rule out the possible contributions that could come from stronger monomer-monomer interactions mediated by the aforementioned residues. It is possible that a salt-bridge is established between the Glu148 of StnII and the corresponding Lys residue of StnI or StnII (Lys123/124, respectively). This comparatively stronger interaction could shift the equilibrium toward the multimeric ensembles, which could in turn facilitate membrane binding and later oligomerization.

It is also worth noting that these results are all compatible with the pore structure obtained for FraC using X-ray. Altogether, these observations support that the stoichiometry of the pores of actinoporins is always the same regardless of the specific proteins that form the pores, indicating that it would mainly depend on protein shape.

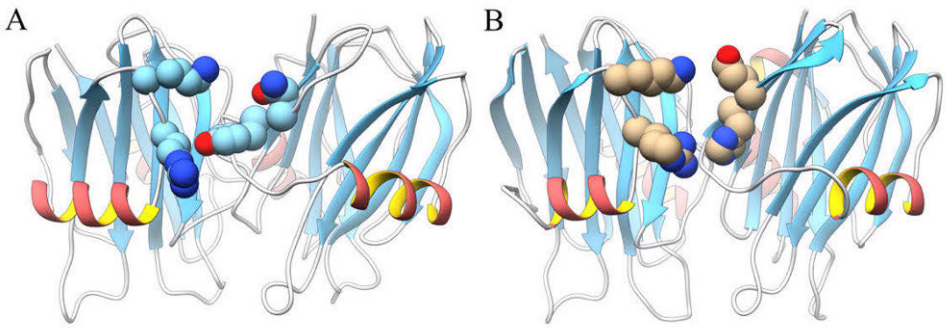

Figure 38. *Homodimers of StnI (***A***) and StnII (***B***). Side chains shown are those of the same amino acids in both cases for the monomer on the left, Lys124 and Arg126 of StnI (Lys123 and Arg125 of StnII). For the monomer on the right, the amino acids differ. For StnI, they are Tyr148 and Gln149, whereas for StnII, they are His147 and Glu148. The orientation of the residues is not necessarily that found upon oligomerization since the structures used to create the illustration were obtained in solution (A) and by crystallization (B). The Arg could interact with either of the aromatic residues either by hydrogen bonding or by a cation-π interaction. The latter kind of interaction can, in fact, be observed in the dimer structure published for FraC (PDB ID: 4TSL [35]) between its equivalent amino acids. Lys residues probably form a hydrogen bond with Gln149 and a salt bridge with Glu148. Adapted from publication IV.*

6.4.4. Results in the absence of Chol suggest binding by oligomers

The results yielded by the experiments using membranes that lack Chol can seem surprising at first. The predictions are not followed in any case (Figure 29 andFigure **31**). Furthermore, a feasible possibility—that the pores clustered on the membrane—is also discarded since the *E* values observed are not higher than the predictions, as could be expected if clustering had occurred. However, the fact that the first few points are closer to the theory and then stop rising accordingly can suggest that the binding unit for membranes with no Chol would be sticholysin dimers. At low acceptor content in the sample, the expected *E* would be less dependent on acceptors at the $i + 1$ subunit (from a donor placed at i). However, as the acceptor fraction grows, the relevance of the probability of finding acceptors increases simultaneously, at positions $i + 1$ and $i - 1$. Since, for these experiments, donor- and acceptor-labeled proteins are mixed right before the measurements are performed, and in the total final volume, a complete shuffling of the variants in the oligomers might not occur quickly enough. Thus, the oligomers in the sample would rarely have donor-acceptor pairs, yielding the observed effect. This observation is compatible with previous reports pointing to dimers being required for membrane binding in membranes with no Chol [35, 187]. It is possible that Chol's effect on SM's head group [168] orientation aids in SM recognition, allowing the dominant form in solution, monomers, to directly bind those membranes, which would in turn enable a proper shuffling of the subunits, according to the model used.

6.4.5. Further evidence for stable pores

Previously, we have presented evidence showing that sticholysins pores remain open once they are formed (see sections corresponding to paper III). However, these experiments were performed on vesicles with large pore populations. Because of this, these results did not rule out the "remodeling hypothesis" proposed for the noisiness of the electrophysiology measurements, in which the opening of individual pores can be observed [43, 219].

Our present FRET results discard the possibility that the aforementioned noisiness is a consequence of pore remodeling. The timescale of those events was of mere seconds, whereas ours was of the order of two to five minutes—enough, in principle, for the system to reach a new equilibrium, incorporating subunits added later to the sample. In such conditions, no FRET was observed after the addition of acceptor-labelled toxins to previously formed donor-containing complexes (Figure 32), supporting the idea that the pores are not remodeled and that, consequently, they maintain the same subunits once they stabilize.

In light of these results, the comparatively higher noisiness of the actinoporin pores relative to those formed by β-pore forming toxins can be attributed to the thermal-induced motions of the elements of the complex, which would be more significant in these pores due to the looser attachment of the trans-membrane segments, which are, for that reason, more susceptible to nearby lipid motions.

7. OPEN QUESTIONS, PERSPECTIVES, AND OTHER THOUGHTS

The results presented in this thesis provide answers to many questions in the research field. However, at the same time, these same results also show some details and nuances that allow for further discussion and, in the future, could be the starting points of new studies.

7.1.1. Anisotropy change with increasing bilayer thickness

It has been shown that in membranes composed of a single PC species, the thickness of the bilayer varies linearly with acyl chain length for both di-unsaturated and di-monosaturated lipids [220]. Similarly, one could expect a concomitant increase in the hydrophobic contacts between the acyl chains, increasing the overall acyl chain order. The results presented in paper I, using di-monounsaturated PC species, always in presence of 14:0-SM, show precisely that both in the absence and presence of Chol, membrane order is increased with acyl chain length, at least according to the steady-state anisotropy of DPH (Figure 11). However, it is interesting to observe that, at a temperature of 25 °C (Figure 39), when Chol is absent, anisotropy increases almost perfectly linearly with acyl chain length, with only one value falling outside the trend. That value corresponds to the bilayer composed of di-16:1-PC:14:0-SM (4:1 molar ratio). If all systems vary in the same manner relative to one another with just this exception, then this system could be expected to present a unique feature, causing the observed difference.

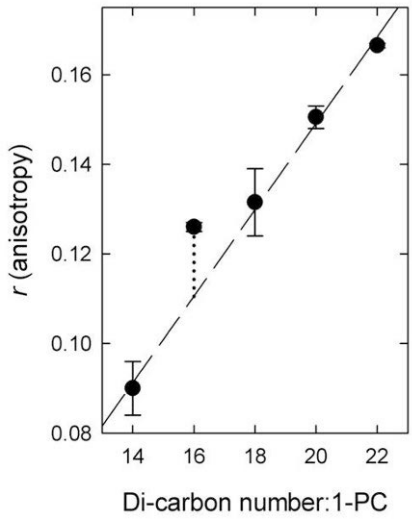

Figure 39. *Steady-state DPH anisotropy in di-X:1-PC:MSM (4:1 molar ratio) bilayers measured at 25 °C. The dashed line is obtained by linear regression ignoring the data from di-16:1-PC membranes (R^2 = 0.997). The dotted line highlights the deviation of the value mentioned in the main text.*

There are two components in all these systems if Chol-containing compositions are left aside (in these, Chol plays a major role and complicates this analysis). On one hand, 14:0-SM has a 14:0 acyl chain. On the other, all di-monounsaturated PCs used have one double bond in both of their acyl chains. The presence of this double bond makes the effective length of those acyl chains (assuming

an all *trans-gauche* isomerization) to be closer to that of an equivalent saturated chain with two fewer carbon atoms. The membranes composed of di-16:1-PC:14:0-SM are the only systems assayed in those experiments in which the hydrophobic mismatch between the PC species and 14:0-SM can be considered, at least theoretically, to be nearly inexistent. It is precisely this composition that displays a higher-than-expected anisotropy. In all the others, either the PC is shorter (di-14:1-PC) or it is larger (acyl chains of 18 to 22 carbons) than the acyl chain of the 14:0-SM, but the mixture always results in systems with a hydrophobic mismatch. The mismatch also varies between systems, but the different degree of mismatch (except when it appears to be zero) does not seem to have any significant effect on the anisotropy displayed by DPH when embedded in these lipid systems. Since DPH anisotropy reports lipid mobility at the membrane core, it is reasonable to think that it can move more freely in those systems that are more poorly packed (i.e., more prone to leave voids) than in similar systems with no or just smaller hydrophobic mismatches.

7.1.2. Does acyl chain order affect membrane binding?

It has been shown that the phase state of the membrane is an essential feature of the membrane if one is to predict binding and pore formation by actinoporins [18, 24, 25, 44, 65, 72, 150, 153, 154]. However, this section is referred to the possibility of smaller differences originating from differences in the acyl chain order of the lipid species of those membranes, assuming that they are all in the same phase state and are suitable targets for actinoporins and, particularly, sticholysins. To that end, the results from SPR measurements will be further discussed.

From a certain point of view, SPR-based methods that measure molecular adsorption (referred to in this work simply as SPR) could be said to work as extremely sensitive balances. In most cases, the k_{on} and k_{off} constants of the interaction of interest can be determined from the signal change over time. These values can then be used to calculate the K_a of the interaction. Moreover, the signal, which corresponds to the changes in the refractive index of the surface of the chip as a consequence of the binding of molecules, can also be readily converted to units of mass/surface (such as ng/cm^2). This value can be then used, if the M_w values of the interacting molecules are known, to estimate the "apparent" stoichiometry of the association. In our case, the L/P molar ratio was calculated. A smaller L/P value indicated more bound protein subunits as the chip-bound amount of lipid was the same in all cases. This last statement was checked using the average molecular weights of each of the lipid compositions used and comparing the expected and observed mass ratios, which were in good agreement in all cases (see section 5.1.3 and Table S1 in paper I).

When the L/P molar ratio was measured using SPR, the overall trend showed that protein binding increased with bilayers having shorter acyl chain lipids. This held true for both Chol-containing and -lacking systems. This trend was almost linear in the Chol-lacking systems. As happened with the anisotropy measurements discussed in the previous section, one of the values stood above what would be expected—the one corresponding to membranes containing di-16:1-PC (Figure 13, panels A and C). Incidentally, this system was also the one that showed higher-than-expected steady-state DPH anisotropy (Figure 39). This suggests that, in addition to bilayer thickness itself, the overall order of the membrane could play a role in membrane binding. To explore this idea, one could plot the values obtained for the L/P ratio as function of the steady-state anisotropy of the corresponding bilayer. If this is done, a linear dependence is obtained for the situations in which Chol-lacking membranes were employed (Figure 40, top panels). If the same is done for the Chol-containing bilayers, the trend is no longer linear (Figure 40, lower panels). Nevertheless, in both cases, these plots are intriguing. In the case where one kept a constant lipid content in the sample, a decreasing L/P molar ratio would indicate an increasing number of membrane-bound protein units. Hence, maximum possible binding would occur as the L/P molar ratio tends to zero. Strictly speaking, and following the above statement, this would mean that an infinite number of proteins has bound each lipid. This has no physical sense, but this hypothetical situation can be related to the effect of membrane-anisotropy on protein binding,

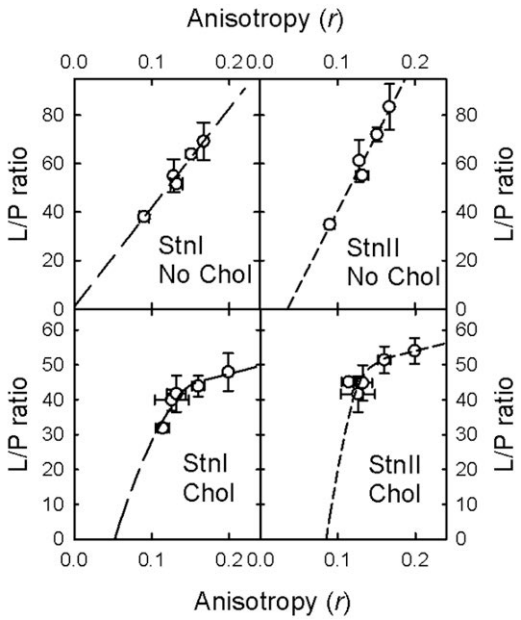

Figure 40. *Plots of the L/P molar ratios obtained from SPR as function of the DPH steady-state anisotropy measured for the same lipid systems. The fits on the top two panels have a R^2 of 0.974 and 0.970 for StnI and StnII, respectively. The lines in the lower panel are only guides to the eye drawn based on the overall trend of the points and not result from fitting.*

Extrapolation from the fits shown in Figure 40 indicates that an L/P molar ratio equal to zero would be reached at $r \approx 0.0$ and $r \approx 0.05$ for StnI and StnII, respectively. Therefore, it could be speculated that in order to achieve maximum possible binding, StnII would be able to overcome the opposing effect of a more ordered membrane. If we consider that the completeness of the pore formation

process (which will be discussed in further detail later) drives membrane binding, it could be said, roughly speaking, that as pores are formed, they leave space for more monomers to bind. This would be expected from the mass action law when applied to a multi-step process. In such case, this ability could be related to the ease by which the N-terminal α-helix is able to penetrate the membrane or, in other words, how easy it is for the membrane to accommodate the helix in its own structure. According to the considerations above, the characteristics of the helix of StnI would be less favorable to that end, at least regarding the initial process of membrane penetration. This could be in fact expected from it having a more polar character than that of StnII (see sequences in Figure 2 and refs. [111, 114]). A similar observation can be made regarding the Chol-containing systems. The presence of Chol, however, would help both proteins in overcoming the energy barrier consequence of lipid order and packing. Possibly, the mechanism could be related to an increased rate of transient void appearance in the membrane, through which the insertion of the helices could be taking place.

Verifying this hypothesis would require a new set of experiments using membrane systems that differed the least possible between one another other than on the acyl chain order of their lipids. If an SPR system capable of maintaining different temperatures was available, the same study could also be performed using a single lipid system at the different temperatures at which its anisotropy had been measured.

7.1.3. How is leakage produced? Comparing calcein and rhodamine 6G

In the sections corresponding to paper III, it has been shown that actinoporins cause the release of LUV-encapsulated probes as a consequence of the process of pore formation rather than through the actual thermodynamically stable pore. Essentially, this would be caused by the insertion of their N-terminal α-helix, since, based on the structure of these proteins, the parts responsible for SM recognition and membrane binding would not reach far enough into the membrane so as to affect both leaflets.

In that same publication, it has also been shown that, at smaller P/L molar ratios, larger leakage is observed when using R6G as the probe instead of calcein. Overall, it might be concluded that R6G experiments are more sensitive. This appears to be obvious when small L/P ratios are used. However, this does not mean that calcein is useless. It just offers a smaller dynamic range than R6G.

Now let us just consider the results from R6G and calcein since H^+ and Tb^{3+} assays were already argued to be not fully comparable due to their potential interactions with the toxins (see section 6.3.2). Since the experiments in paper III were performed with the same protein and always using the same lipid composition, it can be assumed that the membrane perturbations reported for calcein or R6G are the same in all cases.

Considering the results at an P/L molar ratio < 0.0005 from Figure 22a, it can be readily seen that less calcein than R6G is released. This would mean that the number of calcein molecules released per membrane perturbation is smaller, which is also perfectly consistent with the results presented in Figure 22b. In such situations, the release would be controlled by the time for passage that is permitted for each probe, which depends on its molecular characteristics of charge and size as well as the lifetime of the protein-induced membrane perturbations. Dependence on size would be twofold: smaller size entails a larger diffusion coefficient and also a longer time-window during which to pass through (until the membrane "breach" is closed). This last factor would also be affected by charge since short-range electrostatic repulsions would also reduce passage time. Based on this, the molecules that can exit the vesicle when low P/L ratios are used would be those that are within a "diffusible distance" when the membrane breached, being that distance determined by the diffusion coefficient of the probe and its passage time.

When the P/L ratio is larger, however, total release is plateaued. At that point, release is not increased even when the P/L molar ratio is. This could be a consequence of several things. Past ITC experiments have shown that saturation is reached at L/P molar ratios ≥ ~80 (= ~0.0125 P/L molar ratio). In the present leakage experiments, saturation is reached at only a P/L molar ratio of ~0.0005. Therefore, this effect cannot be accounted to no more proteins being incorporated into the membrane after that P/L molar ratio. Another explanation is necessary. One could start from the following. It has been shown that release ceases when pores are formed. This suggests that the faster the pores are formed, the shorter-lived the membrane perturbations are. In other words, the lifetime of the disturbances is inversely proportional to the surface density of toxin monomers, which in turn is proportional to the L/P ratio. Thus, when the amount of toxin used is high enough, only the probe molecules that are in the immediate vicinity of a membrane discontinuity would have time to diffuse through it and leave the vesicle. The consequence of this would be that the effects of probe size and charge are minimized, as is in fact observed experimentally when different probes are compared.

7.1.4. What is sensed by ITC in the case of actinoporins?

ITC quantifies the heat change in the sample as a consequence of sample injection, including that of any reaction or interaction occurring within. Ideally, the sole cause of the temperature change would be the reaction or interaction of interest.[4] Therefore,

[4] This is hardly ever the case. Nevertheless, trivial heat contributions, such as sample dilution, can be accounted for by measuring them separately and subtracting them during data analysis.

regarding actinoporins, it would measure the heat changes due to membrane association, and the subsequent conformational changes. This comprises many different interactions and stages,[5] namely, membrane adsorption and attachment to SM, monomer-monomer interactions, membrane disruption and the rearrangement of lipids, the conformational change of the proteins to form pores, and the associated changes in solvent distribution caused by the variation in the exposed surfaces.

Often, for the sake of explanatory simplicity, the process of pore formation is divided in just two "major" steps: membrane binding, and pore formation. In this sense, it has been said that ITC reflects only the first part of the process, namely, binding, and not the subsequent steps, implicitly assuming that the latter has no effect whatsoever on the thermodynamic constants of the process. This idea might have arisen as follows. In Alegre-Cebollada *et al,* (2008) [107], both StnII-WT and StnII-A10P were characterized using ITC (with DOPC:SM:Chol 1:1:1 vesicles) and hemolysis assays. The ITC isotherms and the thermodynamic parameters of these two proteins were nearly identical, but the hemolytic activity of the mutant was reported to be 0.26 of that of StnII-WT. Since the ITC results were the same, but StnII-A10P was not nearly as hemolytic, and thus presumably not forming pores, ITC was said to report *only* membrane binding.

The ITC characterization of StnII-WT and StnII-A10P was then repeated in García-Linares *et al.* (2015), incorporating the use of POPC:PSM 4:1 vesicles [113]. This time, hemolysis assays were replaced by calcein release experiments. Again, the thermodynamic parameters reported for both proteins were extremely similar, only differing a bit more in the case of Chol-lacking vesicles. This was the calcein release as well. In Chol-containing membranes, StnII-A10P produced essentially *the same* release curves as StnII-WT. While its induced release was reduced in Chol-lacking vesicles, it was still about half of that of the WT protein. Therefore, and according to the calcein release results presented there, StnII-A10P was capable of disrupting those model membranes.

In spite of the calcein release results, it could be argued that StnII-A10P did not form pores, as suggested by the hemolysis assays. This could be the case if the monomers did not fully assemble into a complex and just inserted their helix into the membrane. As mentioned in section 7.1.3, it is extremely unlikely that only SM-recognition and binding could trigger leakage, since the proteins loops responsible for such barely penetrate the outer leaflet of the bilayer. However, in either case, one

[5] The process is artificially divided into stages for clarity. This does not mean that those stages are actually distinguishable from one another in the actual molecular process or that they even occur as such.

would expect the ITC results to differ. Since that did not occur, the most probable scenario would be that StnII-A10P did behave, overall, nearly exactly the same as StnII-WT. The mutation would have had the following two effects: first, hindering membrane penetration in absence of Chol and, second, and most importantly, altering the conformation of the N-terminal α-helices in the final pore assembly. This could narrow the lumen of the pore, hindering cation flow-through. As a consequence, the osmotic shock exerted on the erythrocytes in the hemolysis assays would be greatly reduced. As calcein release experiments reveal, this mutant would still be capable of inducing membrane disruption via the insertion of the α-helix. Nevertheless, the results from paper III suggest that these events are short-lived. Hence, in the case of red blood cells, these may not be enough to cause hemolysis, especially given that the volume of the erythrocytes used for hemolysis is about ~7000 times that of the vesicles typically used for calcein release experiments.[6] Following the discussion in section 7.1.3, only the volume immediately beneath the membrane would be affected by the insertion of the α-helices. Changes in concentration on that fraction of the erythrocyte's content would not be enough to cause them to burst. For this, fully functional pores, which allow for a continuous flow of cations, would be required, such as those of the WT isoform.

Hence, it could be said that ITC does capture contributions from all steps of the process, including pore formation and the associated reorganization of lipids in the membrane. Elucidating what the specific contributions of each sub-process are, given that they could somehow be isolated experimentally, would require the use of a variety of mutants. Such studies might be challenging since they might require high sample concentrations to obtain a detectable signal. However, valuable data would be obtained, increasing the understanding of the process of pore formation. The mutants that come to mind in order to perform such a study would be the following: one whose capability to penetrate the bilayer is, with no doubt, impeded, such as the EqtII-V8C/K69C double mutant [27, 102]; one that does not oligomerize, similar to StnII-G142A, which lost its ability to produce competent oligomerization [179]; and finally one that combines the features of both and could only, in principle, bind to SM. Again, these experiments might be challenging since, given that the process would halt unfinished (the whole point is to hinder pore formation in various ways), monomers would be less prone to bind the bilayer, as expected from the predictions derived from the mass action law.

[6] Sheep erythrocytes have a volume of about 30 fL [243]. Assuming ideal sphericity, vesicles with a diameter of 200 nm would have a volume of ~4.2 aL.

7.1.5. Apparent SPR-ITC disagreement

Based on the above discussion, especially regarding SPR, it could seem that the SPR and ITC results in publication I disagree. SPR reports more binding for thinner membranes by both sticholysins (Figure 13), while ITC shows that the membranes with intermediate thickness are preferred (Figure 14), an observation that is also supported by calcein release experiments (Figure 12). It should be noted, however, that the conditions under which the interaction between sticholysins and LUVs is carried out differ between both methodologies. Not only that, the measured signal arises from different aspects of the interaction. In any case, more binding does not necessarily mean a more productive or affine binding.

In an SPR experiment a constant population of vesicles remains on the chip while a continuous flow of protein maintains the feed of free toxin. Thus, the system is not allowed to equilibrate. Regarding the detection method, SPR senses the presence of protein mass directly. It does not perceive any signal that could originate from protein functionality. As mentioned previously, due to the high affinity binding of actinoporins, a value for the k_{off} could not be retrieved. Hence, in our case, the stoichiometry was measured in place of the affinity constant (which would be calculated from k_{on} and k_{off}). The stoichiometry obtained in this way, that is, by supplying a constant feed of free toxin to system saturation, is related to the maximum capacity of each of the lipid systems to accept toxins. This, in turn, would depend on the effects exerted by the protein on lipid distribution and the arrangement on each particular set of lipids.

On the contrary, the signal sensed by ITC is more complex than that of SPR, as explained in the previous section. Nevertheless, ITC does allow the measurement of the affinity constant directly. Moreover, it also differs from SPR in that, after each injection of the lipid suspension, the system is allowed to equilibrate. Although after each of the first few injections vesicles are in an environment similar to that of SPR, the value of the association constant is determined, essentially, from the heat values obtained when the toxin is no longer in excess and its binding depends most strongly on its affinity for the membrane.

At this point, one could argue, based on this section and the one immediately before, that the affinity constant measured with ITC is not correct. This would be the case only if the ΔH/molecule was not constant. This could be the case if, when the L/P ratio is high enough, not all proteins that bind the membrane and give a measurable signal are able to complete the pore formation process. However, the release results from paper III should be remembered at this point. They show that very small P/L molar ratios are capable of producing probe release, suggesting that at least, most of

the monomers that do bind the membrane are able to produce leakage. Therefore, the ΔH/molecule would be constant (approximately, at least) in each experiment.

7.1.6. Protein shape, α-helix, and stoichiometry

The stoichiometry of sticholysin pores has come up within this text in regard to both paper I, in which it was related to the length of the N-terminal α-helix, and paper IV, which was dedicated entirely to the study this characteristic of the pores of sticholysins. The results of the analyses presented in the two papers agree nicely, both suggesting a stoichiometry of seven or eight monomers per pore as the most likely.

The analysis in paper I was done in a way that might suggest that the length of the N-terminal α-helix, in combination with the thickness of the membrane, might be the determinant of the stoichiometry. This is, however, unlikely. It is more probable that the structure of the β-sandwich is, in fact, the factor that determines the number of monomers per pore. Why? Because its structure is far more complex than that of just the N-terminal α-helix, and it carries out a much more delicate task: the recognition of the head group of SM.

The spatial disposition of the residues required to recognize the SM head group moiety is, *a priori*, much more difficult to achieve than that of an amphipathic α-helix. In other words, once the overall actinoporin structure appeared, the β-sandwich would have been subject to a much stronger selective pressure than the N-terminal α-helix. This can be readily appreciated since it is precisely in the first 30-residue stretch where most differences between actinoporins appear (see Figure 2). While these changes can result in differences in the activity of the toxins [26], they certainly do not unpair it completely, as mutations in the POC-binding site have been shown to do, at least in the absence of Chol [113]. Not only that, but a common mechanism for the appearance of new toxins is the selection of proteins for new, initially similar, tasks, which might change with later specialization [244]. This can occur by random mutation events that, eventually, represent an adaptative advantage for the individuals that possess the mutation. Thus, it is not unlikely that the overall folding motif required for membrane recognition appeared first—associated to a different process but still related to membrane binding and recognition—in the ancestors. The α-helix probably would have been incorporated later as the ancient protein was selected for a toxic functionality. Its length would have been refined later by the evolutionary pressure exerted by the thickness of the membranes that it would act upon. This last part agrees nicely with what was shown in publication I, in which membranes containing di-18:1-PC were, overall, the ones preferred by both sticholysins. The acyl chains of similar lengths as that of the 18:1 acyl chain are precisely the ones most

abundant in many fish species, including the 18:1 acyl chain itself [245]. This study regarding the lipid contents of fish was performed on species from the Mediterranean Sea, where *A. equina*, the sea anemone that produces EqtII (most similar to sticholysins, especially StnI), occurs. These fish are potential prey of sea anemones, and their membranes thus target of actinoporins.

There is still another argument in favor of this point of view. Protein-protein interactions appear to occur, according to the available structures, mainly implying residues located at the β-sandwich, and much less at the α-helix. Therefore, varying stoichiometry would rely on the flexibility of those residues, so that their interactions, which would favor the formation of the complex, could be maintained. This argument also supports the occurrence of higher stoichiometries since the increment in angular displacement that a residue would have to undergo in order to maintain the same interactions is smaller as the number of monomers per pores is increased.

8. CONCLUSIONS

In this thesis, the following aspects of the molecular behavior of sticholysins have been studied: the influence of bilayer thickness on the activity of sticholysins, the relationship between Chol and the activity of these toxins, and the details of the sticholysin-induced permeability of lipid bilayers.

In **paper I**, we determined that sticholysins are more efficient when facing bilayers whose thickness corresponds to that of membranes composed of di-18:1-PC. Our observations and predictions were consistent with the previously measured values of helix tilting and oligomerization numbers. Furthermore, the lipid composition of Mediterranean fish, where *A. equina* (the producer of EqtII) is prevalent, shows a predominance of fatty acids with 16 and 18 carbon atoms [245]. Thus, it appears that the length of the N-terminal α-helix of actinoporins is a result of evolutionary pressure related to the bilayer thickness of the membranes of its preys.

In **paper II**, we determined that the hydroxyl group of Chol was not enough to explain its enhancing effect on the activity of sticholysins, as shown by its comparison with OCer. In fact, Chol induced less acyl chain contacts between SM molecules, as revealed by the experiments with pyr-SM. We showed that StnII was able to change the environment surrounding sterols, using CTL. This fluorescent sterol enabled us as well to show that sterols preferentially partition close to StnII when the toxin is bound to the membrane, particularly next to Trp residues 110 and 114.

In **paper III**, we concluded that the key factor that determines passage through the pores of actinoporins was size. However, we also observed that charge was still important, as revealed by the rates of release of R6G. We determined that the mechanism by which actinoporins cause dye release is, for most assays, mediated by membrane disruption and that passage through the thermodynamically stable pores does not take place for regular, calcein-sized probes.

In **paper IV**, we studied the oligomerization and the stoichiometry of the pores formed by StnI, both on its own and with StnII, and using membranes containing and lacking Chol. We have presented evidence showing that the stoichiometry of the pores is maintained in Chol-containing membranes regardless of the protein composition of the oligomer. Our results also show that StnII promotes the formation of oligomers in solution, an effect that likely aids the recognition and binding of StnI to membranes in which Chol is absent.

9. REFERENCES

1. Eme, L., Spang, A., Lombard, J., Stairs, C.W., Ettema, T.J. (2017). **Archaea and the origin of eukaryotes**. *Nature Reviews Microbiology*, 15 (12), 711.
2. Lesieur, C., Vecseysemjen, B., Abrami, L., Fivaz, M., Vandergoot, F.G. (1997). **Membrane insertion: The strategies of toxins**. *Molecular Membrane Biology*, 14 (2), 45-64.
3. Dal Peraro, M., Van Der Goot, F.G. (2016). **Pore-forming toxins: ancient, but never really out of fashion**. *Nature reviews microbiology*, 14 (2), 77.
4. Parker, M.W., Feil, S.C. (2005). **Pore-forming protein toxins: from structure to function**. *Prog Biophys Mol Biol*, 88 (1), 91-142.
5. Anderluh, G., Lakey, J.H. (2008). **Disparate proteins use similar architectures to damage membranes**. *Trends Biochem Sci*, 33 (10), 482-490.
6. Szczesny, P., Iacovache, I., Muszewska, A., Ginalski, K., Van Der Goot, F.G., Grynberg, M. (2011). **Extending the aerolysin family: from bacteria to vertebrates**. *PLoS One*, 6 (6).
7. Galinier, R., Portela, J., Moné, Y., Allienne, J.F., Henri, H., Delbecq, S., . . . Duval, D. (2013). **Biomphalysin, a new β pore-forming toxin involved in *Biomphalaria glabrata* immune defense against *Schistosoma mansoni***. *PLoS pathogens*, 9 (3).
8. Xiang, Y., Yan, C., Guo, X., Zhou, K., Gao, Q., Wang, X., . . . Zhang, Y. (2014). **Host-derived, pore-forming toxin–like protein and trefoil factor complex protects the host against microbial infection**. *Proc Natl Acad Sci*, 111 (18), 6702-6707.
9. Muller-Eberhard, H.J. (1986). **The membrane attack complex of complement**. *Annual review of immunology*, 4 (1), 503-528.
10. Rivera-de-Torre, E., Martínez-del-Pozo, A., Garb, J.E. (2018). ***Stichodactyla helianthus*' de novo transcriptome assembly: Discovery of a new actinoporin isoform**. *Toxicon*, 150, 105-114.
11. Maček, P. (1992). **Polypeptide cytolytic toxins from sea anemones (Actiniaria)**. *FEMS Microbiol Immunol*, 5 (1-3), 121-129.
12. Anderluh, G., Maček, P. (2002). **Cytolytic peptide and protein toxins from sea anemones (Anthozoa: Actiniaria)**. *Toxicon*, 40 (2), 111-124.
13. Alegre-Cebollada, J., Oñaderra, M., Gavilanes, J.G., Martínez-del-Pozo, A. (2007). **Sea anemone actinoporins: The transition from a folded soluble state to a functionally active membrane-bound oligomeric pore**. *Curr Protein Pept Sci*, 8 (6), 558-572.
14. Caaveiro, J.M., Echabe, I., Gutiérrez-Aguirre, I., Nieva, J.L., Arrondo, J.L., González-Mañas, J.M. (2001). **Differential interaction of equinatoxin II with model membranes in response to lipid composition**. *Biophys J*, 80 (3), 1343-1353.
15. Schön, P., García-Saez, A.J., Malovrh, P., Bacia, K., Anderluh, G., Schwille, P. (2008). **Equinatoxin II permeabilizing activity depends on the presence of sphingomyelin and lipid phase coexistence**. *Biophys J*, 95 (2), 691-698.

16. Barlič, A., Gutiérrez-Aguirre, I., Caaveiro, J.M., Cruz, A., Ruiz-Argüello, M.B., Pérez-Gil, J., González-Mañas, J.M. (2004). **Lipid phase coexistence favors membrane insertion of equinatoxin-II, a pore-forming toxin from *Actinia equina***. *J Biol Chem*, 279 (33), 34209-34216.

17. Varanda, W., Finkelstein, A. (1980). **Ion and nonelectrolyte permeability properties of channels formed in planar lipid bilayer membranes by the cytolytic toxin from the sea anemone, *Stoichactis helianthus***. *J Membr Biol*, 55 (3), 203-211.

18. De los Ríos, V., Mancheño, J.M., Lanio, M.E., Oñaderra, M., Gavilanes, J.G. (1998). **Mechanism of the leakage induced on lipid model membranes by the hemolytic protein sticholysin II from the sea anemone *Stichodactyla helianthus***. *Eur J Biochem*, 252 (2), 284-289.

19. Martínez, D., Otero, A., Álvarez, C., Pazos, F., Tejuca, M., Lanio, M.E., . . . Lissi, E. (2007). **Effect of sphingomyelin and cholesterol on the interaction of St II with lipidic interfaces**. *Toxicon*, 49 (1), 68-81.

20. Bakrač, B., Anderluh, G., **Molecular mechanism of sphingomyelin-specific membrane binding and pore formation by actinoporins**, in: Proteins Membrane Binding and Pore Formation, Springer, 2010, pp. 106-115.

21. Pedrera, L., Fanani, M.L., Ros, U., Lanio, M.E., Maggio, B., Álvarez, C. (2014). **Sticholysin I-membrane interaction: an interplay between the presence of sphingomyelin and membrane fluidity**. *Biochim Biophys Acta (BBA) - Biomembranes*, 1838 (7), 1752-1759.

22. Pedrera, L., Gomide, A.B., Sánchez, R.E., Ros, U., Wilke, N., Pazos, F., . . . Álvarez, C. (2015). **The presence of sterols favors sticholysin I-membrane association and pore formation regardless of their ability to form laterally segregated domains**. *Langmuir*, 31 (36), 9911-9923.

23. Alm, I., García-Linares, S., Gavilanes, J.G., Martínez-del-Pozo, A., Slotte, J.P. (2015). **Cholesterol stimulates and ceramide inhibits sticholysin II-induced pore formation in complex bilayer membranes**. *Biochim Biophys Acta (BBA) - Biomembranes*, 1848, 925-931.

24. García-Linares, S., Palacios-Ortega, J., Yasuda, T., Astrand, M., Gavilanes, J.G., Martínez-del-Pozo, A., Slotte, J.P. (2016). **Toxin-induced pore formation is hindered by intermolecular hydrogen bonding in sphingomyelin bilayers**. *Biochim Biophys Acta (BBA) - Biomembranes*, 1858 (6), 1189-1195.

25. Palacios-Ortega, J., García-Linares, S., Astrand, M., Al Sazzad, M.A., Gavilanes, J.G., Martínez-del-Pozo, A., Slotte, J.P. (2016). **Regulation of Sticholysin II-Induced Pore Formation by Lipid Bilayer Composition, Phase State, and Interfacial Properties**. *Langmuir*, 32 (14), 3476-3484.

26. García-Linares, S., Rivera-de-Torre, E., Morante, K., Tsumoto, K., Caaveiro, J.M., Gavilanes, J.G., . . . Martínez-del-Pozo, Á. (2016). **Differential effect of membrane composition on the pore-forming ability of four different sea anemone actinoporins**. *Biochemistry*, 55 (48), 6630-6641.

27. Wacklin, H.P., Bremec, B.B., Moulin, M., Rojko, N., Haertlein, M., Forsyth, T., . . . Norton, R.S. (2016). **Neutron reflection study of the interaction of the eukaryotic pore-forming actinoporin equinatoxin II with lipid membranes reveals intermediate states in pore formation**. *Biochim Biophys Acta (BBA) - Biomembranes*, 1858 (4), 640-652.

28. Marchioretto, M., Podobnik, M., Dalla Serra, M., Anderluh, G. (2013). **What planar lipid membranes tell us about the pore-forming activity of cholesterol-dependent cytolysins**. *Biophys Chem*, 182, 64-70.

29. Mancheño, J.M., Martín-Benito, J., Martínez-Ripoll, M., Gavilanes, J.G., Hermoso, J.A. (2003). **Crystal and electron microscopy structures of sticholysin II actinoporin reveal insights into the mechanism of membrane pore formation**. *Structure*, 11 (11), 1319-1328.

30. García-Linares, S., Castrillo, I., Bruix, M., Menéndez, M., Alegre-Cebollada, J., Martínez-del-Pozo, A., Gavilanes, J.G. (2013). **Three-dimensional structure of the actinoporin sticholysin I. Influence of long-distance effects on protein function**. *Arch Biochem Biophys*, 532 (1), 39-45.

31. Athanasiadis, A., Anderluh, G., Maček, P., Turk, D. (2001). **Crystal structure of the soluble form of equinatoxin II, a pore-forming toxin from the sea anemone *Actinia equina***. *Structure*, 9 (4), 341-346.

32. Hinds, M.G., Zhang, W., Anderluh, G., Hansen, P.E., Norton, R.S. (2002). **Solution structure of the eukaryotic pore-forming cytolysin equinatoxin II: Implications for pore formation**. *J Mol Biol*, 315 (5), 1219-1229.

33. Mechaly, A.E., Bellomio, A., Morante, K., González-Mañas, J.M., Guerin, D.M. (2009). **Crystallization and preliminary crystallographic analysis of fragaceatoxin C, a pore-forming toxin from the sea anemone *Actinia fragacea***. *Acta Crystallogr Sect F Struct Biol Cryst Commun*, 65 (4), 357-360.

34. Mechaly, A.E., Bellomio, A., Gil-Carton, D., Morante, K., Valle, M., González-Mañas, J.M., Guerin, D.M. (2011). **Structural insights into the oligomerization and architecture of eukaryotic membrane pore-forming toxins**. *Structure*, 19 (2), 181-191.

35. Tanaka, K., Caaveiro, J.M., Morante, K., González-Mañas, J.M., Tsumoto, K. (2015). **Structural basis for self-assembly of a cytolytic pore lined by protein and lipid**. *Nat Commun*, 6 (1), 1-11.

36. Welsh, J.H. (1964). **Composition and mode of action of some invertebrate venoms**. *Annual Review of Pharmacology*, 4 (1), 293-304.

37. Baslow, M.H. (1971). **Marine toxins**. *Annual Review of Pharmacology*, 11 (1), 447-454.

38. Lane, C. (1968). **Toxins of marine origin**. *Annual Review of Pharmacology*, 8 (1), 409-426.

39. Devlin, J.P. (1974). **Isolation and partial purification of hemolytic toxin from sea anemone, *Stoichactis helianthus***. *Journal of pharmaceutical sciences*, 63 (9), 1478-1480.

40. Bernheimer, A.W., Avigad, L.S. (1976). **Properties of a toxin from the sea anemone *Stoichactis helianthus*, including specific binding to sphingomyelin**. *Proc Natl Acad Sci*, 73 (2), 467-471.

41. Linder, R., Bernheimer, A.W. (1978). **Effect on sphingomyelin-containing liposomes of phospholipase D from *Corynebacterium ovis* and the cytolysin from *Stoichactis helianthus***. *Biochim Biophys Acta (BBA) - Biomembranes*, 530 (2), 236-246.

42. Linder, R., Bernheimer, A.W., Kim, K.S. (1977). **Interaction between sphingomyelin and a cytolysin from the sea anemone *Stoichactis helianthus***. *Biochim Biophys Acta (BBA) - Biomembranes*, 467 (3), 290-300.

43. Michaels, D.W. (1979). **Membrane damage by a toxin from the sea anemone *Stoichactis helianthus*. I. Formation of transmembrane channels in lipid bilayers**. *Biochim Biophys Acta (BBA) - Biomembranes*, 555 (1), 67-78.

44. Shin, M.L., Michaels, D.W., Mayer, M.M. (1979). **Membrane damage by a toxin from the sea anemone *Stoichactis helianthus*. II. Effect of membrane lipid composition in a liposome system**. *Biochim Biophys Acta (BBA) - Biomembranes*, 555 (1), 79-88.

45. Kem, W., Doyle, J., Dunn, B., Blumenthal, K., **Purification and Characterization of Sea Anemone (*Stoichactis*) Cytotoxins**, in: Federation Proceedings, vol. 41, Federation Amer Soc Exp Biol 9650 Rockville Pike, Bethesda, MD 20814-3998, 1982, pp. 1643-1643.

46. Blumenthal, K., Kem, W. (1983). **Primary structure of *Stoichactis helianthus* cytolysin III**. *J Biol Chem*, 258 (9), 5574-5581.

47. Kem, W.R., Dunn, B.M. (1988). **Separation and characterization of four different amino acid sequence variants of a sea anemone (*Stichodactyla helianthus*) protein cytolysin**. *Toxicon*, 26 (11), 997-1008.

48. Doyle, J.W., Kem, W.R. (1989). **Binding of a radiolabeled sea anemone cytolysin to erythrocyte membranes**. *Biochim Biophys Acta (BBA) - Biomembranes*, 987 (2), 181-186.

49. Doyle, J.W., Kem, W.R., Vilallonga, F.A. (1989). **Interfacial activity of an ion channel-generating protein cytolysin from the sea anemone *Stichodactyla helianthus***. *Toxicon*, 27 (4), 465-471.

50. Kem, W.R., Parten, B., Pennington, M.W., Price, D.A., Dunn, B.M. (1989). **Isolation, characterization, and amino acid sequence of a polypeptide neurotoxin occurring in the sea anemone *Stichodactyla helianthus***. *Biochemistry*, 28 (8), 3483-3489.

51. Ávila, A., De Acosta, C.M., Lage, A. (1988). **A new immunotoxin built by linking a hemolytic toxin to a monoclonal antibody specific for immature T lymphocytes**. *International journal of cancer*, 42 (4), 568-571.

52. Ávila, A., Mateo Acosta, C.D., Lage, A. (1989). **A carcinoembryonic antigen - directed immunotoxin built by linking a monoclonal antibody to a hemolytic toxin**. *International journal of cancer*, 43 (5), 926-929.

53. Ferlan, I., Lebez, D. (1974). **Equinatoxin, a lethal protein from *Actinia equina*—I Purification and characterization**. *Toxicon*, 12 (1), 57-58.

54. Sket, D., Drašlar, K., Ferlan, I., Lebez, D. (1974). **Equinatoxin, a lethal protein from *Actinia equina*—II. Pathophysiological action**. *Toxicon*, 12 (1), 63-68.

55. Giraldi, T., Ferlan, I., Romeo, D. (1976). **Antitumour activity of equinatoxin**. *Chemico-biological interactions*, 13 (3-4), 199-203.

56. Ferlan, I., Jackson, K.W. (1983). **Partial amino acid sequence of equinatoxin**. *Toxicon*, 21, 141-144.

57. Maček, P., Lebez, D. (1981). **Kinetics of hemolysis induced by equinatoxin, a cytolytic toxin from the sea anemone *Actinia equina*. Effect of some ions and pH**. *Toxicon*, 19 (2), 233-240.

58. Lafranconi, W.M., Ferlan, I., Russell, F.E., Huxtable, R.J. (1984). **The action of equinatoxin, a peptide from the venom of the sea anemone, *Actinia equina*, on the isolated lung**. *Toxicon*, 22 (3), 347-352.

59. Ho, C., Ko, J., Lue, H., Lee, C., Ferlan, I. (1987). **Effects of equinatoxin on the guinea-pig atrium**. *Toxicon*, 25 (6), 659-664.

60. Maček, P., Lebez, D. (1988). **Isolation and characterization of three lethal and hemolytic toxins from the sea anemone *Actinia equina* L**. *Toxicon*, 26 (5), 441-451.

61. Teng, C.-M., Lee, L.-G., Lee, C.-Y., Ferlan, I. (1988). **Platelet aggregation induced by equinatoxin**. *Thrombosis research*, 52 (5), 401-411.

62. Turk, T., Maček, P., Gubensek, F. (1989). **Chemical modification of equinatoxin II, a lethal and cytolytic toxin from the sea anemone *Actinia equina* L**. *Toxicon*, 27 (3), 375-384.

63. Batista, U., Maček, P., Sedmak, B. (1990). **The cytotoxic and cytolytic activity of equinatoxin II from the sea anemone *Actinia equina***. *Cell Biol Int Rep*, 14 (11), 1013-1024.

64. Zorec, R., Tester, M., Maček, P., Mason, W.T. (1990). **Cytotoxicity of equinatoxin II from the sea anemone *Actinia equina* involves ion channel formation and an increase in intracellular calcium activity**. *J Membr Biol*, 118 (3), 243-249.

65. Belmonte, G., Pederzolli, C., Maček, P., Menestrina, G. (1993). **Pore formation by the sea anemone cytolysin equinatoxin-II in red blood cells and model lipid membranes**. *J Membr Biol*, 131, 11-22.

66. Maček, P., Belmonte, G., Pederzolli, C., Menestrina, G. (1994). **Mechanism of action of equinatoxin II, a cytolysin from the sea anemone *Actinia equina* L. belonging to the family of actinoporins**. *Toxicology*, 87 (1-3), 205-227.

67. Belmonte, G., Menestrina, G., Pederzolli, C., Krizaj, I., Gubensek, F., Turk, T., Maček, P. (1994). **Primary and secondary structure of a pore-forming toxin from the sea anemone, *Actinia equina L.*, and its association with lipid vesicles**. *Biochim Biophys Acta (BBA) - Biomembranes*, 1192, 197-204.

68. Anderluh, G., Pungerear, J., Strukelj, B., Maček, P., Gubensk, F. (1996). **Cloning, sequencing and expression of equinatoxin II**. *Biochem Biophys Res Commun*, 220, 437-442.

69. Morera, V., Gómez, J., Besada, V., Estrada, R., Pons, T., Álvarez, C., . . . Pazos, F. (1994). **Primary structure analysis of the haemolytic polypeptide sticholysin isolated from a sea anemone**.

70. Alvarez, C., Tejuca, M., Morera, V., Besada, V., Pazos, F., Veitia, R., . . . Lanio, M. (1994). **Some characteristics of sticholysin: a novel cytolysin from *Stichodactyla helianthus***. *Adv Mod Biotechnol*, 2, 135-146.

71. Alvarez, C., Tejuca, M., Morera, V., Besada, V., Pazos, F., Lanio, M., Padrón, G. (1996). **Novel primary structure of sticholysin and its interaction with membranes**. *Toxicon*, 3 (34), 301.

72. Tejuca, M., Dalla Serra, M., Ferreras, M., Lanio, M.E., Menestrina, G. (1996). **Mechanism of membrane permeabilization by sticholysin I, a cytolysin isolated from the venom of the sea anemone *Stichodactyla helianthus***. *Biochemistry*, 35 (47), 14947-14957.

73. Bellomio, A., Morante, K., Barlič, A., Gutiérrez-Aguirre, I., Viguera, A.R., González-Mañas, J.M. (2009). **Purification, cloning and characterization of fragaceatoxin C, a novel actinoporin from the sea anemone *Actinia fragacea***. *Toxicon*, 54 (6), 869-880.

74. Vincent, J., Balerna, M., Barhanin, J., Fosset, M., Lazdunski, M. (1980). **Binding of sea anemone toxin to receptor sites associated with gating system of sodium channel in synaptic nerve endings in vitro**. *Proc Natl Acad Sci*, 77 (3), 1646-1650.

75. Barhanin, J., Hugues, M., Schweitz, H., Vincent, J.-P., Lazdunski, M. (1981). **Structure-function relationships of sea anemone toxin II from *Anemonia sulcata***. *J Biol Chem*, 256 (11), 5764-5769.

76. Bernheimer, A.W., Avigad, L.S., Lai, C. (1982). **Purification and properties of a toxin from the sea anemone *Condylactis gigantea***. *Arch Biochem Biophys*, 214 (2), 840-845.

77. Bernheimer, A.W., Avigad, L.S. (1982). **Toxins of the sea anemone *Epiactis prolifera***. *Arch Biochem Biophys*, 217 (1), 174-180.

78. Bernheimer, A.W., Avigad, L.S., Branch, G., Dowdle, E., Lai, C.Y. (1984). **Purification and properties of a toxin from the South African sea anemone, *Pseudactinia varia***. *Toxicon*, 22 (2), 183-191.

79. Bernheimer, A.W., Lai, C.Y. (1985). **Properties of a cytolytic toxin from the sea anemone, *Stoichactis kenti***. *Toxicon*, 23 (5), 791-799.

80. El-Sherif, N., Fozzard, H.A., Hanck, D.A. (1992). **Dose-dependent modulation of the cardiac sodium channel by sea anemone toxin ATXII**. *Circulation Research*, 70 (2), 285-301.

81. Khoo, K.S., Kam, W.K., Khoo, H.E., Gopalakrishnakone, P., Chung, M.C. (1993). **Purification and partial characterization of two cytolysins from a tropical sea anemone, *Heteractis magnifica***. *Toxicon*, 31 (12), 1567-1579.

82. Aneiros, A., García, I., Martínez, J.R., Harvey, A.L., Anderson, A.J., Marshall, D.L., . . . Karlsson, E. (1993). **A potassium channel toxin from the secretion of the sea anemone *Bunodosoma granulifera*. Isolation, amino acid sequence and biological activity**. *Biochim Biophys Acta (BBA) - General Subjects*, 1157 (1), 86-92.

83. Tkacheva, E., Leychenko, E., Monastyrnaya, M., Issaeva, M., Zelepuga, E., Anastuk, S., . . . Kozlovskaya, E. (2011). **New actinoporins from sea anemone *Heteractis crispa*: Cloning and functional expression**. *Biochemistry*, 76 (10), 1131.

84. Norton, R.S., Bobek, G., Ivanov, J.O., Thomson, M., Fiala-Beer, E., Moritz, R.L., Simpson, R.J. (1990). **Purification and characterisation of proteins with cardiac stimulatory and haemolytic activity from the anemone *Actinia tenebrosa***. *Toxicon*, 28 (1), 29-41.

85. Jiang, X., Chen, H., Yang, W., Liu, Y., Liu, W., Wei, J., . . . Xu, A. (2003). **Functional expression and characterization of an acidic actinoporin from sea anemone *Sagartia rosea***. *Biochem Biophys Res Commun*, 312 (3), 562-570.

86. Tejuca, M., Dalla Serra, M., Potrich, C., Álvarez, C., Menestrina, G. (2001). **Sizing the Radius of the Pore Formed in Erythrocytes and Lipid Vesicles by the Toxin Sticholysin I from the Sea Anemone *Stichodactyla helianthus***. *J Membr Biol*, 183 (2), 125-135.

87. Saier Jr, M.H., Reddy, V.S., Tsu, B.V., Ahmed, M.S., Li, C., Moreno-Hagelsieb, G. (2016). **The transporter classification database (TCDB): recent advances**. *Nucleic acids research*, 44 (D1), D372-D379.

88. Iacovache, I., van der Goot, F.G., Pernot, L. (2008). **Pore formation: an ancient yet complex form of attack**. *Biochim Biophys Acta (BBA) - Biomembranes*, 1778 (7-8), 1611-1623.

89. Mueller, M., Grauschopf, U., Maier, T., Glockshuber, R., Ban, N. (2009). **The structure of a cytolytic α-helical toxin pore reveals its assembly mechanism**. *Nature*, 459 (7247), 726-730.

90. Mueller, M., Ban, N. (2010). **Enhanced SnapShot: Pore-forming toxins**. *Cell*, 142 (2), 334, 334 e331.

91. Geny, B., Popoff, M.R. (2006). **Bacterial protein toxins and lipids: pore formation or toxin entry into cells**. *Biol Cell*, 98 (11), 667-678.

92. González, M.R., Bischofberger, M., Pernot, L., van der Goot, F.G., Freche, B. (2008). **Bacterial pore-forming toxins: the (w)hole story?** *Cell Mol Life Sci*, 65 (3), 493-507.

93. Law, R.H., Lukoyanova, N., Voskoboinik, I., Caradoc-Davies, T.T., Baran, K., Dunstone, M.A., . . . Whisstock, J.C. (2010). **The structural basis for membrane binding and pore formation by lymphocyte perforin**. *Nature*, 468 (7322), 447-451.

94. Basulto, A., Pérez, V.M., Noa, Y., Varela, C., Otero, A.J., Pico, M.C. (2006). **Immunohistochemical targeting of sea anemone cytolysins on tentacles, mesenteric filaments and isolated nematocysts of *Stichodactyla helianthus***. *J Exp Zoolog A Comp Exp Biol*, 305 (3), 253-258.

95. Rivera-de-Torre, E., García-Linares, S., Alegre-Cebollada, J., Lacadena, J., Gavilanes, J.G., Martínez-del-Pozo, A. (2016). **Synergistic action of actinoporin isoforms from the same sea anemone species assembled into functionally active heteropores**. *J Biol Chem*, 291 (27), 14109-14119.

96. Wang, Y., Yap, L.L., Chua, K.L., Khoo, H.E. (2008). **A multigene family of *Heteractis* magnificalysins (HMgs)**. *Toxicon*, 51 (8), 1374-1382.

97. Monastyrnaya, M., Leychenko, E., Isaeva, M., Likhatskaya, G., Zelepuga, E., Kostina, E., . . . Kozlovskaya, E. (2010). **Actinoporins from the sea anemones, tropical *Radianthus***

***macrodactylus* and northern *Oulactis orientalis*: Comparative analysis of structure-function relationships**. *Toxicon*, 56 (8), 1299-1314.

98. Turk, T. (1991). **Cytolytic toxins from sea anemones**. *Toxin Reviews*, 10 (3), 223-262.

99. De los Ríos, V., Oñaderra, M., Martínez-Ruiz, A., Lacadena, J., Mancheño, J.M., Martínez-del-Pozo, A., Gavilanes, J.G. (2000). **Overproduction in *Escherichia coli* and purification of the hemolytic protein sticholysin II from the sea anemone *Stichodactyla helianthus***. *Protein Expr Purif*, 18 (1), 71-76.

100. The-UniProt-Consortium. (2018). **UniProt: a worldwide hub of protein knowledge**. *Nucleic Acids Research*, 47 (D1), D506-D515.

101. Hoang, Q.T., Cho, S.H., McDaniel, S.F., Ok, S.H., Quatrano, R.S., Shin, J.S. (2009). **An actinoporin plays a key role in water stress in the moss *Physcomitrella patens***. *New Phytol*, 184 (2), 502-510.

102. Hong, Q., Gutiérrez-Aguirre, I., Barlič, A., Malovrh, P., Kristan, K., Podlesek, Z., . . . Anderluh, G. (2002). **Two-step Membrane Binding by Equinatoxin II, a Pore-forming Toxin from the Sea Anemone, Involves an Exposed Aromatic Cluster and a Flexible Helix**. *J Biol Chem*, 277 (44), 41916-41924.

103. Norton, R.S. (2009). **Structures of sea anemone toxins**. *Toxicon*, 54 (8), 1075-1088.

104. Malovrh, P., Viero, G., Serra, M.D., Podlesek, Z., Lakey, J.H., Maček, P., . . . Anderluh, G. (2003). **A novel mechanism of pore formation: membrane penetration by the N-terminal amphipathic region of equinatoxin**. *J Biol Chem*, 278 (25), 22678-22685.

105. Kristan, K., Podlesek, Z., Hojnik, V., Gutiérrez-Aguirre, I., Guncar, G., Turk, D., . . . Anderluh, G. (2004). **Pore Formation by Equinatoxin, a Eukaryotic Pore-forming Toxin, Requires a Flexible N-terminal Region and a Stable b-Sandwich**. *J Biol Chem*, 279 (45), 46509-46517.

106. Alegre-Cebollada, J., Martínez-del-Pozo, A., Gavilanes, J.G., Goormaghtigh, E. (2007). **Infrared spectroscopy study on the conformational changes leading to pore formation of the toxin sticholysin II**. *Biophys J*, 93 (9), 3191-3201.

107. Alegre-Cebollada, J., Cunietti, M., Herrero-Galán, E., Gavilanes, J.G., Martínez-del-Pozo, A. (2008). **Calorimetric scrutiny of lipid binding by sticholysin II toxin mutants**. *J Mol Biol*, 382 (4), 920-930.

108. Pettersen, E.F., Goddard, T.D., Huang, C.C., Couch, G.S., Greenblatt, D.M., Meng, E.C., Ferrin, T.E. (2004). **UCSF Chimera--a visualization system for exploratory research and analysis**. *J Comput Chem*, 25 (13), 1605-1612.

109. Casallanovo, F., de Oliveira, F.J., de Souza, F.C., Ros, U., Martínez, Y., Penton, D., . . . Schreier, S. (2006). **Model peptides mimic the structure and function of the N-terminus of the pore-forming toxin sticholysin II**. *Biopolymers*, 84 (2), 169-180.

110. Lima de Oliveira, A., Maffud Cilli, E., Ros, U., Crusca, E., Jr., Lanio, M.E., Alvarez, C., . . . Spisni, A. (2018). **Insights on the structure-activity relationship of peptides derived from Sticholysin II**. *Peptide Science*, 110 (5), e23097.

111. Ros, U., Pedrera, L., Diaz, D., Karam, J.C., Sudbrack, T.P., Valiente, P.A., . . . Avarez, C. (2012). **The membranotropic activity of N-terminal peptides from the pore-forming**

proteins sticholysin I and II is modulated by hydrophobic and electrostatic interactions as well as lipid composition. *J Biosci*, 36 (5), 781-791.

112. Morante, K., Caaveiro, J.M., Tanaka, K., González-Mañas, J.M., Tsumoto, K. (2015). **A pore-forming toxin requires a specific residue for its activity in membranes with particular physicochemical properties**. *J Biol Chem*, 290 (17), 10850-10861.

113. García-Linares, S., Alm, I., Maula, T., Gavilanes, J.G., Slotte, J.P., Martínez-del-Pozo, A. (2015). **The effect of cholesterol on the long-range network of interactions established among sea anemone Sticholysin II residues at the water-membrane interface**. *Mar Drugs*, 13 (4), 1647-1665.

114. Rivera-de-Torre, E., Palacios-Ortega, J., García-Linares, S., Gavilanes, J.G., Martínez-del-Pozo, A. (2017). **One single salt bridge explains the different cytolytic activities shown by actinoporins sticholysin I and II from the venom of *Stichodactyla helianthus***. *Arch Biochem Biophys*, 636, 79-89.

115. Casallanovo, F., de Oliveira, F.J.F., Souto, A.L.C.F., de Souza, F.C., Cilli, E.M., Martínez, Y., . . . Álvarez, C., **Peptides from the N-terminal domain of a pore-forming toxin, Sticholysin II. Conformation and activity.**, in: 48th Annual Meeting of the Biophysical Society, Biophys J, *Baltimore, MD*, 2004.

116. Ros, U., Souto, A.L., de Oliveira, F.J., Crusca, E., Jr., Pazos, F., Cilli, E.M., . . . Alvarez, C. (2013). **Functional and topological studies with Trp-containing analogs of the peptide StII1-30 derived from the N-terminus of the pore forming toxin sticholysin II: contribution to understand its orientation in membrane**. *Biopolymers*, 100 (4), 337-346.

117. De Planque, M.R., Kruijtzer, J.A., Liskamp, R.M., Marsh, D., Greathouse, D.V., Koeppe, R.E., 2nd, . . . Killian, J.A. (1999). **Different membrane anchoring positions of tryptophan and lysine in synthetic transmembrane a-helical peptides**. *J Biol Chem*, 274 (30), 20839-20846.

118. Alegre-Cebollada, J., Lacadena, V., Oñaderra, M., Mancheño, J.M., Gavilanes, J.G., Martínez-del-Pozo, A. (2004). **Phenotypic selection and characterization of randomly produced non-haemolytic mutants of the toxic sea anemone protein sticholysin II**. *FEBS Lett*, 575 (1-3), 14-18.

119. Anderluh, G., Razpotnik, A., Podlesek, Z., Maček, P., Separovic, F., Norton, R.S. (2005). **Interaction of the eukaryotic pore-forming cytolysin equinatoxin II with model membranes: ^{19}F NMR studies**. *J Mol Biol*, 347 (1), 27-39.

120. Bakrač, B., Gutierrez-Aguirre, I., Podlesek, Z., Sonnen, A.F., Gilbert, R.J., Maček, P., . . . Anderluh, G. (2008). **Molecular determinants of sphingomyelin specificity of a eukaryotic pore-forming toxin**. *J Biol Chem*, 283 (27), 18665-18677.

121. Pardo-Cea, M.A., Alegre-Cebollada, J., Martínez-del-Pozo, A., Gavilanes, J.G., Bruix, M. (2010). **^{1}H, ^{13}C, and ^{15}N NMR assignments of StnII-Y111N, a highly impaired mutant of the sea anemone actinoporin Sticholysin II**. *Biomol NMR Assign*, 4 (1), 69-72.

122. Pardo-Cea, M.A., Castrillo, I., Alegre-Cebollada, J., Martínez-del-Pozo, A., Gavilanes, J.G., Bruix, M. (2011). **Intrinsic local disorder and a network of charge-charge**

interactions are key to actinoporin membrane disruption and cytotoxicity. *FEBS J*, 278 (12), 2080-2089.

123. Maula, T., Isaksson, Y.J., García-Linares, S., Niinivehmas, S., Pentikainen, O.T., Kurita, M., . . . Slotte, J.P. (2013). **2NH and 3OH are crucial structural requirements in sphingomyelin for sticholysin II binding and pore formation in bilayer membranes**. *Biochim Biophys Acta (BBA) - Biomembranes*, 1828 (5), 1390-1395.

124. Bakrač, B., Kladnik, A., Maček, P., McHaffie, G., Werner, A., Lakey, J.H., Anderluh, G. (2010). **A toxin-based probe reveals cytoplasmic exposure of golgi sphingomyelin**. *J Biol Chem*, 285 (29), 22186-22195.

125. Yeagle, P.L. 2004. **The structure of biological membranes**, CRC press.

126. Yeagle, P.L. 2016. **The membranes of cells**, Academic Press.

127. Tanford, C. (1978). **The hydrophobic effect and the organization of living matter**. *Science*, 200 (4345), 1012-1018.

128. Voelker, D.R., **Lipid assembly into cell membranes**, in: Biochemistry of Lipids, Lipoproteins and Membranes, Elsevier, 2008, pp. 441-484.

129. Nyholm, T.K., Lindroos, D., Westerlund, B., Slotte, J.P. (2011). **Construction of a DOPC/PSM/cholesterol phase diagram based on the fluorescence properties of trans-parinaric acid**. *Langmuir*, 27 (13), 8339-8350.

130. Björkqvist, Y.J., Nyholm, T.K., Slotte, J.P., Ramstedt, B. (2005). **Domain formation and stability in complex lipid bilayers as reported by cholestatrienol**. *Biophys J*, 88 (6), 4054-4063.

131. Engberg, O., Yasuda, T., Hautala, V., Matsumori, N., Nyholm, T.K., Murata, M., Slotte, J.P. (2016). **Lipid Interactions and Organization in Complex Bilayer Membranes**. *Biophys J*, 110 (7), 1563-1573.

132. Klose, C., Ejsing, C.S., García-Sáez, A.J., Kaiser, H.-J., Sampaio, J.L., Surma, M.A., . . . Simons, K. (2010). **Yeast lipids can phase-separate into micrometer-scale membrane domains**. *J Biol Chem*, 285 (39), 30224-30232.

133. De Almeida, R.F., Fedorov, A., Prieto, M. (2003). **Sphingomyelin-Phosphatidylcholine-Cholesterol phase diagram: boundaries and composition of lipid rafts**. *Biophys J*, 85 (4), 2406-2416.

134. De Almeida, R.F., Loura, L.M., Fedorov, A., Prieto, M. (2005). **Lipid rafts have different sizes depending on membrane composition: a time-resolved fluorescence resonance energy transfer study**. *J Mol Biol*, 346 (4), 1109-1120.

135. Nyholm, T.K., Nylund, M., Slotte, J.P. (2003). **A calorimetric study of binary mixtures of dihydrosphingomyelin and sterols, sphingomyelin, or phosphatidylcholine**. *Biophys J*, 84 (5), 3138-3146.

136. Cooper, G.M., Hausman, R., **A molecular approach**, in: The Cell., Sunderland, MA: Sinauer Associates, 2000.

137. Van Meer, G., Voelker, D.R., Feigenson, G.W. (2008). **Membrane lipids: where they are and how they behave**. *Nature reviews: Molecular cell biology*, 9 (2), 112-124.

138. Cevc, G. (1987). **How membrane chain melting properties are regulated by the polar surface of the lipid bilayer**. *Biochemistry*, 26 (20), 6305-6310.

139. Cevc, G., Watts, A., Marsh, D. (1981). **Titration of the phase transition of phosphatidylserine bilayer membranes. Effects of pH, surface electrostatics, ion binding, and head-group hydration**. *Biochemistry*, 20 (17), 4955-4965.

140. Jouhet, J. (2013). **Importance of the hexagonal lipid phase in biological membrane organization**. *Frontiers in plant science*, 4, 494.

141. Kumar, V. (1991). **Complementary molecular shapes and additivity of the packing parameter of lipids**. *Proc Natl Acad Sci*, 88 (2), 444-448.

142. Yeagle, P.L. (1985). **Cholesterol and the cell membrane**. *Biochim Biophys Acta (BBA) - Reviews on Biomembranes*, 822 (3-4), 267-287.

143. Shieh, H.-S., Hoard, L., Nordman, C. (1981). **The structure of cholesterol**. *Acta Crystallographica Section B: Structural Crystallography Crystal Chemistry*, 37 (8), 1538-1543.

144. Sankaram, M.B., Thompson, T.E. (1990). **Modulation of phospholipid acyl chain order by cholesterol. A solid-state deuterium nuclear magnetic resonance study**. *Biochemistry*, 29 (47), 10676-10684.

145. Lönnfors, M., Doux, J.P., Killian, J.A., Nyholm, T.K., Slotte, J.P. (2011). **Sterols Have Higher Affinity for Sphingomyelin than for Phosphatidylcholine Bilayers even at Equal Acyl-Chain Order**. *Biophys J*, 100 (11), 2633-2641.

146. Slotte, J.P. (2016). **The importance of hydrogen bonding in sphingomyelin's membrane interactions with co-lipids**. *Biochim Biophys Acta (BBA) - Biomembranes*, 1858 (2), 304-310.

147. Ramstedt, B., Slotte, J.P. (2002). **Membrane properties of sphingomyelins**. *FEBS Lett*, 531 (1), 33-37.

148. Jain, M.K., Wagner, R.C., **Introduction to biological membranes**, in, Wiley New York, 1988.

149. Silvius, J.R., Delgiudice, D., Lafleur, M. (1996). **Cholesterol at different bilayer concentrations can promote or antagonize lateral segregation of phospholipids of differing acyl chain length**. *Biochemistry*, 35 (48), 15198-15208.

150. Valcarcel, C.A., Dalla Serra, M., Potrich, C., Bernhart, I., Tejuca, M., Martínez, D., . . . Menestrina, G. (2001). **Effects of lipid composition on membrane permeabilization by sticholysin I and II, two cytolysins of the sea anemone *Stichodactyla helianthus***. *Biophys J*, 80 (6), 2761-2774.

151. Alegre-Cebollada, J., Rodríguez-Crespo, I., Gavilanes, J.G., Martínez-del-Pozo, A. (2006). **Detergent-resistant membranes are platforms for actinoporin pore-forming activity on intact cells**. *FEBS J*, 273 (4), 863-871.

152. Bakrač, B., Anderluh, G. (2009). **Molecular mechanism of sphingomyelin-specific membrane binding and pore formation by actinoporins**. *Avd Exp Med Biol*, 677, 106-115.

153. Rojko, N., Dalla Serra, M., Maček, P., Anderluh, G. (2016). **Pore formation by actinoporins, cytolysins from sea anemones**. *Biochim Biophys Acta (BBA) - Biomembranes*, 1858 (3), 446-456.

154. Martínez, D., Campos, A.M., Pazos, F., Álvarez, C., Lanio, M.E., Casallanovo, F., . . . Lissi, E. (2001). **Properties of St I and St II, two isotoxins isolated from *Stichodactyla helianthus*: a comparison**. *Toxicon*, 39 (10), 1547-1560.

155. Busto, J.V., Fanani, M.L., De Tullio, L., Sot, J., Maggio, B., Goni, F.M., Alonso, A. (2009). **Coexistence of immiscible mixtures of palmitoylsphingomyelin and palmitoylceramide in monolayers and bilayers**. *Biophys J*, 97 (10), 2717-2726.

156. Castro, B.M., de Almeida, R.F., Silva, L.C., Fedorov, A., Prieto, M. (2007). **Formation of ceramide/sphingomyelin gel domains in the presence of an unsaturated phospholipid: a quantitative multiprobe approach**. *Biophys J*, 93 (5), 1639-1650.

157. Chiantia, S., Kahya, N., Ries, J., Schwille, P. (2006). **Effects of ceramide on liquid-ordered domains investigated by simultaneous AFM and FCS**. *Biophys J*, 90 (12), 4500-4508.

158. Meinardi, E., Florin-Christensen, M., Paratcha, G., Azcurra, J.M., Florin-Christensen, J. (1995). **The molecular basis of the self/nonself selectivity of a coelenterate toxin**. *Biochem Biophys Res Commun*, 216 (1), 348-354.

159. Anderluh, G., Podlesek, Z., Maček, P. (2000). **A common motif in proparts of Cnidarian toxins and nematocyst collagens and its putative role**. *Biochim Biophys Acta (BBA) - Protein Structure Molecular Enzymology*, 1476 (2), 372-376.

160. Meinardi, E., Azcurra, J.M., Florin-Christensen, M., Florin-Christensen, J. (1994). **Coelenterolysin: a hemolytic polypeptide associated with the coelenteric fluid of sea anemones**. *Comparative Biochemistry Physiology Part B: Comparative Biochemistry*, 109 (1), 153-161.

161. Hori, T., Nozawa, Y., **Phosphonolipids**, in: New comprehensive biochemistry, vol. 4, Elsevier, 1982, pp. 95-128.

162. Hilderbrand, R.L., Henderson, T.O., **Phosphonic acids in nature**, in: The role of phosphonates in living systems, 1983, pp. 5-30.

163. Simon, G., Rouser, G. (1967). **Phospholipids of the sea anemone: Quantitative distribution; absence of carbon - phosphorus linkages in glycerol phospholipids; structural elucidation of ceramide aminoethylphosphonate**. *Lipids*, 2 (1), 55-59.

164. Joseph, J.D. (1979). **Lipid composition of marine and estuarine invertebrates: Porifera and Cnidaria**. *Progress in lipid research*, 18 (1), 1-30.

165. Nelson, M.M., Phleger, C.F., Mooney, B.D., Nichols, P.D. (2000). **Lipids of gelatinous Antarctic zooplankton: Cnidaria and Ctenophora**. *Lipids*, 35 (5), 551-559.

166. Meneses, P., Navarro, N. (1992). **^{31}P NMR phospholipid profile study of seven sea anemone species**. *Comparative Biochemistry Physiology Part B: Comparative Biochemistry*, 102 (2), 403-407.

167. Huang, J., Buboltz, J.T., Feigenson, G.W. (1999). **Maximum solubility of cholesterol in phosphatidylcholine and phosphatidylethanolamine bilayers**. *Biochim Biophys Acta (BBA) - Biomembranes*, 1417 (1), 89-100.

168. Björkbom, A., Róg, T., Kaszuba, K., Kurita, M., Yamaguchi, S., Lönnfors, M., . . . Slotte, J.P. (2010). **Effect of Sphingomyelin Headgroup Size on Molecular Properties and Interactions with Cholesterol**. *Biophys J*, 99 (10), 3300-3308.

169. Jaikishan, S., Björkbom, A., Slotte, J.P. (2010). **Sphingomyelin analogs with branched N-acyl chains: the position of branching dramatically affects acyl chain order and sterol interactions in bilayer membranes**. *Biochim Biophys Acta (BBA) - Biomembranes*, 1798 (10), 1987-1994.

170. Feinstein, M., Fernandez, S., Sha'Afi, R. (1975). **Fluidity of natural membranes and phosphatidylserine and ganglioside dispersions: Effects of local anesthetics, cholesterol and protein**. *Biochim Biophys Acta (BBA) - Biomembranes*, 413 (3), 354-370.

171. Aittoniemi, J., Rog, T., Niemelä, P., Pasenkiewicz-Gierula, M., Karttunen, M., Vattulainen, I. (2006). **Tilt: major factor in sterols' ordering capability in membranes**. *The Journal of Physical Chemistry B*, 110 (51), 25562-25564.

172. Róg, T., Pasenkiewicz-Gierula, M. (2006). **Cholesterol-sphingomyelin interactions: a molecular dynamics simulation study**. *Biophys J*, 91 (10), 3756-3767.

173. Bruzik, K.S., Sobon, B., Salamonczyk, G.M. (1990). **Nuclear magnetic resonance study of sphingomyelin bilayers**. *Biochemistry*, 29 (16), 4017-4021.

174. Cosentino, K., Ros, U., García-Sáez, A.J. (2016). **Assembling the puzzle: Oligomerization of a-pore forming proteins in membranes**. *Biochim Biophys Acta (BBA) - Biomembranes*, 1858 (3), 457-466.

175. Álvarez, C., Mancheño, J.M., Martínez, D., Tejuca, M., Pazos, F., Lanio, M.E. (2009). **Sticholysins, two pore-forming toxins produced by the Caribbean sea anemone *Stichodactyla helianthus*: Their interaction with membranes**. *Toxicon*, 54 (8), 1135-1147.

176. Martínez, D., Álvarez, C., Tejuca, M., Pazos, F., Valle, A., Calderón, L., . . . Lanio, M.E. (2006). **Los lípidos de la membrana actúan como moduladores de la actividad permeabilizante de Sticholisina II, una toxina formadora de poros con aplicaciones biomédicas.** *Biología Aplicada*, 23 (3), 251-254.

177. Anderluh, G., Dalla Serra, M., Viero, G., Guella, G., Maček, P., Menestrina, G. (2003). **Pore formation by equinatoxin II, a eukaryotic protein toxin, occurs by induction of nonlamellar lipid structures**. *J Biol Chem*, 278 (46), 45216-45223.

178. Ruoslahti, E. (1988). **Fibronectin and its receptors**. *Annual review of biochemistry*, 57 (1), 375-413.

179. García-Linares, S., Richmond, R., García-Mayoral, M.F., Bustamante, N., Bruix, M., Gavilanes, J.G., Martínez-del-Pozo, A. (2014). **The sea anemone actinoporin (Arg-Gly-Asp) conserved motif is involved in maintaining the competent oligomerization state of these pore-forming toxins**. *FEBS J*, 281 (5), 1465-1478.

180. Tanaka, K., Caaveiro, J.M.M., Morante, K., Tsumoto, K. (2017). **Haemolytic actinoporins interact with carbohydrates using their lipid-binding module**. *Philos Trans R Soc Lond B Biol Sci*, 372 (1726), 20162016.

181. García-Linares, S., Rivera-de-Torre, E., Palacios-Ortega, J., Gavilanes, J.G., Martínez-del-Pozo, A., **The metamorphic transformation of a water-soluble monomeric protein into an oligomeric transmembrane pore**, in: Iglič, A., Rappolt, M., García-Sáez, A.J. (Eds.) Advances in Biomembranes and Lipid Self-Assembly, vol. 26, 2017, pp. 51-97.

182. García-Ortega, L., Alegre-Cebollada, J., García-Linares, S., Bruix, M., Martínez-del-Pozo, A., Gavilanes, J.G. (2011). **The behavior of sea anemone actinoporins at the water-membrane interface**. *Biochim Biophys Acta (BBA) - Biomembranes*, 1808 (9), 2275-2288.

183. Castrillo, I., Araujo, N.A., Alegre-Cebollada, J., Gavilanes, J.G., Martínez-del-Pozo, A., Bruix, M. (2010). **Specific interactions of sticholysin I with model membranes: an NMR study**. *Proteins*, 78 (8), 1959-1970.

184. De los Ríos, V., Mancheño, J.M., Martínez-del-Pozo, A., Alfonso, C., Rivas, G., Oñaderra, M., Gavilanes, J.G. (1999). **Sticholysin II, a cytolysin from the sea anemone *Stichodactyla helianthus*, is a monomer-tetramer associating protein**. *FEBS Lett*, 455 (1-2), 27-30.

185. Morante, K., Bellomio, A., Gil-Carton, D., Redondo-Morata, L., Sot, J., Scheuring, S., . . . Caaveiro, J.M.M. (2016). **Identification of a Membrane-bound Prepore Species Clarifies the Lytic Mechanism of Actinoporins**. *Journal of Biological Chemistry*, 291 (37), 19210-19219.

186. Rojko, N., Kristan, K.C., Viero, G., Zerovnik, E., Maček, P., Dalla Serra, M., Anderluh, G. (2013). **Membrane damage by an a-helical pore-forming protein, Equinatoxin II, proceeds through a succession of ordered steps**. *J Biol Chem*, 288 (33), 23704-23715.

187. Subburaj, Y., Ros, U., Hermann, E., Tong, R., García-Sáez, A.J. (2015). **Toxicity of an a-pore-forming toxin depends on the assembly mechanism on the target membrane as revealed by single-molecule imaging**. *J Biol Chem*, 290 (8), 4856-4865.

188. Valle, A., Lopez-Castilla, A., Pedrera, L., Martinez, D., Tejuca, M., Campos, J., . . . Schreier, S. (2011). **Cys mutants in functional regions of Sticholysin I clarify the participation of these residues in pore formation**. *Toxicon*, 58 (1), 8-17.

189. Martín-Benito, J., Gavilanes, F., de Los Ríos, V., Mancheño, J.M., Fernández, J.J., Gavilanes, J.G. (2000). **Two-dimensional crystallization on lipid monolayers and three-dimensional structure of sticholysin II, a cytolysin from the sea anemone *Stichodactyla helianthus***. *Biophys J*, 78 (6), 3186-3194.

190. Rojko, N., Cronin, B., Danial, J.S., Baker, M.A., Anderluh, G., Wallace, M.I. (2014). **Imaging the lipid-phase-dependent pore formation of equinatoxin II in droplet interface bilayers**. *Biophys J*, 106 (8), 1630-1637.

191. Antonini, V., Perez-Barzaga, V., Bampi, S., Penton, D., Martinez, D., Dalla Serra, M., Tejuca, M. (2014). **Functional Characterization of Sticholysin I and W111C Mutant Reveals the Sequence of the Actinoporin's Pore Assembly**. *PLoS One*, 9 (10), e110824.

192. Baker, M.A., Rojko, N., Cronin, B., Anderluh, G., Wallace, M.I. (2014). **Photobleaching Reveals Heterogeneous Stoichiometry for Equinatoxin II Oligomers**. *Chembiochem*, 15 (14), 2139-2145.

193. Kristan, K., Viero, G., Maček, P., Dalla Serra, M., Anderluh, G. (2007). **The equinatoxin N-terminus is transferred across planar lipid membranes and helps to stabilize the transmembrane pore**. *FEBS J*, 274 (2), 539-550.

194. Cohen, R., Barenholz, Y., Gatt, S., Dagan, A. (1984). **Preparation and characterization of well defined D-*erythro* sphingomyelins**. *Chemistry and physics of lipids*, 35 (4), 371-384.

195. Fischer, R.T., Stephenson, F.A., Shafiee, A., Schroeder, F. (1984). **$\Delta^{5,7,9(11)}$-Cholestatrien-3β-ol: A fluorescent cholesterol analogue**. *Chemistry and physics of lipids*, 36 (1), 1-14.

196. Térová, B., Slotte, J.P., Nyholm, T.K. (2004). **Miscibility of acyl-chain defined phosphatidylcholines with N-palmitoyl sphingomyelin in bilayer membranes**. *Biochim Biophys Acta*, 1667 (2), 182-189.

197. Alegre-Cebollada, J., Clementi, G., Cunietti, M., Porres, C., Oñaderra, M., Gavilanes, J.G., Martínez-del-Pozo, A. (2007). **Silent mutations at the 5'-end of the cDNA of actinoporins from the sea anemone *Stichodactyla helianthus* allow their heterologous overproduction in *Escherichia coli***. *J Biotechnol*, 127 (2), 211-221.

198. García-Linares, S., Maula, T., Rivera-de-Torre, E., Gavilanes, J.G., Slotte, J.P., Martínez-del-Pozo, A. (2016). **Role of the tryptophan residues in the specific interaction of the sea anemone *Stichodactyla helianthus*'s actinoporin Sticholysin II with biological membranes**. *Biochemistry*, 55 (46), 6406-6420.

199. Ho, S.F., Hunt, H.D., Horton, R.M., Pullen, J.K. and Pease, L.R. (1989). **Site-directed mutagenesis by overlap extension using the polymerase chain reaction**. *Gene*, 77 (1), 51-59.

200. Lakowicz, J.R. 2006. **Principles of fluorescence spectroscopy**, Springer Science & Business Media.

201. Melo, A.M., Fedorov, A., Prieto, M., Coutinho, A. (2014). **Exploring homo-FRET to quantify the oligomer stoichiometry of membrane-bound proteins involved in a cooperative partition equilibrium**. *Physical Chemistry Chemical Physics*, 16 (34), 18105-18117.

202. Valeur, B., Berberan-Santos, M.N., **Molecular Fluorescence, Principles and Applications**, in, Wiley-VCH Verlag GmbH & Co. KGaA, 2012.

203. Wimley, W.C. (2015). **Determining the Effects of Membrane-Interacting Peptides on Membrane Integrity**. *Methods Mol Biol*, 1324, 89-106.

204. Rouser, G., Fkeischer, S., Yamamoto, A. (1970). **Two dimensional thin layer chromatographic separation of polar lipids and determination of phospholipids by phosphorus analysis of spots**. *Lipids*, 5 (5), 494-496.

205. Andersson, A., Danielsson, J., Gräslund, A., Mäler, L. (2007). **Kinetic models for peptide-induced leakage from vesicles and cells**. *Eur Biophys J*, 36 (6), 621-635.

206. Schroeder, F., Nemecz, G., Gratton, E., Barenholz, Y., Thompson, T.E. (1988). **Fluorescence properties of cholestatrienol in phosphatidylcholine bilayer vesicles**. *Biophys Chem*, 32 (1), 57-72.

207. Davenport, L., Dale, R.E., Bisby, R.H., Cundall, R.B. (1985). **Transverse location of the fluorescent probe 1,6-diphenyl-1,3,5-hexatriene in model lipid bilayer membrane systems by resonance excitation energy transfer**. *Biochemistry*, 24 (15), 4097-4108.

208. Heymann, J.B., Zakharov, S.D., Zhang, Y.L., Cramer, W.A. (1996). **Characterization of electrostatic and nonelectrostatic components of protein membrane binding interactions**. *Biochemistry*, 35, 2717-2725.

209. Hille, J.D., Donne-Op den Kelder, G.M., Sauve, P., De Haas, G.H., Egmond, M.R. (1981). **Physicochemical studies on the interaction of pancreatic phospholipase A2 with a micellar substrate analog**. *Biochemistry*, 20 (14), 4068-4073.

210. Wiseman, T., Williston, S., Brandts, J.F., Lin, L.-N. (1989). **Rapid measurement of binding constants and heats of binding using a new titration calorimeter**. *Analytical biochem*, 179 (1), 131-137.

211. Hresko, R.C., Sugar, I.P., Barenholz, Y., Thompson, T.E. (1986). **Lateral distribution of a pyrene-labeled phosphatidylcholine in phosphatidylcholine bilayers: fluorescence phase and modulation study**. *Biochemistry*, 25 (13), 3813-3823.

212. Hresko, R.C., Sugar, I.P., Barenholz, Y., Thompson, T.E. (1987). **The lateral distribution of pyrene-labeled sphingomyelin and glucosylceramide in phosphatidylcholine bilayers**. *Biophys J*, 51 (5), 725-733.

213. Jones, M.E., Lentz, B.R. (1986). **Phospholipid lateral organization in synthetic membranes as monitored by pyrene-labeled phospholipids: effects of temperature and prothrombin fragment 1 binding**. *Biochemistry*, 25 (3), 567-574.

214. Kullberg, A., Ekholm, O.O., Slotte, J.P. (2016). **Miscibility of Sphingomyelins and Phosphatidylcholines in Unsaturated Phosphatidylcholine Bilayers**. *Biophys J*, 109 (9), 1907-1916.

215. Wang, T.Y., Silvius, J.R. (2003). **Sphingolipid partitioning into ordered domains in cholesterol-free and cholesterol-containing lipid bilayers**. *Biophys J*, 84 (1), 367-378.

216. Koivusalo, M., Alvesalo, J., Virtanen, J.A., Somerharju, P. (2004). **Partitioning of pyrene-labeled phospho- and sphingolipids between ordered and disordered bilayer domains**. *Biophys J*, 86 (2), 923-935.

217. Holt, A., de Almeida, R.F., Nyholm, T.K., Loura, L.M., Daily, A.E., Staffhorst, R.W., . . . Killian, J.A. (2008). **Is there a preferential interaction between cholesterol and tryptophan residues in membrane proteins?** *Biochemistry*, 47 (8), 2638-2649.

218. Runnels, L.W., Scarlata, S.F. (1995). **Theory and application of fluorescence homotransfer to melittin oligomerization**. *Biophys J*, 69, 1569-1583.

219. Kristan, K.C., Viero, G., Dalla Serra, M., Maček, P., Anderluh, G. (2009). **Molecular mechanism of pore formation by actinoporins**. *Toxicon*, 54 (8), 1125-1134.

220. Lewis, B.A., Engelman, D.M. (1983). **Lipid bilayer thickness varies linearly with acyl chain length in fluid phosphatidylcholine vesicles**. *J Mol. Biol.*, 166 (2), 211-217.

221. Marsh, D. (1999). **Thermodynamic analysis of chain-melting transition temperatures for monounsaturated phospholipid membranes: dependence on *cis*-monoenoic double bond position**. *Biophys J*, 77 (2), 953-963.

222. Wang, Z.-q., Lin, H., Li, S., Huang, C.-H. (1994). **Calorimetric studies and molecular mechanics simulations of monounsaturated phosphatidylethanolamine bilayers**. *J Biol Chem*, 269 (38), 23491-23499.

223. Stockton, G.W., Smith, I.C. (1976). **A deuterium nuclear magnetic resonance study of the condensing effect of cholesterol on egg phosphatidylcholine bilayer membranes. I. Perdeuterated fatty acid probes**. *Chem Phys Lipids*, 17 (2-3), 251-263.

224. Kučerka, N., Nieh, M.-P., Pencer, J., Sachs, J.N., Katsaras, J. (2009). **What determines the thickness of a biological membrane**. *J Gen Physiol Biophys*, 28 (2), 117-125.

225. Seelig, J. (1997). **Titration calorimetry of lipid-peptide interactions**. *Biochim Biophys Acta (BBA) - Reviews on Biomembranes*, 1 (1331), 103-116.

226. Nyholm, T.K., Grandell, P.-M., Westerlund, B., Slotte, J.P. (2010). **Sterol affinity for bilayer membranes is affected by their ceramide content and the ceramide chain length**. *Biochim Biophys Acta (BBA) - Biomembranes*, 1798 (5), 1008-1013.

227. Westerlund, B., Grandell, P.-M., Isaksson, Y.J.E., Slotte, J.P. (2010). **Ceramide acyl chain length markedly influences miscibility with palmitoyl sphingomyelin in bilayer membranes**. *Eur Biophys J*, 39 (8), 1117-1128.

228. Eftink, M.R., **Fluorescence quenching reactions**, in: Biophysical and biochemical aspects of fluorescence spectroscopy, Springer, 1991, pp. 1-41.

229. Morante, K., Caaveiro, J.M., Viguera, A.R., Tsumoto, K., González-Mañas, J.M. (2015). **Functional characterization of Val60, a key residue involved in the membrane-oligomerization of fragaceatoxin C, an actinoporin from *Actinia fragacea***. *FEBS Lett*, 589 (15), 1840-1846.

230. Carretero, G.P.B., Vicente, E.F., Cilli, E.M., Alvarez, C.M., Jenssen, H., Schreier, S. (2018). **Dissecting the mechanism of action of actinoporins. Role of the N-terminal amphipathic alpha-helix in membrane binding and pore activity of sticholysins I and II**. *PLoS One*, 13 (8), e0202981.

231. Soto, C., Del Valle, A., Valiente, P.A., Ros, U., Lanio, M.E., Hernandez, A.M., Alvarez, C. (2017). **Differential binding and activity of the pore-forming toxin sticholysin II in model membranes containing diverse ceramide-derived lipids**. *Biochimie*, 138, 20-31.

232. Ros, U., Carretero, G.P.B., Paulino, J., Crusca, E., Jr., Pazos, F., Cilli, E.M., . . . Alvarez, C. (2019). **Self-association and folding in membrane determine the mode of action of peptides from the lytic segment of sticholysins**. *Biochimie*, 156, 109-117.

233. Mesa-Galloso, H., Delgado-Magnero, K.H., Cabezas, S., Lopez-Castilla, A., Hernandez-Gonzalez, J.E., Pedrera, L., . . . Valiente, P.A. (2017). **Disrupting a key hydrophobic pair in the oligomerization interface of the actinoporins impairs their pore-forming activity**. *Protein Sci*, 26 (3), 550-565.

234. Laborde, R.J., Sanchez-Ferras, O., Luzardo, M.C., Cruz-Leal, Y., Fernandez, A., Mesa, C., . . . Lanio, M.E. (2017). **Novel Adjuvant Based on the Pore-Forming Protein**

Sticholysin II Encapsulated into Liposomes Effectively Enhances the Antigen-Specific CTL-Mediated Immune Response. *J Immunol*, 198 (7), 2772-2784.

235. Marcus, Y. (2012). **Volumes of aqueous hydrogen and hydroxide ions at 0 to 200 °C**. *J Chem Phys*, 137 (15), 154501.

236. Alvarez, C., Casallanovo, F., Shida, C.S., Nogueira, L.V., Martínez, D., Tejuca, M., . . . Schreier, S. (2003). **Binding of sea anemone pore-forming toxins sticholysins I and II to interfaces-Modulation of conformation and activity, and lipid-protein interaction**. *Chem Phys Lipids*, 122 (1-2), 97-105.

237. Tamba, Y., Ariyama, H., Levadny, V., Yamazaki, M. (2010). **Kinetic pathway of antimicrobial peptide magainin 2-induced pore formation in lipid membranes**. *J Phys Chem B*, 114 (37), 12018-12026.

238. Mustafa, M.B., Tipton, D.L., Barkley, M.D., Russo, P.S., Blum, F.D. (1993). **Dye Diffusion in Isotropic and Liquid-Crystalline Aqueous (Hydroxypropyl)Cellulose**. *Macromolecules*, 26 (2), 370-378.

239. Müller, C.B., Loman, A., Pacheco, V., Koberling, F., Willbold, D., Richtering, W., Enderlein, J. (2008). **Precise measurement of diffusion by multi-color dual-focus fluorescence correlation spectroscopy**. *EPL (Europhys Lett)*, 83 (4), 46001.

240. Šuput, D. (1986). **Effects of Equinatoxin on the membrane of skeletal-muscle fiber**. *Period. Biol.*, 88 (2), 210-211.

241. Krauson, A.J., He, J., Wimley, W.C. (2012). **Determining the mechanism of membrane permeabilizing peptides: identification of potent, equilibrium pore-formers**. *Biochim Biophys Acta (BBA) - Biomembranes*, 1818 (7), 1625-1632.

242. Krauson, A.J., He, J., Wimley, W.C. (2012). **Gain-of-function analogues of the pore-forming peptide melittin selected by orthogonal high-throughput screening**. *J Am Chem Soc*, 134 (30), 12732-12741.

243. Mock, D.M., Matthews, N.I., Strauss, R.G., Burmeister, L.F., Schmidt, R., Widness, J.A. (2009). **Red blood cell volume can be independently determined in vitro using sheep and human red blood cells labeled at different densities of biotin**. *J Transfusion*, 49 (6), 1178-1185.

244. Calvete, J.J. (2017). **Venomics: integrative venom proteomics and beyond**. *Biochem. J.*, 474 (5), 611-634.

245. Prato, E., Biandolino, F. (2012). **Total lipid content and fatty acid composition of commercially important fish species from the Mediterranean, Mar Grande Sea**. *Food Chemistry*, 131 (4), 1233-1239.

10. APPENDIX

10.1. Excitation anisotropy spectrum of ATTO-488

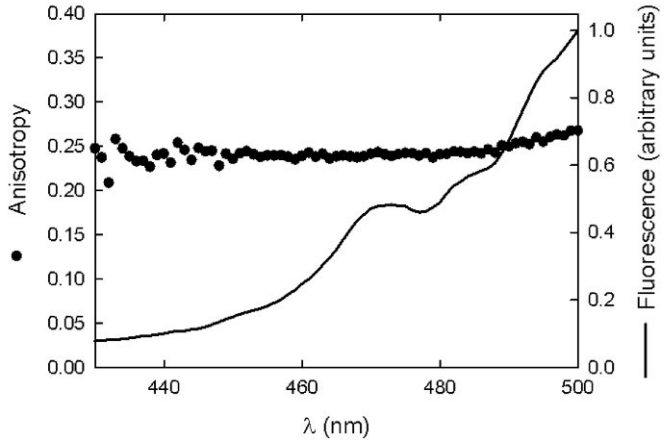

Figure A1. *Excitation anisotropy spectrum (solid circles) and excitation intensity spectrum (solid line) of ATTO-488 in 87% glycerol (v/v) at room temperature using 520 nm for emission wavelength. Notice that the values agree nicely with the* r*(0) values obtained in the anisotropy decays measured for ATTO-labeled StnI (the resolution of the instrument did not allow to resolve the r(0) value for the free label).*

10.2. Structural characterization of StnI-T43C

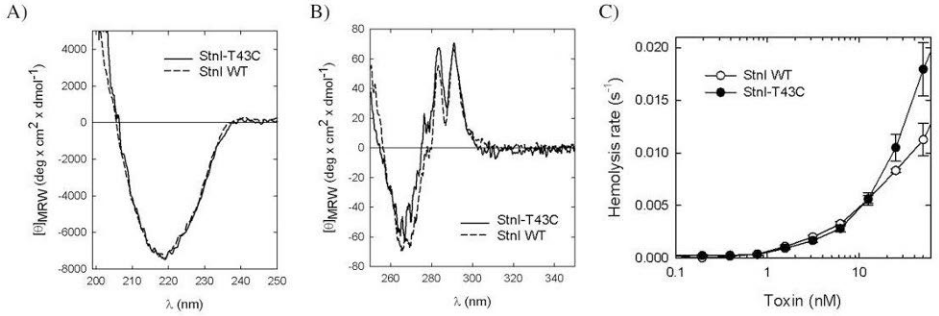

Figure A2. A) *Far-UV circular dichroism of the mutant (solid line) and StnI-WT (dashed line).* **B)** *Near-UV circular dichroism of the mutant (solid line) and StnI-WT (dashed line).* **C)** *Hemolysis rates of erythrocyte preparations when exposed to the indicated concentrations of StnI-WT (open circles) or StnI-T43C (solid circles).*

10.3. Mutated position of StnI-T43C

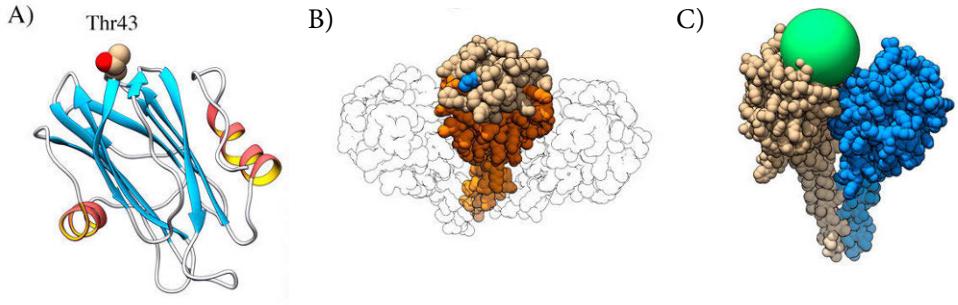

Figure A3. A) *Three-dimensional structure of StnI with Thr43 shown as spheres.* **B)** *Three StnI monomers (as spheres) arranged according to the octameric structure of FraC, showing the position of Thr43 in blue. Residues in orange were considered to be especially relevant for StnI functionality, and hence should preferably not be mutated.* **C)** *Two StnI-monomers arranged as in B, with a green sphere representing the maximum possible reach of the fluorescent labels used. It can be readily seen that the label will hardly interfere with the interaction with the neighboring monomer.*

10.4. Python program used to predict FRET efficiencies in the pores of sticholysins as a function of acceptor percentage in the sample

```
#!/usr/bin/env python3
# -*- coding: utf-8 -*-
"""
Last version. Included on this file on Thu Jun 11 13:17:34 2020
@author: Juan Palacios Ortega
Separation of the comments on the program has been adjusted for better display when
printed with this thesis
"""
import matplotlib.pyplot as plt
import numpy as np
from itertools import combinations as cmb

# General parametes & adjustments

r_mm = 29.0          # Distance between labelled positions
R0DD = 00.0          # R0 for D-D transfer; = 0.0 for D-D not affecting signal
R0DA = 63.8          # R0 for D-A transfer
t_D  = 4.1           # Average lifetime of the donor
ktd  = 1/t_D         # Decay rate of the D

fD   = 5             # Fraction of D, usually constant; max 100-fA

stoich = list(range(11,1,-1)) # Stoichiometries; as range(max,min-1,interval)

breakdown = 0        # Prints number of combinations for a stoich.
roff      = 10.0     # Distance from prot. center to label
aloff = np.pi/180*66 # Angle of the offset relative to line to oligomer center

#Output options
plotter = 0          # Show the plots of the oligomers
labs    = 0          # Show the distance labels
labs_c  = 0          # Show the distance to the center
```

```
rel_siz = 0          # Plot olig. so that 1 unit is NOT same in all (if == 1)
save_drw= 0          # Saves the schemes of the oligomers

sel_fA  = 0.06       # fA at which to plot FRET(stoich)
subdiv  = 4          # Resolution on x axis of the final traces is 1/subdiv

#------------------------------------------------------------------------
finalE = [184]
for N in stoich:
    # Geometrical calculations

    Cn   = r_mm/(2*np.sin(np.pi/N))        # Distance to the center
    Cn   = np.sqrt((Cn+roff*np.cos(aloff))\
           **2+(roff*np.sin(aloff))**2)   # Distance to center from fluorophore
    ri   = [0]              # Distances from 0 to i, calculated in the next loop
    ralf = [0]

    for i in range(1,N):
        ri.append(2*Cn*np.sin((np.pi*i)/N))
        ralf.append(2*np.pi*(i)/N)

#========================================================================
# Plot of the oligomers

    x    = []              # Stores x coordinates of the poligon
    y    = []              # Stores y cooridnates of the poligon

    for j in ralf:         # Loop to calculate x,y coordinates
        if rel_siz == 1:
            x.append(np.cos(j)*Cn)
            y.append(np.sin(j)*Cn)
        else:
            x.append(np.cos(j)*Cn)
            y.append(np.sin(j)*Cn)

    x.append(x[0])         # Adds first to have the last line in the diagram
    y.append(y[0])

    if N == max(stoich):
        xm   = max(x)*1.2  # Adjust the maximum values of the axis
        ym   = max(y)*1.2

        if xm > ym:
            ym = xm
        else:
            xm = ym

        if ym < 0.02:
            ym = 1.2
            xm = ym

    fig  = plt.figure(figsize = [6,6])     # Creates the plot

    plt.plot(x,y, 'k:')                    # Plots the exterior line
    plt.plot(x,y, 'o', markersize = 10, color = 'none', \
             mec = 'k', mew = 2)           # Plots the points in the vertices

    for j in range(1,int(N/2+1)):          # Loop that plots the non-symmetric ri and
the values of the distances
        plt.plot([x[0],x[j]],[y[0],y[j]],'b--', lw = 2, dashes = [5,2*j])
        if labs == 1:
            plt.text((x[0]+x[j]*1.3)/2,(y[0]+y[j]*1.25)/2,\
                 'r'+str(j)+' = '+str(ri[j])[:5], fontsize = 12, color = 'b')

    plt.plot([x[N-1],0],[y[N-1],0],'r-.', lw = 2)   # Plot of the line to the center
    if labs_c == 1:
        plt.text(x[N-1]/2,y[N-1]*1.1/2,'$C_n $= '+str(Cn)[:5]+' Å',\
             fontsize = 15, color = 'r')            # Plot of the distance to the center

    for j in range(len(x)-1):                       # Plot of subunit numbering
        plt.text(x[j]*1.4,y[j]*1.4,str(j+1), fontsize = 15)
```

```
    ax = plt.gca()                                  # Adjustments of the axis
    ax.set_xlim([-xm,xm])
    ax.set_ylim([-ym,ym])
    ax.axis('off')

    if save_drw == 1:
        plt.savefig(str(N)+'mer_Distances.png',\
                            transparent = True,dpi = 150)
        plt.savefig(str(N)+'mer_Distances.pdf',dpi = 150)
    if plotter == 1:
        plt.show()
    plt.close()

#=========================================================================
# Combinatorial calculations
# We consider that a donor is always placed at a fixed position (1) of the oligomer.
That way, redundances due to rotational symmetry are avoided

    combs = {}          # Dict. for the combinations. Name is COMBinationS

    for D in range(1,N+1):     # Loop that creates "all" the combinations
        combs[D] = {}  # Dict. for all the combinations for each number of Ds

        if D == 1:   # The possible donor combinations, NOT having 1 fixed
            d = list(cmb(range(0,1),D))
        elif D == N:
            d = tuple(range(N))
            combs[D][0] = d
        else:
            d = list(cmb(range(0,N),D))
# Combinations of A, removes the redundances, inforces the "1 fixed" rule
        for A in range(1,N-D+1):
            combs[D][A] = []
            a = list(cmb(range(N),A))
            for i in d:
                for m in a:
                    if 0 in i:
                        U = True
                        for j in i:
                            if j not in m:
                                continue
                            else:
                                U = False
                        if U:
                            combs[D][A].append((i,m))

    ck = list(combs.keys())
    for i in ck:      # Loop to get the combinations for the donors if A = 0
        if i < N:
            varl = []
            vark = list(combs[i].keys())
            for j in vark:
                if j == max(ck)-i:
                    for k in combs[i][j]:
                        if type(k) is tuple:
                            varl.append(tuple(k[0]))
                    combs[i][0] = varl

    combs[0] = {}
    for i in ck:            # Loop to get the combinations of A when D = 0
        combs[0][i] = combs[i][0]

    combs[0][0] = ['none']  # Definition, D & A = 0, all are empty

    ck = list(combs.keys()) # Update of the dict. key list

    if breakdown == 1:
        suma = 0            # Counting combinations produced; check point
        for i in ck:
            for j in combs[i]:
```

```
                if type(combs[i][j]) is list:
                    print(i, 'D ',j,'A ->\t',\
                          len(combs[i][j]),'\tcombinations')
                    suma += len(combs[i][j])
                else:
                    print(i, 'D ',j,'A ->\t 1\tcombinations')
                    suma += 1

        print('Total    ->\t',suma,'combinations\n')

#=============================================================================
    rate_comp = {}          # Stores transfer rates for each configuration
    for i in ck:
        rate_comp[i] = {}
        for j in combs[i]:
            rate_comp[i][j] = []
            for k in combs[i][j]:
                if i != ck[-1]:
                    if type(k) is tuple:
# This "if" calculates them for the combinations that A != 0
                        if type(k[0]) is tuple:
                            rates = 0
                            for m in k[1]:
                                rates += ktd*(R0DA/ri[m])**6
                            for m in k[0]:
# This "if" takes into account D-D transfer, if it is possible (D>1)
                                if m != 0:
                                    rates += ktd*(R0DD/ri[m])**6
                            rate_comp[i][j].append(rates)
                        if type(k[0]) is not tuple:   # Same for A = 0
                            rates = 0
                            for m in k:
                                if m != 0:
                                    rates += ktd*(R0DD/ri[m])**6
                            rate_comp[i][j].append(rates)

    rates = 0
    if N > 2:
        for i in ck:    # Same for D = N
            rates += ktd*(R0DD/ri[m])**6
        rate_comp[N][0].append(rates)

#_____________________________________________________________
    E_vals = {}

    for i in ck:
        E_vals[i] = {}
        for j in rate_comp[i]:
            E = 0
            rounds = 0
            for k in rate_comp[i][j]:
                E += k/(k+ktd)
                rounds += 1
            if rounds != 0:
                E_vals[i][j] = []
                E_vals[i][j].append(E/rounds)

#=============================================================================

    fact = {}
    for i in ck:
        fact[i] = np.math.factorial(i)

    emp_combs = {}
    for i in ck:
        emp_combs[i] = {}
        if i != 0:
            for j in E_vals[i]:
                emp_combs[i][j] = int(fact[N-1]/\
                                  (fact[i-1]*fact[j]*fact[N-i-j]))
```

```
    fA   = np.arange(0,subdiv*100-subdiv*fD,1)/(100*subdiv) # Fraction of A, usually
variable; max 100-fD

    finalE[N] = []

    for u in range(len(fA)):
        value  = 0
        wei_E = {}
        tot = 0

        for i in emp_combs:
            wei_E[i] = {}
            for j in emp_combs[i]:
                wei_E[i][j] = emp_combs[i][j]*(fD/100)**(i-1)\
                              *fA[u]**j*(1-(fD/100)-fA[u])**(N-i-j)
                tot += wei_E[i][j]

        for i in E_vals:
            for j in E_vals[i]:
                value += E_vals[i][j][0]*wei_E[i][j]

        finalE[N].append(value)

# Plot of the results
fig_Es = plt.figure(figsize = [6,6])
for N in finalE:
    plt.plot(fA,finalE[N])

ax = plt.gca()
ax.set_xlim([0,1])
ax.set_ylabel('FRET Efficiency')
ax.set_ylim([0,1])
ax.set_xlabel('Fraction of acceptor')
ax.tick_params(axis = 'both',direction = 'in', top = True,right=True)

fA_plt = int(np.where(fA == sel_fA)[0])

fig_Egx = plt.figure(figsize = [4,4])
for N in finalE:
    plt.plot(N,finalE[N][fA_plt],'ko')

ax2 = plt.gca()
ax2.set_title('FRET efficiency at $f_A =$'+str(fA[fA_plt]))
ax2.set_ylabel('FRET efficiency')
ax2.set_xlabel('Stoichiometry')
ax2.tick_params(axis = 'both',direction = 'in', top = True,right=True)

# Export the results to a .txt file in the current folder
with open('Predicts.txt','w') as f:
    f.write('\t')
    for N in finalE:
        f.write(str(N)+'\t')
    f.write('\n')
    for i in range(len(finalE[2])):
        f.write(str(fA[i]).replace('.',',')+'\t')
        for N in finalE:
            f.write(str(finalE[N][i])[:7].replace('.',',')+'\t')
        f.write('\n')
```

11. ORIGINAL PUBLICATIONS

Paper I is reprinted with permission from Palacios-Ortega, J., García-Linares, S., Rivera-de-Torre, E., Gavilanes, J. G., Martínez-del-Pozo, A., & Slotte, J. P. (2017). **Differential effect of bilayer thickness on sticholysin activity**. *Langmuir*, 33(41), 11018-11027.
https://doi.org/10.1021/acs.langmuir.7b01765

Paper II is reprinted with permission from Palacios-Ortega, J., García-Linares, S., Rivera-de-Torre, E., Gavilanes, J. G., Martínez-del-Pozo, Á., & Slotte, J. P. (2019). **Sticholysin, sphingomyelin, and cholesterol: a closer look at a tripartite interaction**. *Biophysical journal*, 116(12), 2253-2265.
https://doi.org/10.1016/j.bpj.2019.05.010

Paper III is reprinted with permission from Palacios-Ortega, J., Rivera-de-Torre, E., Gavilanes, J. G., Slotte, J. P., & Martínez-del-Pozo, Á. (2020). **Evaluation of different approaches used to study membrane permeabilization by actinoporins on model lipid vesicles**. *Biochimica et Biophysica Acta (BBA)-Biomembranes*, 1862(9), 183311.
https://doi.org/10.1016/j.bbamem.2020.183311

Paper IV is reprinted with permission from Palacios-Ortega, J., Rivera-de-Torre, E., García-Linares, S., Gavilanes, J. G., Martínez-del-Pozo, Á., & Slotte, J. P. (2021). **Oligomerization of Sticholysins from Förster Resonance Energy Transfer**. *Biochemistry*, 60(4), 314-323.
https://pubs.acs.org/doi/abs/10.1021/acs.biochem.0c00840

ISBN 978-952-12-4074-4